CR-152022

UNSTEADY HOVERING WAKE PARAMETERS IDENTIFIED FROM DYNAMIC MODEL TESTS

Part I of Final Report under contract NAS2-7613

Prepared for the Ames Directorate, USAAMRDL
at Ames Research Center, Moffett Field, California

by

K. H. Hohenemser
and
Sam T. Crews
Department of Mechanical Engineering

Washington University
School of Engineering and Applied Science
St. Louis, Missouri 63130

June 1977

UNSTEADY HOVERING WAKE PARAMETERS IDENTIFIED FROM DYNAMIC MODEL TESTS

Part I of Final Report under contract NAS2-7613

Prepared for the Ames Directorate, USAAMRDL
at Ames Research Center, Moffett Field, California

by

K. H. Hohenemser
and
Sam T. Crews
Department of Mechanical Engineering

Washington University
School of Engineering and Applied Science
St. Louis, Missouri 63130

June 1977

UNSTEADY HOVERING WAKE PARAMETERS IDENTIFIED FROM DYNAMIC MODEL TESTS

Part I of Final Report under Contract NAS2-7613

Abstract

This paper reports on the development of a 4-bladed model rotor that can be excited with a simple eccentric mechanism in progressing and regressing modes with either harmonic or transient inputs. Parameter identification methods were applied to the problem of extracting parameters for linear perturbation models, including rotor dynamic inflow effects, from the measured blade flapping responses to transient pitch-stirring excitations. These perturbation models were then used to predict blade flapping response to other pitch-stirring transient inputs, and rotor wake and blade-flapping responses to harmonic inputs. The viability and utility of using parameter identification methods for extracting the perturbation models from transients are demonstrated through these combined analytical and experimental studies.

Preface to Final Report under Contract NAS2-7613

Work under Contract NAS2-7613 started on July 1, 1973. The contract was originally awarded for a 3 year period.

Due to the slower than anticipated progress of the experimental work, not all research goals had been achieved by 30 June 1976. Since less than the anticipated cost for personnel and equipment had been spent, the research contract was extended by a year without increase in funding.

The research goals as stated in the contract were:

(a) Assess analytically the effects of fuselage motions on stability and random response. The problem is to develop an adequate but not overly complex flight dynamics analytical model and to study the effects of structural and electronic feedback, particularly for hingeless rotors.

(b) Study by computer and hardware experiments the feasibility of adequate perturbation models from non-linear trim conditions. The problem is to extract an adequate linear perturbation model for the purpose of stability and random motion studies. The extraction is to be performed on the basis of transient responses obtained either by computed time histories or by model tests.

(c) Extend the experimental methods to assess rotor wake-blade interactions by using a 4-bladed rotor model with the capability of progressing and regressing blade pitch excitation (cyclic pitch stirring), by using a 4-bladed rotor model with hub tilt stirring, and by testing rotor models in sinusoidal up or side flow.

Including the final report, 10 reports under Contract NAS2-7613 have been submitted. They are listed as P. 1 to P. 10 at the end of the Preface. P. 1 and P. 10 pertain to research goal (a). P. 2, P. 4, P. 6, P. 7, P. 8, P. 9, pertain to research goal (b). P. 3 and P. 5 pertain to research goal (c). The latter is not as yet complete since neither hub tilt stirring nor testing is sinusoidal up or side flow has been performed. While P. 10 describes only work done during FY 1977, P. 8 and P. 9 combine both FY 1977 work results and summaries of earlier results, so that the three parts of the Final Report can be read without recourse to the earlier reports. P. 8 includes much new material not available when the preceding Yearly Report P. 7 was written. The experimental data of P. 9 have all been obtained in FY 77.

So far 3 publications came out of the research under Contract NAS2-7613. They are listed as P. 11, P. 12, P. 13.

List of Reports and Papers under Contract NAS2-7613

P 1. Hohenemser, K. H. and Yin, S. K., "Methods Studies Toward Simplified Rotor-Body Dynamics", Part I of First Yearly Report under Contract NAS2-7613, June 1974.

P 2. Hohenemser, K. H. and Yin, S. K., "Computer Experiments in Preparation of System Identification from Transient Rotor Model Tests", Part II of First Yearly Report under Contract NAS2-7613, June 1974.

P 3. Hohenemser, K. H. and Crews, S. T., "Experiments with a Four-Bladed Cyclic Pitch Stirring Model Rotor", Part III of First Yearly Report under Contract NAS2-7613.

P 4. Hohenemser, K. H., Banerjee, D. and Yin, S. K., "Methods Studies on System Identification from Transient Rotor Tests", Part I of Second Yearly Report under Contract NAS2-7613, June 1975.

P 5. Hohenemser, K. H. and Crews, S. T., "Additional Experiments with a Four-Bladed Cyclic Pitch Stirring Model Rotor". Part II of Second Yearly Report under Contract NAS2-7613, June 1975.

P 6. Hohenemser, K. H., Banerjee, D. and Yin, S. K., "Rotor Dynamic State and Parameter Identification from Simulated Forward Flight Transients", Part I of Third Yearly Report under Contract NAS2-7613, June 1976.

P 7. Hohenemser, K. H. and Crews, S. T., "Rotor Dynamic State and Parameter Identification from Hovering Transients", Part II of Third Yearly Report under Contract NAS2-7613, June 1976.

P 8. Hohenemser, K. H. and Crews, S. T., "Unsteady Hovering Rotor Wake Parameters Identified from Dynamic Model Tests", Part I of Final Report under Contract NAS2-7613, June 1977.

P 9. Hohenemser, K. H. and Banerjee, D., "Application of System Identification to Analytic Rotor Modeling from Simulated and Wind Tunnel Dynamic Test Data", Part II of Final Report under Contract NAS2-7613, June 1977.

P 10. Hohenemser, K. H. and Yin, S. K., "Finite Element Stability Analysis for Coupled Rotor and Support Systems", Part III of Final Report under Contract NAS2-7613, June 1977.

P 11. Hohenemser, K. H. and Yin, S. K., "On the Use of First Order Rotor Dynamics in Multiblade Coordinates", 30th Annual National Forum of the American Helicopter Society, May 1974, Preprint 831.

P 12. Banerjee, D. and Hohenemser, K., "Optimum Data Utilization for Parameter Identification with Application to Lifting Rotors", Journal of Aircraft, Vol. 13, No. 12, December 1976, pp. 1014-1016.

P 13. Banerjee, D., Crews, S. T., Hohenemser, K. H. and Yin, S. K., Identification of State Variables and Dynamic Inflow from Rotor Model Dynamic Tests", Journal American Helicopter Society, Vol. 22, No. 2, April 1977.

TABLE OF CONTENTS

LIST OF FIGURES

LIST OF TABLES

UNSTEADY HOVERING WAKE PARAMETERS IDENTIFIED FROM DYNAMIC MODEL TESTS

1. INTRODUCTION

While parameter identification from transients is a relatively well developed method to extract rotor derivatives from rotorcraft flight tests (see References 1, 2, 3, 4, 5, and 6) dynamic rotorcraft or model testing has been restricted to frequency response testing (References 7, 8, 9, 10, 11, 12, and 13), limit cycle searches (Reference 14), and studies of the decay of damped modes (References 15, 16, and 17). Frequency response testing implies exciting the rotor with a series of discrete constant frequency inputs over a range of frequencies. A rotor transient test that sweeps this frequency range takes much less testing time. The question then is whether parameter identification techniques are suitable to extract information from transient tests that is equivalent to the information that can be extracted from the harmonic tests.

1.1 SCOPE OF WORK

The work described herein has two goals. One goal was to build a rotor model capable of both harmonic and transient testing, use parameter identification methods to extract information from the transient tests, use traditional frequency response methods to extract information from the harmonic tests, and compare the two methods of testing and data evaluation. Characterization of the hovering rotor dynamic wake is the second major goal. Some experimental work toward this end is presented in Reference 11, which also contains a mathematical model for fitting the experimental results. Reference 18 presents a theory for determining the parameter values of this mathematical model and also extends the model to forward flight.

A four bladed rotor model was designed to study the structure of the rotor dynamic wake. The rotor model can be excited in progressing and regressing modes with either harmonic or transient cyclic pitch

stirring inputs. Collective pitch can be changed from test to test but not during a test run. When harmonic inputs were used, rotor quantities measured were pitch input position, rotor shaft position, one blade flap-bending deflection, and rotor wake velocities at a variety of radial positions. The deflection and velocities were Fourier analyzed at multiples of the excitation frequency. The Fourier coefficients could be compared to coefficients generated by an analytical model. All analytical models are perturbation models about a particular trim condition. When transient inputs were used, rotor quantities measured were pitch input position, rotor shaft position, and four blade flap-bending deflections. Parameter identification methods were used to find the parameter values for analytical models from these measurements. The information obtained from both types of experiments could be compared by using the transient test generated parameters to obtain Fourier coefficients from the analytical models that could then be compared to the harmonic test Fourier coefficients.

Parameter identification methods reduced model testing time by a factor of more than 80 for each collective pitch setting studied, and produced more easily interpretable results with respect to the analytical models studied.

1.2 RELATED WORK

Parameter identification techniques have not been applied to rotorcraft model tests before, so there exists no related work in that area. However, such techniques have been applied to helicopter flight testing (References 1-6). The tests in References 1-4 were used to determine derivative models for the maneuvers performed in the tests. One use for these models could be in constructing pilot training simulators for the particular helicopter that was tested. Another use could be to substantiate or improve the analysis, though this use was not emphasized in the cited references. In contrast parameter values identified from the tests presented in the following are directly compared with mathematical model parameter values. In other words, the parameter identification techniques are used here to directly explore the relationship between mathematical model and the physical dynamic system.

The oldest mathematical rotor models were based on the actuator disc concepts developed by Glauert and Lock in the 1920's and used

momentum theory to derive values for the induced inflow through the disc and its effects on rotor thrust. These models did not attempt to describe the rotor structural motions (rotor dynamics) or transient thrust effects, except for the damping from steady pitch or roll rates. These models assumed a static uniform wake structure, the effects of the dynamic wake on rotor dynamics was ignored. Steady state models and their modern day extensions give fairly good values of gross rotor performance.

Recently much effort has been devoted to the study of rotor wakes, primarily for performance prediction. A good survey of the work done in the Western world is presented in Reference 19. The Russian treatment of this same subject appears in Reference 20. These works lean heavily toward vortex theory in their treatment of the wake. Vortex theories appear to be quite promising for predicting quasi-steady rotor wake-structural coupling at moderate to high advance ratios (References 20, 21) where certain simplifying assumptions can be made about the distribution of wake vorticity. It is still an open question as to how useful general vortex theory will become for predicting dynamic rotor wake-structural coupling because of the complexity of the problem.

Theoretical and experimental studies of the effects of steady wake asymmetries have shown that wake-structural coupling is responsible for deficiencies in control effectiveness and for changes in static derivatives not only at low but at high advance ratios (References 22, 23, 24, 25). Reference 24 presents a momentum theory formulation for predicting the quasi-steady rotor wake-structural coupling and compares this theory to experiment, vortex theory, and an empirical (best fit to the data) wake.

The classical work by Loewy, Reference 26, on the unsteady aerodynamics of rotors, represents an extension of the Theodorsen and Kussner theory of oscillating airfoils in plane flow to the lifting rotor in the substall region at zero advance ratio and predicts an appreciable reduction in the aerodynamic damping of flap-bending modes in regions where the flap-bending frequency is an integral multiple of the rotation frequency. The Loewy theory was verified in experiments conducted by Daughaday et al, Reference 13. The Loewy effect is substantial only at low rotor lift.

Carpenter in 1953, Reference 15, introduced dynamic induced downwash in a study of the effect of transient collective pitch changes on thrust behavior. Carpenter et al were apparently the first and until now only group to make direct measurements of a dynamic wake, although many measurements have been made of quasi-steady wakes (see Reference 19 for a partial literature survey). They showed that for rotors subject to collective pitch ramp inputs, rotor behavior could be predicted by including an unsteady wake which is based on the concept of a participating air mass. This air mass is equivalent to the air mass that participates in the axial acceleration of a circular disk of the same radius as the rotor.

The little that is known to date about coupled rotor wake and cyclic flap-bending characteristics has been deduced from the rotor flapping frequency response to cyclic pitch input tests reported in References 7-10. Correlations of such test data with a simple dynamic rotor wake model based upon a time delayed momentum wake are given in Reference 11. Theoretical values of the wake time constants are determined in Reference 18 from potential flow around a solid disk.

2. THE FOUR BLADED ROTOR MODEL

The four bladed rotor model was designed specifically for the purpose of studying rotor flapping response to dynamic pitch stirring inputs. A dynamic pitch stirring input is a cyclic pitch input where the position of the maximum pitch input angle either progresses around the rotor azimuth angle in the direction of rotor rotation, or regresses around the rotor azimuth angle opposite to the direction of rotor rotation. The complicated control system needed to control a rotor in flight is not needed to produce dynamic pitch stirring inputs. In fact a flight control system in a model rotor, which is built to study a particular aspect of flight dynamics, is a liability. The many bearings necessary to achieve a flight control system usually produce excessive dead areas, play, or slop in control systems of model rotors. Our model rotor has only six bearings, four pitch feathering bearings, one for each blade, and two cyclic pitch stirring input bearings. There is no measurable play in the control system. The rotor was designed and built to minimize rotor pitch-flap and flap-lag structural coupling over the range of experimental test conditions. There is no structural inter-blade coupling because the hub is very stiff compared to the blades. Therefore the only possible inter-blade coupling is through the wake structure. There are no test stand natural frequencies in range of the test excitation frequencies to interfere with test results. Flapping response to cyclic pitch stirring inputs for this model rotor have been effectively isolated from structural coupling with other rotor structural motions.

2.1 THE ROTOR HEAD

Figure 1 is a schematic of the rotor head and Figure 2 is a photograph of the rotor head. The blades are driven by the hub, which is screwed into the rotor shaft RS, through flanged extended inner ring micro-precision bearings. The cyclic pitching motion is generated by an inner shaft I whose rotation can be independent of the rotor shaft RS. Relative rotation of the inner shaft I to the rotor shaft RS produces via eccentric E, bending flexures B and pitch shafts S feathering oscillations of the pair of opposing blades connected with flapping flexures F to pitch shafts S. The amplitude of cyclic pitch transmitted to the blades is proportional to the eccentricity of the

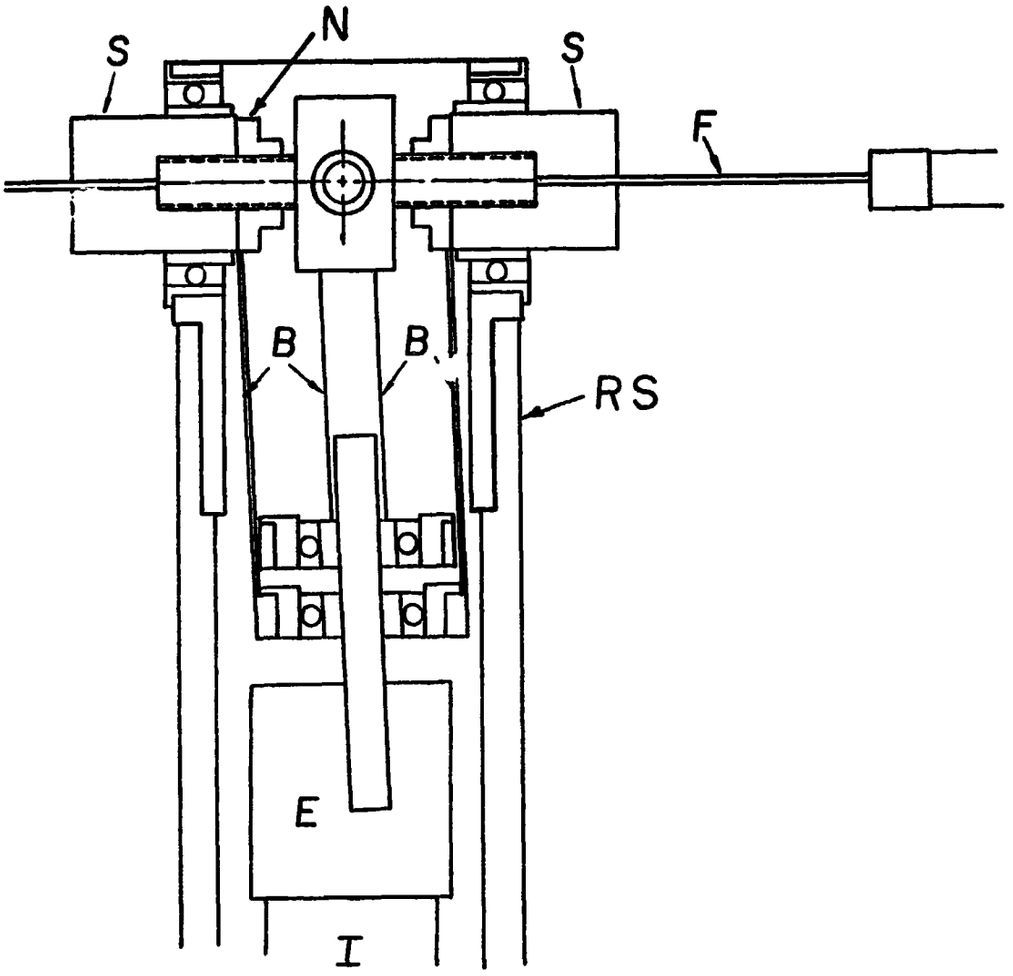

Figure 1 Rotor Head Schematic

rod in the eccentric E. When the inner shaft is not rotating, a steady cyclic pitch excitation is transmitted to the blades. The difference in angular velocities of the eccentric shaft I and rotor shaft RS then produces progressing or regressing cyclic pitch excitations. If I rotates in the same direction as RS, then the cyclic pitch is progressing in the direction of rotor rotation. If I rotates in the opposite direction from RS, then the cyclic pitch is regressing. The bearings attached to the bending flexures B will take a plus or minus 3^{o} misalignment. All tests were conducted with a 1.4^{o} eccentric.

2.1.1 Rotor Head Properties

The rotor was designed to fit into a wind tunnel with a 24" by 24"

Figure 2 Rotor Head Photograph

cross-section. A rotor diameter of 16.5" was chosen. The NACA 0012 fiberglass coated styrofoam blades are described in References 27 and 28. The blade cord is 1" yielding a rotor solidity ratio of .154.

Measurements to determine the structural properties of the blade and the blade-hub attachment were made with a stationary rotor. The blade fixture nut (Figure 2) was excited with a variable frequency magnetic field. The blade flapping, edgewise (or lead-lag), and torsion (or pitch) response were monitored by appropriate wiring of the 4 flapping strain gages (Figure 2), and resonant frequencies were determined. The measurements gave 14.0 Hz and 166 Hz for the first and second flap bending natural frequencies, 180 Hz and 271 Hz for the first and second torsion natural frequencies and 114 Hz for first lag bending natural frequency.

The blade and blade hub attachment mass distribution was measured. A finite element analysis (described in References 27 and 29) with 20 elements used the experimentally determined non-rotating first and second natural frequencies to construct the unknown flap bending stiffness distribution of the blade and blade hub attachment. The analysis was then used to determine the first and second natural flap bending frequencies during rotation, the mode shapes, and the flap bending moments. The computed bending moments per unit tip deflection of the first mode were found to be independent of rotor velocity at the center of the bending flexure strain gages (Figure 3). The value .573 lbf-in./in. tip deflection could be used independent of rotor velocity. This value was checked experimentally by applying simulated centrifugal forces. For both analysis and experiment the flapping angle β is arbitrarily defined by the straight line from the rotor center to the first mode deflection at .7 radius. One inch tip deflection represents 6.32^{o} flapping angle. The flap bending moment of the strain gage per degree of flapping angle is .091 in.-lbf/degree.

Tests were conducted at rotor rotational frequencies (n) of approximately 21, 27, and 36 Hz (Table 1). The maximum frequency of excitation was 1.5 n. Because of the substantial frequency spread between excitation and the higher natural frequencies (Table 1), second mode flap bending, elastic flap torsion coupling and elastic flap lag coupling were ignored in the dynamic theories used to predict experimental results.

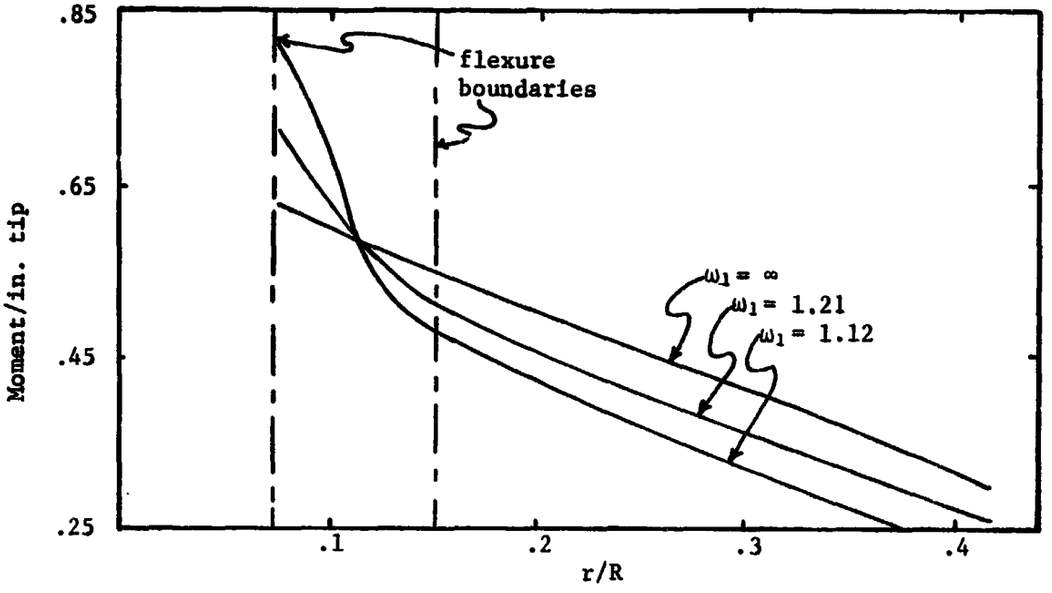

Figure 3 First Mode Bending Moments

Table 1

Natural Frequencies at Test Rotor Speeds

rotor speed-n	1st natural flap bending	2nd natural flap bending	1st natural torsion	1st natural edgewise	maximum pitch excitation
21 Hz	1.26 n	8.1 n	8.6 n	5.4 n	1.5 n
27 Hz	1.18 n	6.4 n	6.7 n	4.2 n	1.2 n
36 Hz	1.12 n	4.9 n	5.0 n	3.2 n	1.2 n

All quantities used to calculate the blade Lock number γ are known within three digits except for the blade lift slope a. The blade Reynolds number at .7 radius varies from .3 to .6 x 10^5 through the test range. Published test data (References 30 and 31) indicate that the 0012 airfoil should have a lift slope of about 5.7 at low angle of attack near these Reynolds numbers. However different sources of published data on the same airfoil can show characteristics that differ by as much as 5 percent (Reference 32). These differences can probably be attributed to surface differences between the respective airfoils tested. The Lock number for the test blades is 3.6 ± .2.

2.1.2 Rotor Head Adjustments

The blades are attached to the hub at the blade root fixtures shown in Figure 2. There is a cutout on one side of the blade root that allows the blade to slip into the fixture channel. Two screws are

used to hold the blade to the fixture. Blade pre-cone can be eliminated by trial and error shimming of the blade root to the fixture nut. Pre-lag can also be eliminated by careful blade placement before tightening the screws. A special fixture was built to facilitate the elimination of blade pre-lag.

Collective pitch is adjusted by locking the feathering shafts S (Figure 1) into different positions with respect to the eccentric bending flexures B by tightening the feathering nuts N. Collective pitch can only be adjusted with the rotor stopped between test runs. Relative collective pitch changes are measured with an optical device, Figure 4.

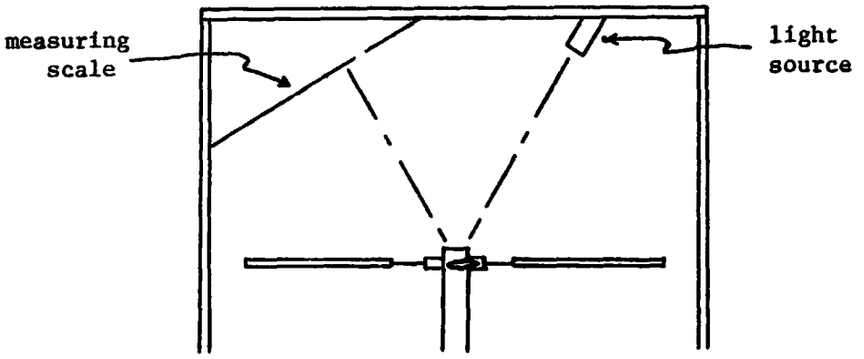

Figure 4 Collective Pitch Adjustment

Light strikes the mirror (Figure 2) on the blade flexure root and reflects on the measuring scale. With this device collective pitch changes on each blade can be made to accuracies of $\pm.05^{o}$. The reference value of the collective pitch of each blade, which was used for the base of the blade pitch changes, is difficult to find. Four sets of hovering tests were conducted. Between each set of tests, refinements were made in setting the reference value of collective pitch for each blade. Table 4 in Section 2.4 defines the physical condition of the rotor for the four sets of tests. All blade pitch changes were carefully recorded.

The rotor shaft is outfitted with pieces of reflecting tape at the azimuthal positions of each blade. A photo-electric pickup causes a stroboscope to fire as each blade passes the pickup. The viewer sees the 4 blade tips (each a different color) at the same vertical spacial

location. Tracking the rotor-getting all the blades to run in the same plane - is achieved by adjusting the individual blade pitch settings until all the blade tips are super-imposed upon each other. The rotor can be tracked to an accuracy of greater than $.1^{o}$ in flapping angle.

Frequency response tests were conducted first. During these tests, downwash velocities were measured with a hot wire anemometer. Keeping the rotor tracked, the point of near zero flow velocity was found by adjustment of the rotor collective pitch setting. Tests were run at plus 2, 5, and 8 degrees pitch from this point with a pitch stirring excitation of 1.4^{o} and with the rotor 1.28 radii above the ground plane. A steady cyclic pitch input moves each blade through one complete sinusoidal pitching cycle per revolution. Therefore, if the perturbations are linear, the blade flapping response should contain only Fourier components of once per revolution. During analysis the second Fourier coefficient of the flapping response was found to be approximately 10 percent of the first. Careful measurement revealed that some of the blades had pre-cone angles other than zero degrees. The spread was approximately .3 degrees. Because of the pre-cone spread the tracked blades also had a collective pitch spread of $\pm.7^{o}$. The collective pitch given for the frequency response tests is an average value.

The pre-cone was then corrected and transient tests set 1 were conducted at collective pitch settings of 1.5, 4.5, and 7.5 degrees. During analysis, the second Fourier coefficients of the blade flapping responses to a one per revolution pitch excitation were found to be 6 to 8 percent of the first. Careful measurements revealed that some of the blades had pre-lag angles other than zero. The spread was approximately $.7^{o}$. Because of the geometry of the blade root attachment, a pre-lag causes a pre-cone. The collective pitch spread for this set of tests was $\pm.4^{o}$.

The pre-lag and its respective pre-cone were then corrected and transient tests set 2 were conducted at collective pitch settings of 3.3, 6.3, and 9.3 degrees. During analysis the second Fourier coefficients of the blade flapping responses to a 1 per revolution pitching excitation were now found to be 2 to 4 percent of the first Fourier coefficients rather than the 6 to 8 percent found in transient tests set 1.

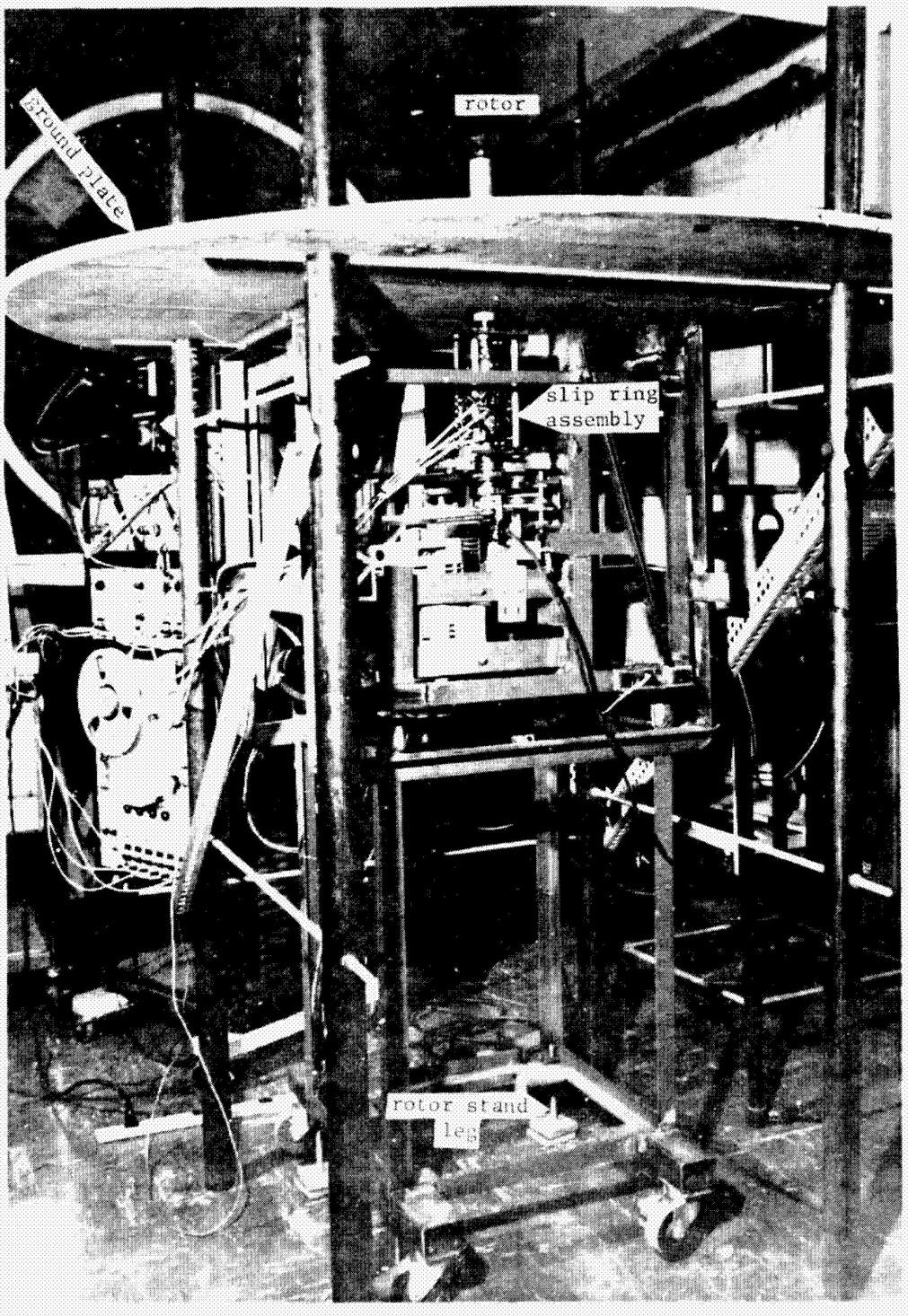

Figure 5 Rotor Hovering Test Stand

At this point the rotor was put into the wind tunnel at zero shaft angle of attack and at zero collective pitch setting. This position yielded a near zero flapping response from all blades at high advance ratio and zero cyclic pitch. Thus the zero collective pitch baseline determined previously was confirmed.

The rotor was then removed from the wind tunnel and transient pitch stirring tests set 3, with 5 degree collective pitch angle, were run.

2.2 ROTOR TEST SET-UP

The rotor test set-up consists of the test stand and the analog measurement system. The design of the measurement system was in part the result of decisions that had to be made as to how much of the signal processing and measurement functions should be done with analog devices and how much should be done with digital algorithms on the various mini-computers used for data processing. Signal processing and measurement functions were implemented on the digital side whenever possible in order to reduce hardware costs. The digital measurement functions are described in detail in Section 3.

2.2.1 Test Stand

The rotor hovering test stand can be seen in Figure 5. The ground height is adjusted by moving the ground plate support rods (Figure 5). The rotor height above the ground plate for each series of tests is given in Table 4 section 2.4. The ground plate was constructed to achieve (as far as possible) an azimuthally symmetric test condition. The rotor center is 4 rotor radii from the edge of the ground plate. The ground plate support legs are 2.8 rotor radii away from the rotor center and present an obstruction over 5 percent of the circumference. The nearest object, apart from the ground plate, to the rotor is the ceiling which is about 9 radii away from the rotor center. There is no air circulation system in the room. With the windows closed, local air velocities are near zero.

The rotor is leveled by adjusting the lengths of the 4 legs of the rotor stand. The rotor is level when a rotor blade has the same height above the ground plate (Figure 5) at all azimuth angles. The rotor stand is described in References 27 and 33. The only major change that has been made to the rotor stand is the replacement of the 12 slip ring assembly by a 20 slip ring assembly.

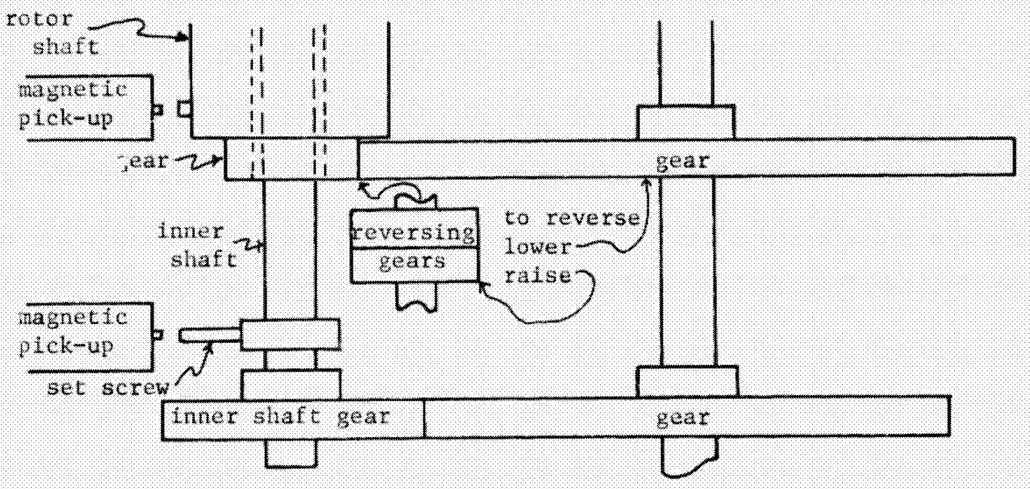

Figure 6 Harmonic Pitch Stirring Excitation System

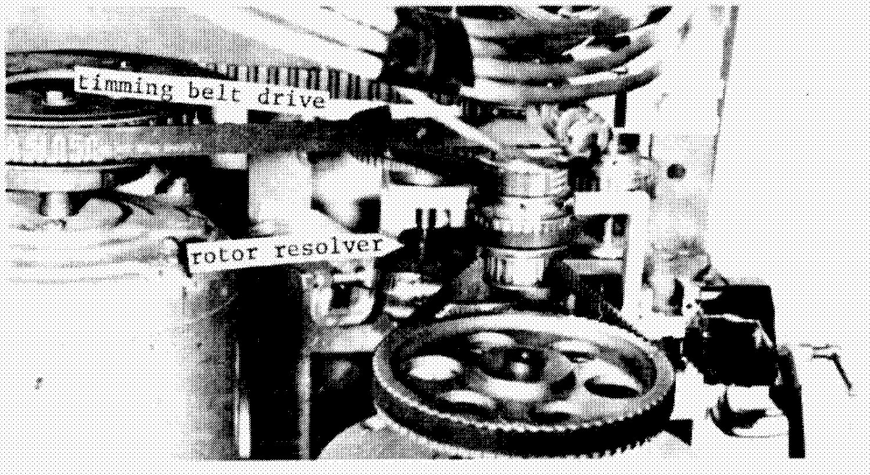

Figure 7 Transient Pitch Stirring Excitation System

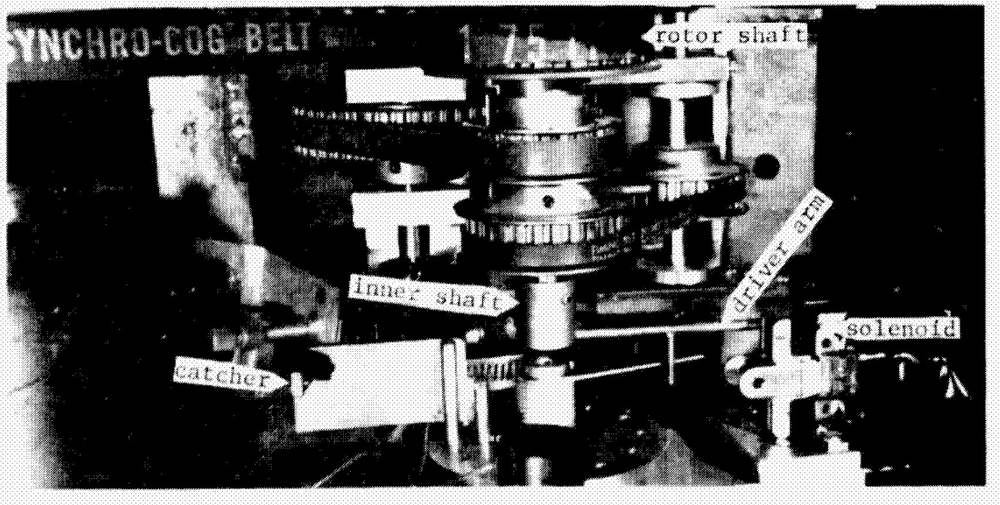

Figure 8 Short Transient Pitch Stirring Excitation System

The pitch stirring condition can be described by

$$\theta_I = \sin(\psi_p(t))$$
$$\theta_{II} = \cos(\psi_p(t)) \quad (1)$$

where ψ_p is the inner shaft azimuthal position and is defined so that θ_I and θ_{II} are forward and left cyclic pitch inputs respectively. Three cyclic pitch stirring excitation systems can be mounted on the rotor stand.

The harmonic cyclic pitch stirring excitation system is shown in Figure 6 and is described extensively in References 27 and 29. The drive motor turns the rotor shaft RS (Figure 1) through a timing belt drive. The rotor shaft drives the inner shaft I (Figure 1) through a reversible gear train (Figure 6). The gear ratios can be changed. Due to the reversing gears, the inner shaft I can be driven in the same direction as the rotor shaft, thus providing a progressing pitch stirring excitation, or opposite to the direction of rotor shaft rotation, thus providing a regressing pitch stirring excitation. Gear ratios are available for providing cyclic pitch stirring excitations in a space fixed reference system of $\omega_n = \pm.067, \pm.1, \pm.2, \pm.4, \pm.6, \pm.8$.

A transient pitch stirring excitation system that makes use of a variant of the double motor drive described in References 27 and 28 is shown in Figure 7. The inner shaft (Figures 1 and 7) is driven by a variable speed reversible motor through a 1 to 8 speed ratio timing belt drive (Figure 7). When the inner shaft motor is stationary the rotor cyclic pitch is constant with a space fixed excitation frequency of 0. Engaging the inner shaft motor accelerates the inner shaft to a preselected constant speed and produces either a progressing or regressing constant frequency value (depending upon the direction of motor rotation). The transient between these two steady values is used for parameter identification. This transient takes the form

$$\theta_I = \sin(\psi_{po} + \psi_p(t)\cdot t)$$
$$\theta_{II} = \cos(\psi_{po} + \psi_p(t)\cdot t) \quad (2)$$

where ψ_{po} is a constant. $\psi_p(t)$ is zero until the transient starts, the inner shaft motor is engaged. $\psi_p(t)$ is monotonically increasing during the transient, as the motor accelerates. $\psi_p(t)$ is constant after the transient is over, the motor reaches constant speed. Friction between the rotor shaft RS (Figure 1) and the inner shaft I will drive the

inner shaft (and the inner shaft motor) in the direction of rotor rotation. In transient tests sets 1 and 2 (Table 4), the inner shaft was restrained by hand until the inner shaft motor was engaged. In transient tests set 3, the inner shaft was released by a solenoid (Figure 7) that frees the inner shaft for rotation at the same time the inner shaft motor is engaged.

A second method of generating a transient cyclic pitch excitation is presented in Figure 8. This device has a driver arm attached to the inner shaft which is driven by a spring that wraps around a mandrel which is below the inner shaft. A solenoid is engaged that releases the driver arm. The spring accelerates the driver until it hits a catcher which is designed to eliminate rebound of the driver arm. The catcher can be positioned so that it allows an inner shaft travel of 90°, 180°, or 270°. The spring torque can be increased by winding it up more. This excitation takes the form

$$\theta_I = \sin(\psi_{po} + \psi_p(t))$$
$$\theta_{II} = \cos(\psi_{po} + \psi_p(t)) \qquad (3)$$

where ψ_{po} is a constant. $\psi_p(t) = 0$ before the transient starts, before the solenoid releases the driver arm. $\psi_p(t)$ accelerates during the test, as the driver travels to the catcher. $\psi_p(t)$ achieves a constant value at the transient end point, when the driver hits the catcher.

2.2.2 Analog Measurement Systems and Control Units

Blade angles were measured by strain gages on the flapping flexures (Figures 1 and 2). Similar flapping angle measurements are described extensively in References 27 and 29. The four strain gages on each flexure were wired into a Wheatstone bridge. The bridge remains balanced for blade edgewise and torsional deflections. The bridge responds only to blade flap-bending deflections. Each bridge circuit is separate. 3600 Hz 5 volt rms power is supplied, in the space fixed reference system, to each bridge, in the rotating reference system, through 3 of the circuits in the 20 circuit slip ring assembly. This signal is amplified by an A. C. amplifier (Figure 9) and is recorded on a 6 channel F. M. analog tape recorder (Figure 9). The output level of the amplifiers was adjusted to give a one volt output signal per degree of blade flapping, when possible, so that flapping angle amplitudes could be easily monitored on oscilloscopes during testing. The input to the flapping angle tape recording

channels could be switched for calibration purposes from the amplifiers to 2 D. C. voltage levels generated by a mercury battery circuit.

There are control circuits for two variable speed motor drives (Figure 9). These controls are described in References 27 and 29. The control circuits of the inner shaft and rotor motor are wired so that a 2.8 volt D. C. signal is recorded on the tape recorder channels used for monitoring the shaft azimuth angles until the motors are engaged. When the switch that engages a motor is thrown, the 2.8 volt signal is switched off and is replaced by the shaft azimuth angle measurement which varies between .2 and 1.8 volts. Thus the starting point of a transient test is clearly defined by a sudden voltage shift. For transient tests set 3, Table 4, the inner shaft motor switch also engages a solenoid that releases the inner shaft when the motor is engaged. This same switch was used in the spring excitation system to mark the start of the transient and release the driver arm (Figure 8).

Rotor shaft position, ψ, and inner shaft position, ψ_p, were determined by blips generated by magnetic pick-ups (Figure 6) passing set screws in the shafts in harmonic testing. The signals generated by the pick-ups were recorded on two channels of the tape recorder (Figure 9). Rotor shaft and inner shaft travel at constant speed in harmonic testing, consequently one does not need continuous measurements of their position during a test. It is sufficient to know their rate and a position at one given time during a test. Their position at any other time in the test can be calculated from these two factors. During a transient test continuous measurements of the azimuthal position of the inner shaft, ψ_p, must be made so that the cyclic pitch input condition can be determined (see (''' The blips cannot fulfill this function so tney were replaced.

Two resolvers (Figure 7) driven through timing belt drives were installed to make continuous measurements of ψ and ψ_p. The resolvers were purchased from a used parts catalog for a nominal sum. Operating specifications were not available. Experiments showed that these resolvers produced a repeatable 2 per revolution signal instead of a repeatable 1 per revolution signal. The rotor resolver drive ratio was changed from 1:1 to 1:½. The inner shaft resolver drive ratio remained 1:1 since the starting position of the inner shaft was known

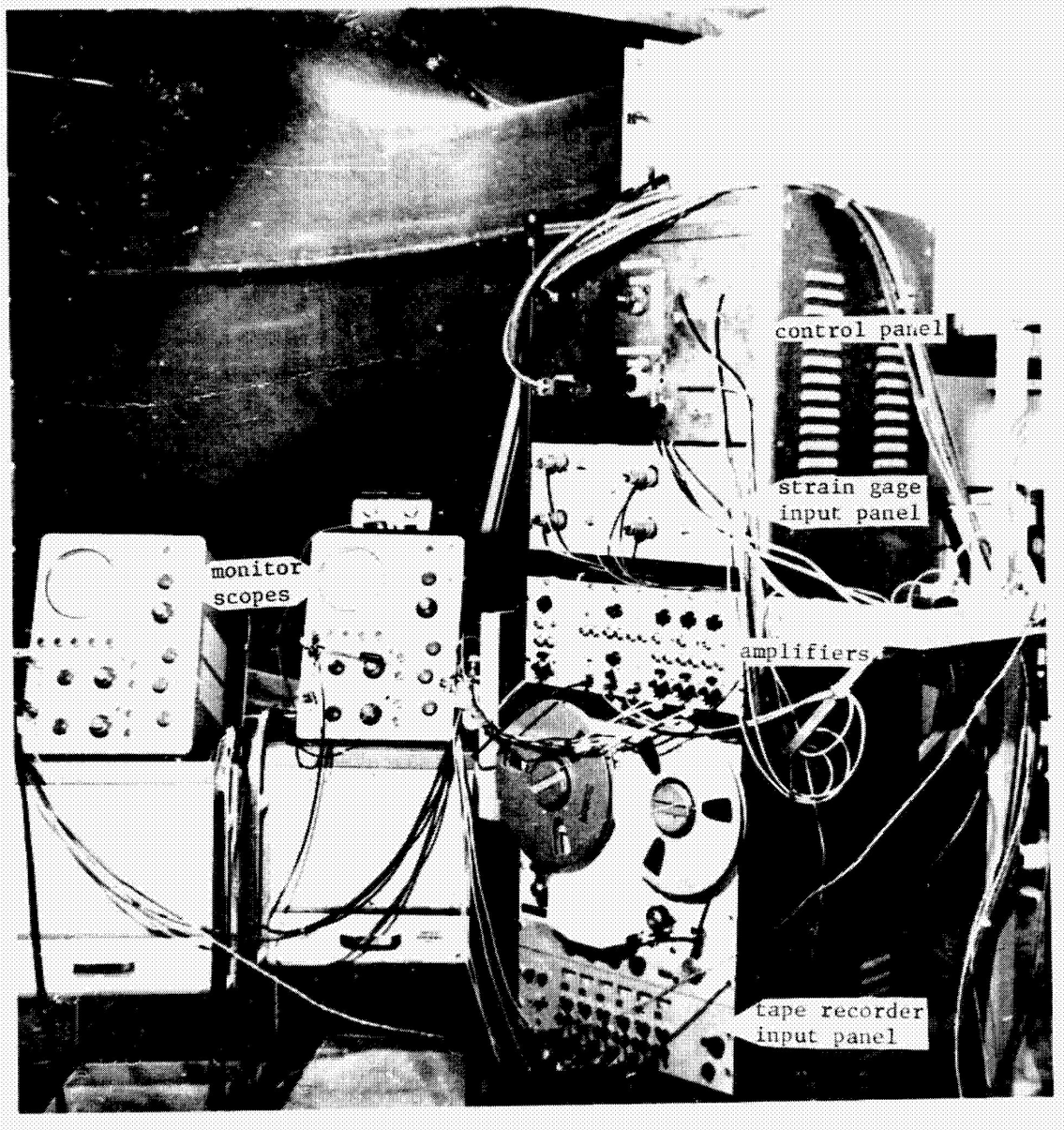

Figure 9 Instrumentation System

at the beginning of the test and the repeatable 2 per revolution signal provided more accuracy in the ψ_p measurement than a repeatable 1 per revolution signal could. Power was provided to the resolvers by audio oscillators operating at about 10,000 Hz. The output of the resolver is a 10,000 Hz signal attenuated by factors which vary with shaft position. The maximum modulation frequency is 100 Hz. The resolver output passes through a full wave rectifier and then through a low pass filter with a frequency cut-off of approximately 1000 Hz. The resulting signal is a repeatable 1 or 2 per shaft revolution waveform. In transient tests sets 1 and 2 (Table 4) the resolver signals were contaminated by inner resolver feedback through the single driving audio oscillator. This happened because the output impedence of the oscillator was not low enough compared tc the impedence of the two resolver circuits. Consequently there is a 1 per revolution error signal in the measurement of the inner shaft azimuth position (ψ_p). The error signal maximum amplitude is 5 percent of the maximum amplitude of the inner shaft resolver output. This error signal was eliminated in transient test set 3 by driving the two resolvers with different audio oscillators.

The resolver signals were recorded on the analog tape recorder. Converting the resolver signals into ψ and ψ_p measurements was done with digital algorithms in the computer and is described in Section 3.

Wake measurements were made with conventional hot wire anemometry. Two probes were calibrated in a calibration chamber for 0 to 20 ft/sec flow velocities. Linearization coefficients for the 4th order polynomial signal linearizers were obtained from the calibrations. A probe stand (Figure 10), which allows probes to be positioned at various azimuthal and radial positions below the rotor, was constructed. Probe height can also be adjusted. The measurement stations used in the set of harmonic tests of Table 4 are shown in Figure 11. Wake measurement signals were recorded on the analog tape recorder. The wake measurement signals were also processed on a RMS voltmeter with a time period of 1 sec. and on a D. C. Voltmeter while the tests were in progress.

The 6 channel Ampex SP-300 F. M. tape recorder (Figure 9) records D. C. voltage levels between -4 and +4 volts. At the recording speed used for all tests, 3.75 ips, the recorded signal remains undistorted

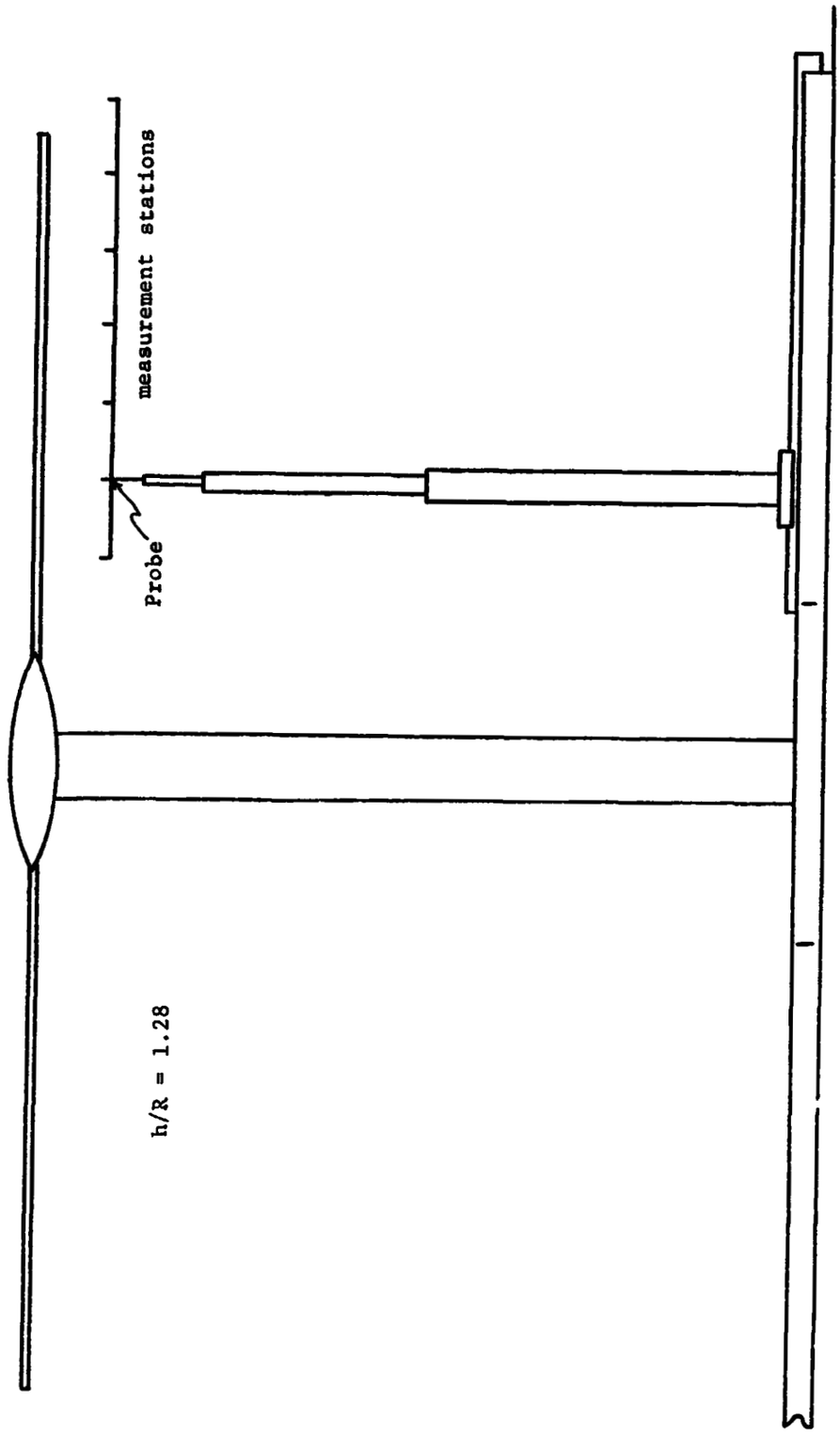

Figure 10 Hot Wire Anemometer Prob Stand

up to frequencies of 625 Hz. The recording level can be adjusted so that the signal actually recorded can be from .5 to 3.5 times the actual input signal. 1 to 1 input signal to recorded signal ratios requires very careful adjustment of the 6 level controls. The D. C. output level can be adjusted across a .5 volt range. At 3.75 ips, the tape drive reaches steady state speed in about 3 inches of tape from the stopped position. During a test, approximately 1 foot of tape is allowed to pass the record heads before recording is initiated.

Measurements recorded on the tape recorder during harmonic tests were:

channel 1 Rotor shaft blip for determining rotor azimuth position

channel 2 Inner shaft blip for determining cyclic pitch azimuth position

channel 3 β_1

channel 4 Hot wire measurement of rotor wake.

Measurements recorded on the tape recorder during transient tests were:

channel 1 Rotor shaft resolver for continuous rotor azimuth position

channel 2 Inner shaft resolver for continuously determining cyclic pitch azimuth position

channel 3 β_1

channel 4 β_2

channel 5 β_3

channel 6 β_4

2.3 CALIBRATION AND TEST PROCEDURES

In all tests the measurement signals were recorded on the 6 channel F. M. analog tape recorder. Some measurement functions (Section 3) and all analysis (Section 5) were performed on minicomputers. The interface between analog signals and digital signals was provided by the analog-digital converters controlled by the computer. The testing procedure was designed around this interface. The analog to digital converter accepts signals between 0 and 2 volts. It assigns voltages of 0 to $-\infty$ the integer value -512. It assigns voltages of 2 to ∞ the integer value 512. All signal levels recorded on analog tape were maintained between 0 and 2 volts except for the pretransient signal recorded on the inner shaft azimuth position channel. The A/D converter can address 8 input lines and sample at a rate of once every

16 micro-seconds.

2.3.1 Harmonic Test Calibration and Testing Procedure

Calibration of the harmonic test flapping measurement required accurate knowledge of three calibration numbers:

1. The amplifier output voltage per inch of tip deflection, which was measured by loading the blade tip and producing a known root moment and therefore a known tip deflection.
2. The tape recorder recording level amplification or attenuation which was carefully adjusted by recording known input signal levels and playing them back.
3. The precise A/D converter mapping of voltage level into the ±512 integer range, which was measured by sampling known D. C. voltage levels and displaying the results. The linearity of the conversion process was verified during this measurement.

The hot wire wake measurements were normalized so that 0 to 20 ft/sec yielded 0 to 2 volts output. The tape recorder record levels were carefully set and the A/D converter channels were studied for attenuation or amplification. The maximum signal level of the rotor and inner shaft blips have to be .3 to .8 volts for the program to find their relative position.

The test procedure is as follows. The collective pitch and the ground height are set at the desired test condition. A gear ratio is chosen, for example one that yields $\omega_n = .2$. The hot wire probe is positioned at a particular radial position (Figure 11). The rotor is run up to speed. The tape recorder drive is engaged and a foot of tape allowed to pass the recording head then the recorder is put into record mode. Three feet of tape are recorded, a meter keeps track of tape position. While the signal is being recorded, the average wake value (the D. C. signal level) and the RMS wake value are recorded by hand. The rotor is stopped and the hot wire probe is moved to a new position. The sequence is repeated until 7 radial positions (Figure 11) of the hot wire probe have been recorded. The reversing gear is engaged so that $\omega_n = -.2$ and a set of 7 wake measurements is made. This process is repeated until all 6 sets of gear ratios have been used. The whole test condition takes about 500 minutes (Table 3) to survey.

2.3.2 Transient Test Calibration and Test Procedure

Table 2 presents the interface between instrumentation, mini-

Table 2

Calibration and Test Procedure-Transient Tests

Data Use		Calibration Procedure			Test Procedure		
tape channel number	measurement or D. C. volts	computer sample			computer sample		
Ch. 1	Rotor resolver or 2.5V	2046 pnts at 180 pnts/rev rotor and inner resolver	nothing	nothing	rotor motor on triggers sampling. 1024 pnts per channel are saved of each measurement. Yeilds a transient in ω_1 the structural parameter.	Sampling is arbitrarily triggered by operator. 1024 pnts per channel are saved of each measurement. Yeilds the 'trim' or pretransient condition.	Inner shaft motor on triggers sampling. 1024 pnts per channel of each measurement are saved. Yeilds transient.
Ch. 2	Inner shaft resolver or 2.5 V						
Ch. 3	$_1$ or D. C. voltage	nothing	1024 pnts of 1.4 V	1024 pnts of 1.4 V.			
Ch. 4	$_2$ or D. C. voltage						
Ch. 5	$_3$ or D. C. voltage						
Ch. 6	$_4$ or D. C. voltage						

Tape operations
tape speed
3.75 ips
Model manipulations

5 ft | 10 ft | 3 ft | 3 ft | 3 ft

A
1. link shafts
2. inner shaft resolver switch--on
3. rotor resolver switch--on
4. rotor motor engaged

B
1. rotor off
2. unlink shafts
3. inner shaft resolver switch--off
4. test voltage—1.4V

C
1. test voltage --.4 V

D
1. rotor motor--on

E
1. inner shaft motor--on

F
1. inner shaft motor--off
2. rotor motor --off

computer, calibration procedure and testing procedure for the transient tests. Much greater use was made of the mini-computer in transient test calibration than in the frequency response test calibration.

A set of calibration runs was conducted before each set of tests. Each blade was loaded at its tip with a known mass which produced a known root moment and consequently a known flapping angle. The output of the amplifier for each blade flapping angle strain gage circuit was adjusted to give 1 volt per degree. The combined tape recorder and analog digital converter amplification and/or attenuation per channel were determined by recording 2 known D. C. voltage levels on (Table 2) 4 flapping angle recorder channels. The tape was played back through the computer which averaged the large number of sampled results for the two voltage levels, and determined the ratio of tape recorder input signal level to computer output signal level. The same digital voltmeter used to set the flapping angle amplifier output levels was used to measure the 2 tape recorder D. C. voltage input levels, consequently possible voltmeter calibration errors are avoided. There are then two sources of error in this calibration procedure; misplacement of the mass at the blade tips and D. C. drift of the F. M. tape recorder. The mass can be placed with 1% accuracy and the D. C. drift of the tape recorder yields a further 1% error source. Thus the calibration numbers are known to within 2% of their true values.

The test procedure is as follows. The collective pitch and the ground height are set at the desired test condition. The tape recorder is engaged, the rotor motor is engaged - step D (Table 2), the inner shaft motor is engaged - step E (Table 2), the tape is stopped, and finally the rotor and inner shaft motor are disengaged. The test takes less than 1 minute to perform.

2.4 A COMPARISON OF TEST PROCEDURES AND TEST SET PHYSICAL CONDITIONS

Table 3 presents a comparison of the time involved in conducting a test for the two testing methods. A test condition is defined as a combination of a particular ω_1 value (first rotating flap-bending frequency), a particular collective pitch setting and a particular ground height. It takes about 1 minute to change the rotational speed and consequently the ω_1 value, about 5 minutes to make a ground height change, and about 30 minutes to make a collective pitch change for both

Table 3

Time Comparisons of Test Methods

		Harmonic Test	Transient Test
Time Required to Change Test Condition	ω_1 value	1 min.	1 min.
	Ground Height	5 min.	5 min.
	Collective Pitch	30 min.	30 min.
Test Time		500 min.	1 min.
Model Running Time		80 min.	1 min.
Equivelent IBM 360 Computer Time Required for Digitization and Analysis	Harmonic Test Digitization and Fourier Series	10 min.	
	Transient Digitization and Fourier Coefficients of 1 Ω		13 sec.
	Parameter Identification		1-2 min.

test procedures. The test time for a harmonic test is 500 times that of a transient test. However, the model running time for the harmonic test is 80 times that of a transient test. Much time is spent in the harmonic test changing gear ratios by hand. This task could be done automatically with a mechanically more sophisticated model, so the two procedures should be compared on the basis of running time rather than total testing time.

Table 4 presents the physical condition of the rotor for each test set. For the early tests, the spread in collective pitch setting is large, however the average value of collective pitch for the rotor is quite accurate. In the case of the harmonic tests, the wake measurements take forms which are equivalent to averages over long periods, consequently individual blade differences are not important.

The measurement error of local rotor wake velocity does not exceed 4% of the true value. The error comes from inevitable probe calibration error and local anemometer linearization error. The calibration error for blade flapping angle measurements does not exceed 4% of its true value for the harmonic test and does not exceed 1.5% for the transient test. This random error does not vary from measurement to measurement but is a constant error present

Table 4

Physical Conditions of Tests

	average θ_o	spread of θ_o	ω_1	ground height	spread of pre-lag error	spread of pre-cone error	pitch error signal
Harmonic Tests	2^o 5^o 8^o	$\pm .7^o$	1.18	1.28 R	$.7^o$	$.3^o$	5 %
Transient Tests Set 1	1.5^o 4.5^o 7.5^o	$\pm .4^o$	1.18	1.28 R 1.02 R .78 R	$.7^o$	$.15^o$	5 %
Transient Tests Set 2	3.3^o 6.3^o 9.3^o	$\pm .2^o$	1.18	1.28 R 1.02 R .78 R	$.0^o$	$.0^o$	5 %
Transient Tests Set 3	5.0^o	$\pm .1^o$	1.18	1.02 R	$.0^o$	$.0^o$	5 %
	5.0^o	$\pm .1^o$	1.25 1.18 1.12	1.28 R 1.02 R .78 R	$.0^o$	$.0^o$	1 %

in all measurements. The measurement error of the cyclic pitching excitation angle remains within 1.5% of its true value. The cyclic pitch input azimuth angle is known to within 5% for most tests and to within 1% for the last set of tests conducted.

3. DATA PROCESSING

This chapter describes the manipulations of the transient data from the analog-digital interface through the creation of digital data files in a form suitable for treatment by the identification algorithm. Data processing of the harmonic test data is adequately described in References 27, 28, and 29.

3.1 THE MINI-COMPUTER SYSTEMS

Data processing and the implementation of the identification algorithm were done on mini-computers. The work presented herein would not have been possible without the use of the modern mini-computer. The identification algorithm is essentially a digital algorithm which would cost too much to implement in analog form. This work is also not suitable for implementation on a large scale computer for economic reasons. The computational cost of doing this work on a large scale system would have been approximately 50 times what it cost to do the work on suitable mini-computers. Tasks that require relatively small amounts of memory, large numbers of computations and few peripherals, are perfect for mini-computers and wasteful for large-scale systems since the task charge will include the overhead on large amounts of memory, a much more expensive processor, and many peripherals that are not necessary for the implementation of the task. The minis also offer the user the chance to interact with his data much more frequently than a large-scale system would, thus offering great flexibility in implementation of data manipulation tasks and greater probability of early error detection.

Program development was carried out on a PDP-8 which has a 24 K memory, two disk drives, and a fast line printer. The PDP-8 can communicate with a PDP-12. The PDP-12 was used for data sampling of the analog tape and data reduction. The PDP-12 has an 8 K memory, two disk drives, two file oriented tape drives, analog-digital converters, a processor controlled scope with a 512x512 matrix, and a teletype. The reduced data were written on tape and taken to another PDP-12, which has a hardware floating point processor and a 32 K memory, to be analyzed by the identification algorithm. The results were then written on tape, taken back to the first

PDP-12, sent to the PDP-8 and printed on the line-printer.

3.2 THE DATA REDUCTION ALGORITHMS

There are three groups of data reduction programs. They are: 1.) sampling programs, 2.) calibration programs, and 3.) reduction programs. The sampling programs interface with the tape operations of Table 2 as shown in Table 5. Calibration and reduction programs are applied to the resulting data sets to produce normalized data sets suitable for the parameter identification algorithms (Table 5).

3.2.1 Sampling Programs

Three F. M. tape sampling programs were written. These are assembly language programs that are similar to each other in many respects. They are written in assembly language because the Fortran callable subroutines that initiate analog-digital conversion will not sample fast enough for these tests.

The PDP-12 analog digital converter is multiplexed to 16 input channels. Eight of the input channel voltage levels are controlled by potentiometers set by the user. The remaining 8 are available for analog data input. The PDP-12 control panel has 5 two-position sense switches which are controlled by the user. The states of these sense switches are program detectable and can therefore be used for branching purposes by the program.

The three sampling programs are called RESOL, ARBSM, and SRSLA. They form the basic link between the tape recorder data and preliminary digital data files. The three programs have two basic operating modes: 1.) sample and display, and 2.) sample and store.

The sample and display modes of the three programs are identical to one another. The sampling rate is controlled by the voltage level of one of the potentiometers. Two of the 6 data channels are sampled at a time. The digital values are scaled and then displayed on the PDP-12 scope. Two "zeroing lines which represent the middle of the channel input levels are displayed also. The D. C. output levels of the tape recorder can be adjusted so that the data signals are properly "zeroed" about the zeroing lines. Sense switches are used to choose between sets of 2 data channel displays. The sample and display mode allows the operator to make all necessary adjustment to the tape recorder output signals such as attenuation and D. C. level control so the the sample and store modes will collect the proper data.

Table 5

Data Reduction

	Tape Recorder Input from Table 2	Program Name	Output Data Structure	Program Name	Output Data Structure	Program Name	Output Data Structure	Program Name	Output Data Structure
Calibration	A-B	RESOL	digitized raw resolver data	CRSLT	normalized pitch and rotor resolver calibration tables				
	B,C	ARBSM	digitized raw voltage levels	BTESTV	flapping calibration numbers				
Test Reduction	D	ARBSM	digitized raw pre-transient data	AVBET1	1 per rev pre-transient single blade data tables and averages	AVBET2	1 per rev multi-blade pre-transient data tables and averages		
	E	SRSLA	digitized raw transient data	NORlDA	normalized (with calibration tables and numbers) single blade transient data			HVOMUL	normalized and zeroed multiblade transient data

The program RESOL is used exclusively for sampling resolver data for calibration purposes. RESOL is used on the taped data that lies between model manipulations A and B of Table 2. The user observes the output of tape channels 1 and 2 with RESOL's sample and display mode and moves directly to the sample and store mode by changing the state of a sense switch when he determines that the correct information is being displayed. The minimum possible time between a sample and store in memory on one channel and a sample and store on another channel is 20 microseconds. If the rotor velocity is 25 Hz , the rotor resolver signal is periodic with a period of 40,000 microseconds and the pitch resolver is periodic with 20,000 microseconds. Taking 360 samples/cycle of the rotor resolver (and therefore 180 samples/ cycle of the pitch resolver) yields 1 sample set every 111 microseconds. The rotor resolver sample and its respective pitch resolver sample are $.2^{c}$apart because of the time between samples. RESOL samples and stores the rotor resolver signal, then the pitch resolver signal, goes into an adjustable delay loop and repeats the process until 2047 samples of each signal are collected. After the sample and store is completed, the user can examine the sampled signal on the scope, by manipulating sense switches, to check signal integrity. If the data is satisfactory, the user directs RESOL to write the sample set onto an empty area of the disk in an integer formatted form.

The program ARBSM is used for calibration data and pretransient data (Table 5). The user can observe tape channels 1 and 2, 3 and 4, or 5 and 6 through sense switch manipulations. When all input channels are adjusted to the user's satisfaction, and when the proper portion of tape is being read, the user triggers the sample and store mode by pressing a sense switch. ARBSM sequentially samples all 6 data channels, stores the results, goes into a delay loop and repeats until 1024 samples of each data channel are collected. The sampling rate is set at 60 sets of samples/cycle for a rotor velocity of 25 cycles/sec. The angular difference between the first and last sample of each set of samples is less than 1^{o}. In the analysis programs, it is assumed that each set of samples is collected simultaneously. This introduces a .3% error into the algorithm which is negligible. After the data is collected, the user can display it on the scope to check its validity (i.e. look for missing data channels). If it is

acceptable it is written onto an empty area of the disk.

The program SRSLA works exactly as ARBSM except that when the user exits "sample and display" the program begins monitoring the pitch resolver data channel. When the signal level drops below 2 volts on this channel,"sample and store"is initiated. The abrupt signal level drop signifies the beginning of the transient excitation.

3.2.2 Calibration Programs

The calibration program BTESTV is used after ARBSM (Table 5). It reads the data left on the disk by ARBSM and computes the average value of the sample sets for each data channel. It also gives the standard deviation of these signals. BTESTV is used only on D. C. calibration signals that are used to define flapping measurement attenuations. The standard deviations are always quite small - on the order of .005 Volts - as compared to the difference between the two calibration signals recorded on every channel - on the order of 1. Volt.

The calibration program CRSLT is used after RESOL to create normalized pitch and rotor resolver tables (Tables 2 and 5). CRSLT reads the rotor resolver digitized data left on the disk by RESOL. The digitized waveform is approximately sinusoidal and is relatively noise free. As many of the 2047 available data points as possible should be used to create the most accurate table of signal amplitude versus azimuth angle. The program 'draws' an arbitrary line through the signal (Figure 12) of magnitude 0 (since the signal varies between -512 and 512). The signal is periodic with the number of

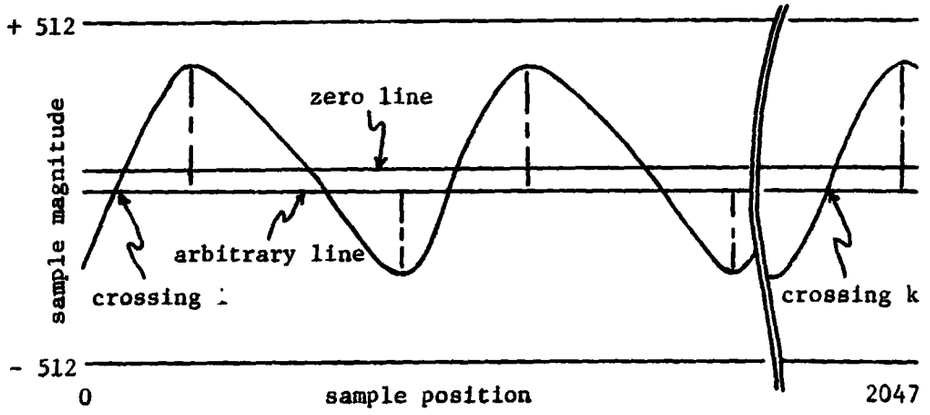

Figure 11 Resolver Normalization

sample positions between the first crossing and the last odd numbered crossing divided by 1/2 the number of crossings - 1. The signal is properly zeroed by averaging the maxima and minima (which are found by polynomial interpolation) between crossings and subtracting that number from every point in the data set. The new maxima and minima are used to locally normalize the signal between crossings so that the signal is normalized between ±1. A 180 point/360 degree table of resolver magnitude versus azimuth angle is produced by averaging the normalized signal magnitudes for each azimuth angle. Linear interpolation is used between data points. The resolver position is adjusted so that the zero azimuth angle occurs when the signal level is 0 with positive slope.

The program CRSLT treats the pitch resolver data exactly the same way as the rotor resolver data. The end products of CRSLT are, therefore, two 180 point/360 degree tables for both the rotor and pitch resolvers.

It is very important that the pitch resolver signal level versus pitch azimuth angle be independent of pitch azimuth angle velocity. This was verified, in the frequency range of the tests, by recording pitch resolver signals of different frequencies, creating the corresponding normalized pitch resolver tables for each frequency, and then comparing the tables. Table values of like azimuth angle were within 1% of each other over a frequency range of .1n to 1.5n.

3.2.3 Reduction Programs and Diagnostics

Each data set that is used for identification purposes is constructed by combining a pre-transient and the corresponding transient data sets for a test condition.

ARBSM is used to collect the pretransient data (Tables 2 and 5). AVBET1 produces normalized 60 point tables of each flapping signal magnitude versus azimuth angle as well as the average value of each signal from the pretransient data. The ARBSM sampling rate is approximately 60 points/rotor revolution or 1 sample every 6^{o}. There are 1024 samples or about 17 rotor revolutions of each data channel. Any one set of 60 points will not produce very accurate measurements of rotor azimuth angle or blade flapping magnitude. But since the waveforms are all periodic, the same sorts of data averaging techniques used to generate resolver calibration tables are used by

AVBET1 to generate pretransient single blade data tables. The correct azimuth angles and the periodicity are determined from the rotor resolver data. The 4 single blade flapping measurement data sets are first zeroed - to eliminate D. C. signal bias - using an average of each signal over the longest available interval in which the signal is periodic (these average values are also saved). The data sets are then averaged at each azimuth angle using linear interpolation between data points. For instance, at an azimuth angle of 36° the table value consists of the average of 17 numbers. These numbers are the result of linear interpolation between the two nearest data points to the 36°azimuth angle in each rotor revolution. Finally each table is normalized with the calibration numbers obtained with BTESTV.

AVBET1 takes the 4 single blade flapping tables and transforms them into 2 multiblade or forward and left tilt tables. Both the 4 single blade and 2 multiblade tables are then Fourier analysed at frequencies of 1, 2, 3, and 4 times the rotor velocity. The Fourier coefficients were used as a diagnostic to make sure all blades were operating under the same condition. For example if the absolute value of the first Fourier coefficient of one blade was very much different from the other 3 blades, then that blade probably had an incorrect collective pitch setting. If the differences were greater than 10% the test condition was thrown out. The absolute values the second Fourier coefficients were useful in diagnosing pre-lag and pre-cone setting errors (see Section 2.1.2).

SRSLA is used to collect the transient data (Tables 2 and 5) that appears on the tape directly after the pretransient data. NORIDA produces normalized pitch resolver azimuth angle measurements and the 4 single blade flapping angle measurements. Of the 6 data tracks only the rotor resolver signal is periodic. This signal is used to determine the number of data points per rotor revolution and the position of the first zero azimuth angle (the azimuth angle of any data point can be calculated using these two quantities) using the averaging techniques that were used to create the resolver calibration tables. The pitch resolver signal is zeroed and then normalized about local maxima and minima (Figure 13). The data values are then compared to the pitch resolver normalized amplitude versus pitch azimuth angle calibration table point by point and are converted into pitch azimuth

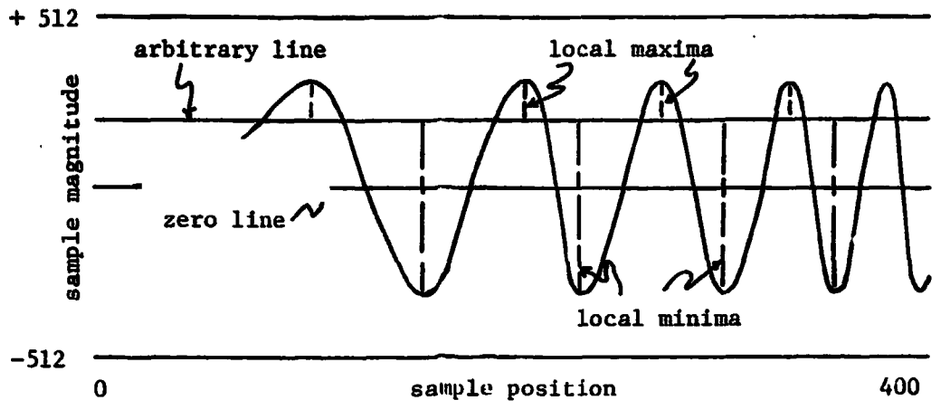

Figure 12 Transient Pitch Resolver Sample Window

angle measurements. The 4 single blade measurement sets are left unchanged by NORlDA.

HVOMUL uses the normalized pretransient data set and the data set created by NORlDA (Table 5) to create the data set used for identification purposes. The identification data set has 5 measurements:

1.) Number of points per cycle
2.) Point of first zero rotor azimuth angle
3.) Pitch azimuth angle
4.) Left tilt
5.) Forward tilt.

The data set has these properties:

1.) Measurements 3), 4), and 5) start with approximately zero value
2.) The tilts are normalized with the amplitude of the excitation eccentric.

The rationale for using these measurements with these properties is given in Chapter 5.

HVOMUL uses the averages of the pretransient single blade measurements to eliminate transient single blade D. C. signal measurement bias. This is possible since the actual signals are recorded only seconds apart (Table 2) which allows little time for instrumentation D. C. drift. The 4 single blade transient data sets are converted to the 2 multiblade measurements using the azimuth angle measurement from NORlDA. These multiblade measurements are 'zeroed' with the pretransient values of forward and left tilt (which are also the

initial conditions of the forward and left tilt for the transient tests). The pitch azimuth angle is 'zeroed' with the average of the first 10 samples of itself. This is possible because the transient starts about 40 samples into the data set.

4. ANALYTICAL TREATMENT OF THE HOVERING UNSTEADY ROTOR WAKE COUPLING

The model rotor is essentially infinitely stiff in the chordwise and torsional directions for the frequency range of pitching excitation that the model is subjected to (Table 2). Therefore only rotor flap-wake interactions need be analysed to predict the rotor model response. For a N bladed rotor operating at zero advance ratio, assuming straight blades flexibly hinged at the rotor center, the single blade equations of motion in a rotating reference system are, Reference 11,

$$\ddot{\beta}_k + A\dot{\beta}_k + \omega_1^2\beta_k = A\theta_k + A''\lambda_k \qquad k=1,\ldots,b \tag{4}$$

where $A=\frac{B^4\gamma}{8}$, A" is a function of the wake distribution over the radius, and λ_k is the generalized wake coordinate. The actual wake velocity is obtained by multiplying λ_k with the appropriate radial wake distribution.

At this point, no assumptions have been made as to the form or structure of the wake. The quantities $A''\lambda_k$ represent the sum of the effects of the wake on the flapping motions of the rotor. In Reference 11 it is established that the hub moments produced by the flapping restraining forces (inertia and spring forces) about the pitching and rolling axes through the rotor center are proportional to a first order expression of the generalized induced flow coordinate

$$\begin{aligned} v_I + \tau\dot{v}_I &= -L\{\sum_{k=1}^{b} (\ddot{\beta}_k + \omega_1^2\beta_k)\cos\psi_k\} \\ v_{II} + \tau\dot{v}_{II} &= -L\{\sum_{k=1}^{b} (\ddot{\beta}_k + \omega_1^2\beta_k)\sin\psi_k\} \end{aligned} \tag{5}$$

where L is the induced flow gain factor and τ the time constant describing the delayed build-up of the wake. v_I and v_{II} are the generalized multiblade induced flow coordinates and are hereafter referred to as the dynamic wake. Transforming the single blade variables to multiblade variables using the transformations (Reference 35)

$$\beta_k = + \beta_I \cos\psi_k + \beta_{II} \sin\psi_k$$

$$\theta_k = - \theta_I \sin\psi_k + \theta_{II} \cos\psi_k \qquad (6)$$

$$\nu_k = \nu_I \cos\psi_k + \nu_{II} \sin\psi_k$$

yields

$$\ddot{\beta}_I + A\dot{\beta}_I + (\omega_1^2 - 1)\beta_I + 2\dot{\beta}_{II} + A\beta_{II} = A(\theta_{II} + \nu_I) \qquad a)$$

$$-2\dot{\beta}_I - A\beta_I + \ddot{\beta}_{II} + A\dot{\beta}_{II} + (\omega_1^2 - 1)\beta_{II} = A(-\theta_I + \nu_{II}) \qquad b)$$

$$\nu_I + \tau\dot{\nu}_I = -L\{\ddot{\beta}_I + (\omega_1^2 - 1)\beta_I + 2\dot{\beta}_{II}\} \qquad c) \qquad (7)$$

$$\nu_{II} + \tau\dot{\nu}_{II} = -L\{\ddot{\beta}_{II} + (\omega_1^2 - 1)\beta_{II} + 2\dot{\beta}_I\} \qquad d)$$

if one assumes $\lambda_k = \nu_k$, that the dynamic wake is the only part of the wake that is important to flapping dynamics. Rearranging (7) yields multiblade equations in state variable form $\dot{x}=Cx+Bu$, that is

$$\begin{bmatrix} \dot{\beta}_I \\ \ddot{\beta}_I \\ \dot{\beta}_{II} \\ \ddot{\beta}_{II} \\ \dot{\nu}_I \\ \dot{\nu}_{II} \end{bmatrix} = \begin{bmatrix} 0 & 1 & 0 & 0 & 0 & 0 \\ -P2 & -A & -A & -2 & A & 0 \\ 0 & 0 & 0 & 1 & 0 & 0 \\ A & 2 & -P2 & -A & 0 & A \\ 0 & L^* & L^* & 0 & -\tau^* & 0 \\ -L^* & 0 & 0 & L^* & 0 & -\tau^* \end{bmatrix} \begin{bmatrix} \beta_I \\ \dot{\beta}_I \\ \beta_{II} \\ \dot{\beta}_{II} \\ \nu_I \\ \nu_{II} \end{bmatrix} + \begin{bmatrix} 0 & 0 \\ 0 & A \\ 0 & 0 \\ -A & 0 \\ 0 & -L^* \\ L^* & 0 \end{bmatrix} \begin{bmatrix} \theta_I \\ \theta_{II} \end{bmatrix} \qquad (8)$$

where $P2=(\omega_1^2-1)$, $L^*=\frac{AL}{\tau}$, $\tau^* = \frac{1+AL}{\tau}$.

No assumptions have been made as to the numerical values of L and τ, which define the dynamic wake. Only a mathematical framework for their use has been provided. Given this framework and a proper set of experiments, the parameter identification algorithm developed in Section 5 can be used to find numerical values of L and τ for the rotor upon which the experiments were conducted. This mathematical framework has one very interesting feature. If the rotor is excited at a constant frequency $\omega = (\omega_1^2-1)$ in pitch, then as can be seen in (5), there can be no dynamic wake (ν_I and ν_{II} are 0). This feature of the mathematical model can be easily checked, at least qualitatively, by performing a simple experiment with the model rotor.

ω = 1.2

Downwash

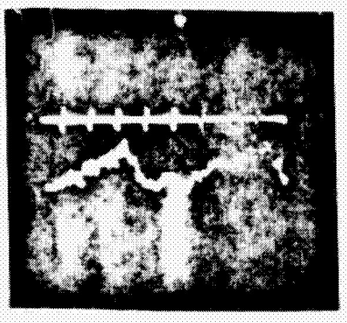

ω_1 = 1.33

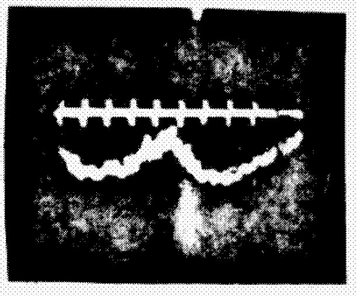

ω_1 = 1.265

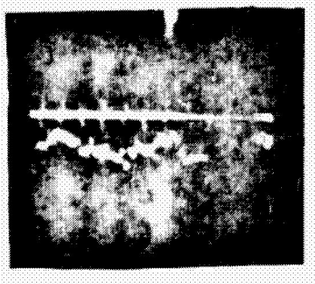

ω_1 = 1.224

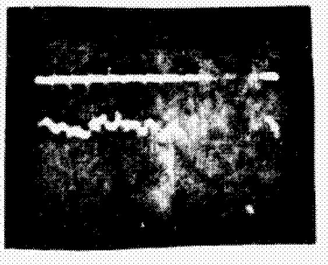

ω_1 = 1.195

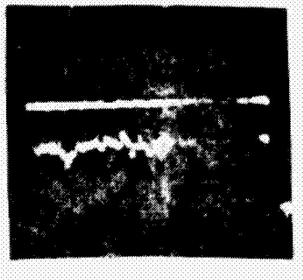

ω_1 = 1.167

Figure 13 Downwash Response with Harmonic Excitation versus ω_1

A hot wire probe was placed at the .82R blade station .2R below the rotor. The rotor was excited with a pitch stirring frequency of $\omega = 1.2$ or $\omega = .2$. The rotor speed was varied from low to high rpm so that ω_1 varied from 1.35 to 1.1. At $\omega_1 = 1.20$, the dynamic wake should disappear. Figure 12 presents a series of oscilloscope photographs of the hot wire output versus ω_1. In the upper trace, each vertical mark represents one rotor revolution. The lower trace is the hot wire measurement of the wake. The "dynamic" part of the wake, if it exists, should be periodic with 5 rotor revolutions. The photographs show that there is indeed a wake component periodic with 5 rotor revolutions that goes toward 0 as ω_1 goes to 1.2. Thus the mathematical framework is promising in that it predicts a measured wake phenomena.

Some interesting variations on and modifications of this mathematical framework are now considered. Rotor drag should induce a flow in the direction of rotor rotation, therefore creating feedback between ν_I and ν_{II}. Thus the right hand sides of equations (7), c) and d) become

$$\begin{matrix} \tau\dot{\nu}_I + \nu_I + H\nu_{II} \\ \tau\dot{\nu}_{II} + \nu_{II} - H\nu_{II} \end{matrix} \qquad (9)$$

Elements 5,6 and 6,5 of the C matrix in equation (8) become $H' = \frac{H}{\tau}$ and $-H'$ respectively.

A logical extension of the time delayed induced flow is to add an acceleration term. The right hand sides of (7), c) and d) become

$$\begin{matrix} T_1^2\ddot{\nu}_I + T_2\dot{\nu}_I + \nu_I \\ T_1^2\ddot{\nu}_{II} + T_2\dot{\nu}_{II} + \nu_{II} \end{matrix} \qquad (10)$$

In state variable form this model becomes

$$\begin{bmatrix} \dot{\beta}_I \\ \ddot{\beta}_I \\ \dot{\beta}_{II} \\ \ddot{\beta}_{II} \\ \dot{\nu}_I \\ \ddot{\nu}_I \\ \dot{\nu}_{II} \\ \ddot{\nu}_{II} \end{bmatrix} = \begin{bmatrix} 0 & 1 & 0 & 0 & 0 & 0 & 0 & 0 \\ -P2 & -A & -A & -2 & A & 0 & 0 & 0 \\ 0 & 0 & 0 & 1 & 0 & 0 & 0 & 0 \\ A & 2 & -P2 & -A' & 0 & 0 & A & 0 \\ 0 & 0 & 0 & 0 & 0 & 1 & 0 & 0 \\ 0 & L' & L' & 0 & -T' & -T & 0 & 0 \\ 0 & 0 & 0 & 0 & 0 & 0 & 0 & 1 \\ L' & 0 & 0 & L' & 0 & 0 & -T' & -T \end{bmatrix} \begin{bmatrix} \beta_I \\ \dot{\beta}_I \\ \beta_{II} \\ \dot{\beta}_{II} \\ \nu_I \\ \dot{\nu}_I \\ \nu_{II} \\ \dot{\nu}_{II} \end{bmatrix} + \begin{bmatrix} 0 & 0 \\ 0 & A \\ 0 & 0 \\ -A & 0 \\ 0 & 0 \\ 0 & -L' \\ 0 & 0 \\ L' & 0 \end{bmatrix} \begin{bmatrix} \theta_I \\ \theta_{II} \end{bmatrix} \qquad (11)$$

where $T = \frac{T_2}{T_1}$, $T' = \frac{1+LA}{T_1^2}$, and $L' = \frac{LA}{T_1^2}$.

If one assumes that the wake gain factor L is adequate for modeling purposes, that $\tau = 0$, equation (8) reduces to

$$\begin{bmatrix} \dot{\beta}_I \\ \ddot{\beta}_I \\ \dot{\beta}_{II} \\ \ddot{\beta}_{II} \end{bmatrix} = \begin{bmatrix} 0 & 1 & 0 & 0 \\ -P2 & -A' & -A' & -2 \\ 0 & 0 & 0 & 1 \\ A' & 2 & -P2 & -A' \end{bmatrix} \begin{bmatrix} \beta_I \\ \dot{\beta}_I \\ \beta_{II} \\ \dot{\beta}_{II} \end{bmatrix} + \begin{bmatrix} 0 & 0 \\ 0 & A' \\ 0 & 0 \\ -A' & 0 \end{bmatrix} \begin{bmatrix} \theta_I \\ \theta_{II} \end{bmatrix} \qquad (12)$$

where $A' = \frac{A}{1+AL}$. A' is similar to the Curtis and Shupe γ^*, 22. This is a quasi-steady wake model where the wake instantly responds to rotor motions.

Equations (12), (8), and (11), in order of increasing complexity, represent three possible mathematical frameworks for treating dynamic rotor wake coupling. They are, respectively, quasisteady, first order unsteady, and second order unsteady treatments of the wake. Equation (9) introduced an interesting variation on (8). The applicability of each of these constructions can be easily studied and compared using the experiments described in Section 2 and the parameter identification algorithm developed in Section 5.

A simple momentum theory of dynamic rotor induced flow is presented in Reference 18. It is based on the assumption that the axial induced flow is uniform over the disk and that the harmonic induced flow given in Equation (5) varies linearly with the radial distance from the rotor center. The air mass participating in the angular pitching and rolling motion is determined from potential flow theory for a solid circular disk. Under these assumptions and under the further assumption of small linear perturbations about trim one obtains for zero advance ratio the following expressions for L and τ:

$$L = a\sigma/(2\gamma\,\bar{v}_o) \quad , \quad \tau = .113/\,\bar{v}_o \qquad (13)$$

Instead of L, Reference 18 gives the factor of the rotor moment coefficients as $1/\bar{v}_o$, while Equation (8) is written in terms of blade moments divided by the blade moment of inertia, M_b/I. To obtain the rotor moment coefficient one must multiply M_b/I by $I(b/2)/\rho\pi R^5$. With $I = a\rho cR^4/\gamma$ and $\sigma = bc/\pi R$ this factor becomes $a\sigma/2\gamma$ and the expression

for L in Equation (13) follows. With $a = 5.6$, $\sigma = .154$, $\gamma = 3.8$ we have $a\sigma/2\gamma = .113$. Thus, according to the theory

$$L = \tau = .113/\bar{\nu}_o \tag{14}$$

Theoretical values of $\bar{\nu}_o$ can be calculated from blade element momentum theory. The experiments were conducted in the vicinity of the ground so the momentum theory must include the effect of the ground on the induced inflow. There are two conflicting methods of doing this. A theory that includes the ground height effect on induced flow for constant circulation (twisted) rotors is described in Reference 36. The theory conflicts with the results of a comprehensive set of tests which measured the hovering performance of various helicopters as a function of ground height. This set of tests is described in Reference 37.

A is a function of the tip loss factor B (Reference 32). B decreases with increasing collective pitch and/or induced inflow. Therefore A can be expected to decrease with increasing collective pitch.

5. DEVELOPMENT OF THE IDENTIFICATION ALGORITHM

The proposed perturbation models of Section 4 have from 6 to 8 state variables and from 4 to 6 parameters. The identification method chosen had to be able to identify all parameters from the transient cyclic pitch stirring tests so that no theoretical assumptions beyond the form of the equations need be made. Only 2 state variables were measured, the left and forward flap-bending deflections. Therefore only two of the 6 to 8 state variables are directly related to the measurements. Thus the identification method must not only identify the parameters, but must also estimate the remaining non-measured state variables, the flapping rates and inflow states. In other words, the method must identify the main system parameters P and A and the feedback parameters without measuring a feedback signal and without measuring half of the main system state variables. In control system engineering this would be considered a formidable task that is solved here by application of the proper identification algorithm to the problem along with some rather stringent requirements on the type and duration of the input transient.

There are many parameter identification methods available in the literature. Extensive simulation work was done to pick out the best method for identifying the parameter models described in Section 4 before the experiments were performed. This simulation work is described in Refer ces 38 and 39. The best method was found to be a modification of the complete maximum likelihood identification algorithm described in Reference 40.

The complete maximum likelihood identification algorithm can be used to identify system parameters in the presence of both process and measurement noise. In order to apply the complete maximum identification algorithm a "likelihood function" has to be maximized subject to several non-linear constra.nt equations (Reference 40). This is a formidable task. The likelihood function can be maximized using a Newton-Raphson iterative technique if one assumes that the best state estimate covariances are constant throughout the data set and that the Kalman filter gain is also constant throughout the data set. If one further assumes that there is no process noise, then the Kalman filter gain is zero and the filtering

equations reduce to the system equations. The following identification algorithm is based on the foregoing assumptions.

5.1 THEORETICAL FORMULATION

The iterative method developed assumes system and measurement equations in the form

$$\dot{x} = f(x,u,\theta) + w \tag{15}$$

$$y = h(x) + v \tag{16}$$

where x is the state vector, u the input vector, θ the parameter vector, w the process noise vector, y the measurement vector, and v the measurement noise vector. The parameter vector θ is estimated in such a way that the criteria function or cost function

$$J(\theta) = (1/2)\sum_{j=1}^{N} \nu_j^T B^{-1} \nu_j \quad \rightarrow \quad \text{minimum} \tag{17}$$

where

$$\nu_j = y_j - h(\hat{x}_j) \tag{18}$$

Here ν_j is called the innovation vector at time j (see Reference 40), $\hat{x}_j$ is the best estimate of the state at time j, N is the number of measurements, and B is the measurement equation error covariance matrix and was updated before proceeding from the k to the k+1 iteration by

$$B_{k+1} = (1/N) \sum_{j=1}^{N} (y-h_k(\hat{x}))_j \, (y-h_k(\hat{x}))_j^T. \tag{19}$$

B in this form is a direct measure of the modeling error of the k^{th} iteration and it is convenient to think of B as the "modeling error." In the complete method B is a function of j.

The cost function (17) was minimized using what is called quasi-linearization with the modified Newton-Raphson method (see Reference 40). This method makes use of the information or sensitivity matrix, M, where

$$M \equiv \partial^2 J / \partial \theta^2 . \tag{20}$$

M^{-1} gives the Cramer-Rao lower bound for the parameter covariances and has a very special importance that will be demonstrated later on. The problem is to find a zero of the gradient of the cost function $\partial J/\partial\theta = 0$. Taking the truncated two term Taylor series expansion of the gradient about the value of θ in the k^{th} iteration,

$$(\partial J/\partial\theta)_{k+1} = (\partial J/\partial\theta)_k + (\partial^2 J/\partial\theta^2)_k \, \Delta\theta_{k+1} = 0 \qquad (21)$$

one obtains with Equation (20) the parameter update increment to be used for the k+1 iteration

$$\theta_{k+1} = \theta_k + \Delta\theta_{k+1}, \qquad \Delta\theta_{k+1} = -M_k^{-1}(\partial J/\partial\theta)_k \qquad (22)$$

In order to obtain the parameter update $\Delta\theta_{k+1}$ one needs the first and second partials of $J(\theta)$,

$$\partial J/\partial\theta = \sum_{j=1}^{N} (\partial\nu/\partial\theta)_j^T \, B^{-1} \, \nu_j \qquad (23)$$

$$M = \partial^2 J/\partial\theta^2 = \sum_{j=1}^{N} (\partial\nu/\partial\theta)_j^T \, B^{-1} \, (\partial\nu/\partial\theta)_j \qquad (24)$$

where higher order partials of ν_j are neglected (quasi-linearization). Computationally, this means that ν_j and $\partial\nu_j/\partial\theta$ are required. ν is obtained from (18) where $\hat{x}$ is obtained from solving the system equation

$$\dot{\hat{x}} = f(\hat{x},\hat{\theta},u) \qquad (25)$$

and $\hat{\theta}$ is the best estimate of the parameters from the previous iteration. Now

$$\partial\nu/\partial\theta = -\partial h/\partial x\big|_{x=\hat{x}} \, \partial\hat{x}/\partial\theta \qquad (26)$$

where $\partial\hat{x}/\partial\theta$ is obtained from solving the sensitivity equations

$$\partial\dot{\hat{x}}/\partial\theta = \partial f/\partial\theta + \partial f/\partial x\big|_{x=\hat{x}} \, \partial\hat{x}/\partial\theta \qquad (27)$$

The initial conditions for $\partial\hat{x}/\partial\theta$ are zero except when x(0) is identified as part of the parameters θ. In this case the initial partials have the value one.

A closer look at (24) and (26) will show that M is not a function of the innovation sequence but is only a function of the theoretical model and the input u weighted with the "modeling error" B from the previous iteration. The diagonal terms of the inverted sensitivity matrix M^{-1} are theoretically a lower bound for estimates of the parameter errors. As the theoretical model approaches a true representation of the experimental model the diagonal terms become a better and better lower bound.

So computationally what is required is:

1) Make reasonable initial estimates of parameter values and B_1.
2) Solve simultaneously system and sensitivity equations.
3) Compute the innovation sequence, $\partial J/\partial \theta$, M, and B_{k+1}.
4) Invert M and calculate parameter iteration.
5) Use updated parameters in step 1).
6) Repeat the process until the parameters converge.

5.2 PRACTICAL CONSIDERATIONS

The above theoretical formulation of the identification algorithm must be properly implemented. Tools that assure the proper application of this algorithm to data sets must be developed. These tools must show the user that the algorithm is doing its job of identifying parameters and that the identification process is working properly.

Convergence of parameters with successive parameter iterations is the most obvious place to start when comparing parameter identification methods and when determining which inputs excite the model sufficiently to identify parameters. If parameter values fail to converge then either the method is at fault or the input is insufficient.

The square root of the average of the "modeling error" or B matrix diagonal

$$RR = \sqrt{(B_{11} + B_{22}) / 2} \tag{28}$$

hereafter called the "fit factor", is a convenient direct measure of how well the theoretical model fits the experimental data set.

Determining the "best" input function for identifying parameters is the most difficult task that faces the experimenter who wishes to use parameter identification methods. Several works on "optimal" input design have been written (References 40 and 41). The experimenter usually does not have the luxury of being able to use a theoretically optimal input in his experiment because of practical considerations such as physical limitations on his model. But, the experimenter can usually devise several different kinds of inputs with which to excite his experimental model. Therefore, he needs methods of comparing the results obtained with various inputs. The experimenter also has to choose how much of a data set to use in the identification process. If he does not use enough data his identification algorithm might not converge. Or worse, the theoretical parameters might be

relatively insensitive to the input function up to that point so that even if the parameter iterations converge, the cost function is locally flat in the area of the identified parameter and a wide range of parameter values would give approximately the same fit between experiment and theory. If he uses data beyond the point where the experiment is generating new information that is relevant to the theoretical model, then he is using excessive processing time and is taking the risk of biasing his parameter estimates with irrelevant information.

Convergence and fit factors can be used to compare parameter identification methods, theoretical models, and inputs, but these two tools by themselves are inadequate for answering all the experimenter's questions with regard to his data and models. A third tool that the experimenter might use that can answer his questions involves computation of the cost criteria, J, as a function of parameter value and data length. This involves excessive computation but can be used as a last resort.

The proper use of M^{-1} is the tool the experimenter needs to answer his questions about the relative value of input functions and how much data from his data sets he needs to use. The use of M^{-1} for determining proper data length is described in References 38 and 42. M^{-1} is a monotonically decreasing function with time (or data length) and is a function of the theoretical model and the experimental input weighted by a constant (the modeling error matrix); see Equation (24), Section 5.1. The experimental input "drives" the value of M^{-1} toward zero. Inputs can be compared by observing how fast they drive M^{-1} toward zero and ultimately by how near M^{-1} gets to zero. If an element of M^{-1} is flat in a particular section of the data, then the algorithm is not making use of the information in that section of data to improve the estimate of the parameter associated with that element of M^{-1}. If there is a particular data length where all the elements of M^{-1} are flat and remain flat for the rest of the available data length, then no further information is gained by using data past that particular data length. This establishes a clearly defined limit on how much data one has to analyse to identify a particular theoretical model. Frequently in early simulation and experimental work insufficient amounts of data

were used for parameter identification and the unsatisfactory results were misinterpreted. The time history of M^{-1} provides a tool for avoiding this pitfall.

Caution should be used when applying the M^{-1} criteria. The "criteria" is only as good as the theoretical model. It "approaches" reality only as the theoretical model "approaches" a true model of the experiment. It should only be used after the parameters have converged to a constant value and therefore offer the best model that the theoretical framework can supply.

Convergence, fit factor, and M^{-1} studies form a powerful set of tools for using the parameter identification algorithm. These three tools are applied intensively to the data sets that were generated in the experiments described in Chapter 2.

Verification of the identified model is accomplished by seeing how well the model response predicts experimental responses not used for identification purposes.

5.3 IMPLEMENTATION OF THE ALGORITHM

Blindly implementing the theoretical algorithm as stated in Section 5.1 would lead to an unnecessarily long and complicated computer program. Careful consideration during implementation can greatly simplify the resulting program and even improve the information content of the program output to the user.

The algorithm was implemented using Fortran IV in 16 K of core memory of the 32 K PDP-12 described in Section 3.1. The program is in Appendix 9.2. The prime consideration in implementing the algorithm was to use as little core memory as possible so that the program could be run on as many machines as possible. The secondary consideration was to minimize the number of computations in the algorithm.

5.3.1 Measurements

The physical measurements taken are (Section 2.2.2) the blade flapping angles in the rotating coordinate system β_1, β_2, β_3, and β_4. The related state variables are the blade flapping angles in the fixed coordinate system, β_I and β_{II}. The true measurement equations are then (Equation (16), Section 5.1)

$$\beta_{k_m} = \beta_I \cos\psi_k + \beta_{II} \sin\psi_k \qquad \text{for } k=1,2,3,4 \qquad (29)$$

Instead of using (29) as the measurement equation, the coordinate transformation

$$\beta_{I_m} = ((\beta_{1_m} - \beta_{3_m})*\cos\psi - (\beta_{2_m} - \beta_{4_m})*\sin\psi) / 2$$
$$\beta_{II_m} = ((\beta_{1_m} - \beta_{3_m})*\sin\psi + (\beta_{2_m} - \beta_{4_m})*\cos\psi) / 2 \quad (30)$$

which is the inverse of (6), was performed during the preprocessing of the data sets (Section 3.2.3) so that the measurement equation becomes

$$\beta_{I_m} = \beta_I + v_1$$
$$\beta_{II_m} = \beta_{II} + v_2 \quad (31)$$

This is done without loss of information.

Using (31) as the measurement equation cuts the measurement storage requirements in half since there are only half as many multiblade measurements as single blade measurements. Each data set consists of approximately 400 measurement vectors. Each number consumes 3 words of storage. Therefore, using multiblade measurement vectors saves 1.6 K of storage. If (29) were used as the measurement equation then the best estimates of β_I and β_{II} from the system equation would have to be translated by (29) into best estimates of the β_k's for each iteration. Using (31) as the measurement equation eliminates this transformation for each iteration. Thus using (31) as the measurement equation saves storage and saves computations.

5.3.2 Choice of Parameters

The parameters that have direct physical significance appear in Equation (7) as (ω_1^2-1), A, L, and τ. When (7) is written in the state variable form, (8), the physically significant parameters become lumped into the groupings (ω_1^2-1) = P2, A, $L^* = AL/\tau$, and $\tau^* = (1+AL)/\tau$. The parameter identification literature (Reference 40) recommends that lumped parameters be used in the identification algorithm. All simulation work was performed identifying lumped parameters (References 38 and 39). Initially the algorithm applied to real data sets was programmed to identify the lumped parameters. However it was found that by identifying the physically significant parameters the algorithm converged more rapidly than lumped parameter identification for real data sets. For example see Table 6. Identifying physical parameters requires using about 10 percent more

Table 6

Parameter Choice Method Studies

Iteration	A	L	τ	$\bar{\beta}_I$	$\bar{\beta}_{II}$	$\beta_I(0)$	$\beta_{II}(0)$	$\nu_I(0)$	$\nu_{II}(0)$	RR
I Physical Parameters plus bias, steady pitch stirring trim										
0	.450	6.0	8.0	.0	.0					.079
1	.283	2.0	4.5	-.05	-.01					.037
2	.303	2.6	6.4	-.05	-.02					.034
3	.307	2.6	6.2	-.05	-.02					.034
4	.307	2.6	6.2	-.05	-.02					.034
5	.307	2.6	6.2	-.05	-.02					
II Lumped Parameters plus bias										
0	.450	6.0	8.0	.0	.0					.079
1	.281	2.0	5.6	-.05	-.02					.038
2	.302	2.7	6.6	-.05	-.02					.036
3	.307	2.6	6.2	-.05	-.02					.034
4	.307	2.6	6.2	-.05	-.02					.034
5	.307	2.6	6.2	-.05	-.02					
III Physical Parameters plus bias and initial conditions, θ_o trim										
0	.450	6.0	8.0	.0	.0	-.19	.33	.0	.0	.092
1	.282	1.2	3.2	.01	.02	-.19	.31	.33	-.23	.039
2	.293	2.3	5.8	.00	.03	-.18	.31	.42	-.33	.028
3	.302	2.4	5.3	.00	.03	-.18	.30	.51	-.34	.027
4	.300	2.4	5.8	.00	.03	-.18	.30	.48	-.35	.027
5	.302	2.4	5.7	.00	.03	-.18	.30	.49	-.35	

Test Condition: $\theta_o = 9.3^o$, h/R = 1.28

Computer Time (PDP-12 with FPP)

	per iteration	iterations required for complete convergence	total time required
I	1. minute	3	3. minutes
II	1. minute	4	4. minutes
III	3. minutes	≃7	21. minutes

terms in the sensitivity equations than identifying lumped parameters, but it can save 1 to 2 iterations. Therefore if it takes 5 iterations for the lumped parameter method to converge, it will take only 3 or 4 iterations for the physical parameter method to converge, using 70 to 90 percent of the computer time of the lumped parameter method. The great advantage that identifying physical parameters over lumped parameters has is that the M^{-1} matrix has direct physical significance with respect to the physical parameters. The elements of M^{-1} can be used to directly determine the relative importance of the physical parameters to the theoretical model for a particular input.

5.3.3 Sensitivity Equations and Matrix

The identification algorithm requires the solution of one sensitivity equation, (27), of the same order as the state equation for each parameter identified. For instance, using the model of equation (8) and identifying the parameter L yields the sensitivity equation (32):

$$\frac{\partial}{\partial L}\begin{bmatrix}\dot{\beta}_I\\ \ddot{\beta}_I\\ \dot{\beta}_{II}\\ \ddot{\beta}_{II}\\ \dot{\nu}_I\\ \dot{\nu}_{II}\end{bmatrix} = \begin{bmatrix}0 & 1 & 0 & 0 & 0 & 0\\ -P2 & -A & -A & -2 & A & 0\\ 0 & 0 & 0 & 1 & 0 & 0\\ A & 2 & -P2 & -A & 0 & A\\ 0 & L^* & L^* & 0 & -\tau^* & 0\\ -L^* & 0 & 0 & L^* & 0 & -\tau^*\end{bmatrix}\frac{\partial}{\partial L}\begin{bmatrix}\beta_I\\ \dot{\beta}_I\\ \beta_{II}\\ \dot{\beta}_{II}\\ \nu_I\\ \nu_{II}\end{bmatrix} + \begin{bmatrix}0 & 0 & 0 & 0 & 0 & 0 & 0 & 0\\ 0 & 0 & 0 & 0 & 0 & 0 & 0 & 0\\ 0 & 0 & 0 & 0 & 0 & 0 & 0 & 0\\ 0 & 0 & 0 & 0 & 0 & 0 & 0 & 0\\ 0 & A/\tau & A/\tau & 0 & -A/\tau & 0 & 0 & -A/\tau\\ -A/\tau & 0 & 0 & A/\tau & 0 & -A/\tau & A/\tau & 0\end{bmatrix}\begin{bmatrix}\beta_I\\ \dot{\beta}_I\\ \beta_{II}\\ \dot{\beta}_{II}\\ \nu_I\\ \nu_{II}\\ \theta_I\\ \theta_{II}\end{bmatrix} \quad (32)$$

The 6x6 matrix of (32) is identical to the 6x6 matrix of Equation (8). The sensitivity equation (32) has the same form as the system equation (8), with a new forcing function, which is $\partial f/\partial x|_{x=\bar{x}}\partial\hat{x}/\partial L$ or the second part of (32). All of the sensitivity equations are of this form, which makes them very easy to program. Using a DO loop, the system equation can be used once for the

system equation, once for each parameter to be identified, and then the forcing function terms can be added outside the DO loop at each time step. This greatly reduces programming time.

In order to perform the parameter iteration the sums of Equations (23) and (24) must be calculated and M must be inverted. If one calculates these sums and then does the inversion at the end of each iteration, then one needs to store values equal to the length of the data set used times the dimension of the measurement vector times 1 plus the number of parameters identified. For example if one uses all 400 measurement vectors in the typical data set and identifies 4 parameters then 400 x 2 x (1+4) = 4000 values must be stored, which requires 12 K words of computer storage. Instead of calculating these sums at the end of each iteration, partial sums were calculated after each 15 time steps (or data vectors), thus reducing the storage requirement to 15 x 2 x (1+4) = 150 values or .45 K words. By inverting the sum of the partial sums which make up M after each 15 time steps one can readily obtain the time history of M^{-1} which one wants on certain occasions for diagnostic purposes (Section 5.2). This capability is incorporated into the program and can be switched on or off at will.

5.3.4 Initial Conditions

When not all state variables are measurable, as is the case here, the identification of the initial state vector in addition to the system parameters is usually required. The model presented in Equation (8) has 6 initial states and 4 system parameters. Therefore if initial conditions must be identified, 10 sensitivity equations are required.

The transient excitations are designed so that up to t=0, θ_I and θ_{II} are in a steady-state condition, Equations (2) and (3). Therefore the multiblade coordinates of the models must have reached a steady state condition, so the initial conditions of rates $\dot{\beta}_I(0)$ and $\dot{\beta}_{II}(0)$ of (8) must be zero. This eliminates 2 initial condition parameter identifications and leads to 4 sensitivity equations for initial condition parameters.

The fact that both inputs (θ_I and θ_{II}) and non-rate states (β_I, β_{II}, ν_I, and ν_{II}) are in steady state at t=0 can be used to eliminate the rest of the initial condition parameters. One simply

"perturbs" the model about the steady state condition. The new measurements are then the difference between their old measured value and their pre-transient, or equivalently their t=0, value ($\beta_{I_m} = \beta_{I_{m_t}} - \beta_{I_{m_{pt}}}(0)$, $\beta_{II_m} = \beta_{II_{m_t}} - \beta_{II_{m_{pt}}}(0)$). This requires subtracting a constant vector from every measurement vector in the data set. This procedure is described in Section 3.2.3. The new inputs become the difference between their old measured value and their pre-transient, or equivalently their t=0, value ($\theta_I = \theta_{I_t} - \theta_{I_{pt}}(0)$, $\theta_{II} = \theta_{II_t} - \theta_{II_{pt}}(0)$). When the measurements and inputs are written in this way, all inputs up to t=0 are zero, therefore all of the perturbation model states up to t=0 are also zero. Now all states have zero initial conditions and no initial condition parameters need be identified. Table 6 presents a comparison of the parameters identified from a typical data set both with and without initial condition identification where the appropriate forms of the input and measurement were used in both cases. There are no essential differences between the results.

Careful design of the input transients reduced the number of potential parameters in Equation (8) from 10 to 8. Careful selection of the form of the measurement vector and input vector further reduced the potential parameters from 8 to 4. Potential computer time was more than halved and the complexity of the problem was greatly reduced.

5.3.5 Measurement Bias

A measurement bias is an arbitrary constant value present in every measurement of the data set. The bias can be considered to be a parameter and can be identified using the identification algorithm. There are at least two ways of including measurement bias in the algorithm.

In the method found in most parameter identification literature, the bias is handled in the system equations. New state variables are defined for the measured states. For example one would make the substitutions

$$\begin{aligned} \beta_{I_{old}} &= \beta_{I_{new}} + \bar{\beta}_I \\ \beta_{II_{old}} &= \beta_{II_{new}} + \bar{\beta}_{II} \end{aligned} \tag{33}$$

in Equation (8). The equation would remain the same except for the new terms

$$+ \begin{bmatrix} 0 & -P2 & 0 & A & 0 & -L^* \\ 0 & -A & 0 & -P2 & L^* & 0 \end{bmatrix}^T \begin{bmatrix} \bar{\beta}_I \\ \bar{\beta}_{II} \end{bmatrix} \tag{34}$$

which would have to be added to the right hand side. The bias $\bar{\beta}_I$ and $\bar{\beta}_{II}$ appear explicitly in the system equation. The cost function remains the same. Writing that cost function using slightly different notation than (17) gives

$$J(\theta) = \tfrac{1}{2} ||\beta_m - \hat{\beta}_{new}||_B \tag{35}$$

where β_m is the measured state vector and $\hat{\beta}_{new}$ the best estimate of that measured state vector. The bias appears implicitly in the cost function, therefore finding $\partial J/\partial \bar{\beta}_I$ and $\partial J/\partial \bar{\beta}_{II}$ requires solving two more sensitivity equations. In general, one must solve a new sensitivity equation of the order of the state equation for each bias identified using this method.

There is no reason not to consider bias explicitly in the cost function, which then becomes

$$J(\theta) = \tfrac{1}{2} ||\beta_m - \hat{\beta}_{old} - \bar{\beta}||_B \tag{36}$$

where $\bar{\beta}$ is the bias vector. Since the bias only appears explicitly, $\partial J/\partial \bar{\beta}_I$ and $\partial J/\partial \bar{\beta}_{II}$ are just $-(\beta_{I_m} - \hat{\beta}_I)$ and $-(\beta_{II_m} - \hat{\beta}_{II})$ which are already available. Thus no sensitivity equations need be solved in order to identify bias. Indeed the quantities one needs to compute to identify bias have already been computed.

The two methods are mathematically identical, but the second is computationally much more efficient.

5.4 PROGRAM DESCRIPTION

A partial listing of the program used to identify the parameters of the model described by Equation (8) is in Appendix 9.2. The program will not be described in great detail here because it is internally documented.

The differential equations were solved forward in time using a modification of a standard 4th order Runga-Kutta subroutine from the IBM Scientific Subroutine Package. The modification was the elimination of the provision for halving the time interval of

integration in the event of a computed order of error becoming larger than a user specified limit. Previous experience has shown that the program almost never made use of the interval halving procedure. Elimination of this procedure reduced the subroutine size by one third.

The matrices were inverted using a standard matrix inversion subroutine (MINV) from the IBM Scientific Subroutine Package.

6. RESULTS AND DISCUSSION

The harmonic test results are presented in Section 6.1. Data length studies, which show how much data has to be used for proper parameter identification, are presented in Section 6.2. Identified parameters are presented in Section 6.3. In Section 6.4 prediction studies that show how well, or poorly, the identified models predict transient response tests are presented. There are also some prediction results presented in Section 6.1 which show how identified models predict frequency response tests. Those predictions presented in Section 6.1 are discussed in Section 6.4. Figures are presented at the end of each section.

6.1 HARMONIC TESTS

The complete set of the harmonic test (Table 4) results, conducted as described in Section 2.3.1, are presented in Reference 34. Sample results of the wake measurements made with a hot wire anemometer for the $\theta_o=5^o$ and $\omega_1=1.17$ case are presented in Figures 14a, b, c and d.

Figures 14a and b present two views of the measurements of the time average of the rotor downwash velocity, $\bar{W}$. In Figure 14a $\bar{W}$ is plotted versus pitch stirring excitation frequency at different radial positions. This plot shows that the average wake is largely independent of the pitch stirring frequency of excitation. The $\theta_o=2^o$ $\bar{W}$ data(Referency 34) shows slightly less frequency dependence. $\bar{W}$ versus radial position at different pitch stirring excitation frequencies is plotted in Figure 14b. The maximum value of $\bar{W}$ always occurs at approximately r/R = .8. Since the wake below a rotor rapidly contracts and since the measurements were taken .12R below the rotor this is a reasonable result.

The $\bar{W}$ data at the three collective pitch settings were averaged over frequency at each radial position. A mean wake velocity at each θ_o was determined by an r weighted average of the frequency averaged radial measurement values. These values are presented in Table 7 where the results are given in units of radians.

Table 7

Average Inflow at h/R = 1.28

θ_o	$\bar{v}_{0\ \text{measured}}$	$\bar{v}_{036}$	$\bar{v}_{037}$	L = τ
2°	.016	.014	.019	7.0
5°	.022	.029	.040	5.1
8°	.033	.040	.057	3.4

Theoretical values of induced inflow were calculated as a function of radius and θ_o using blade element momentum theory at h/R = ∞. The theoretical mean wake velocity at each θ_o was determined by an r weighted average of the theoretical radial wake velocities. Two methods of accounting for the effect of ground on the average induced inflow were used. Reference 32 used the results of Reference 36 to compute plots of h/R and blade radial position versus the reduction of induced inflow for a constant circulation rotor (Section 4). The reduction factor at r = .7R was used to calculate the values $\bar{v}_{036}$ shown in Table 7 from the theoretical values of average inflow at h/R = ∞. Reference 37 derived an empirical formula from tests for computing the reduction of average inflow from h/R (Section 4). This reduction factor was used to calculate the values $\bar{v}_{037}$ shown in Table 7. The L = τ values in Table 7 were calculated with Equation 14 using the $\bar{v}_{0\ \text{measured}}$ values. Since the $\bar{v}_{036}$ values agree better with the tests than the $\bar{v}_{037}$ values, theoretical values of L and τ from (14) were calculated using $\bar{v}_{036}$ values and are presented in Section 6.3.

Figures 14c and d present two views of the measurements of the absolute value of the first Fourier coefficient with respect to the pitch stirring frequency $|F_{1\omega}|_W$ to be highly dependent on pitch stirring frequency. $|F_{1\omega}|_W$ versus radial position at different excitation frequencies is plotted in Figure 14b. The curves consistently peak at approximately r/R = .8.

The dynamic induced flow for a pitch stirring frequency of ω = .933 from Figure 14d is plotted in Figure 15. A linear radial distribution assumption is not well satisfied. Straight line distributions that produce the same hub moment as the experimental distributions were calculated at all pitch stirring frequencies. The straight line in Figure 15 is the equivalent radial dynamic induced flow for the

plotted experimental induced flow. These values are plotted in Figures 16, 17, and 18 for θ_o = 2, 5, and 8 degrees.

Also plotted in Figures 16, 17, and 18 are the experimental frequency flapping responses. The theoretical curves are from the two parameter identification test results described in Section 6.3.

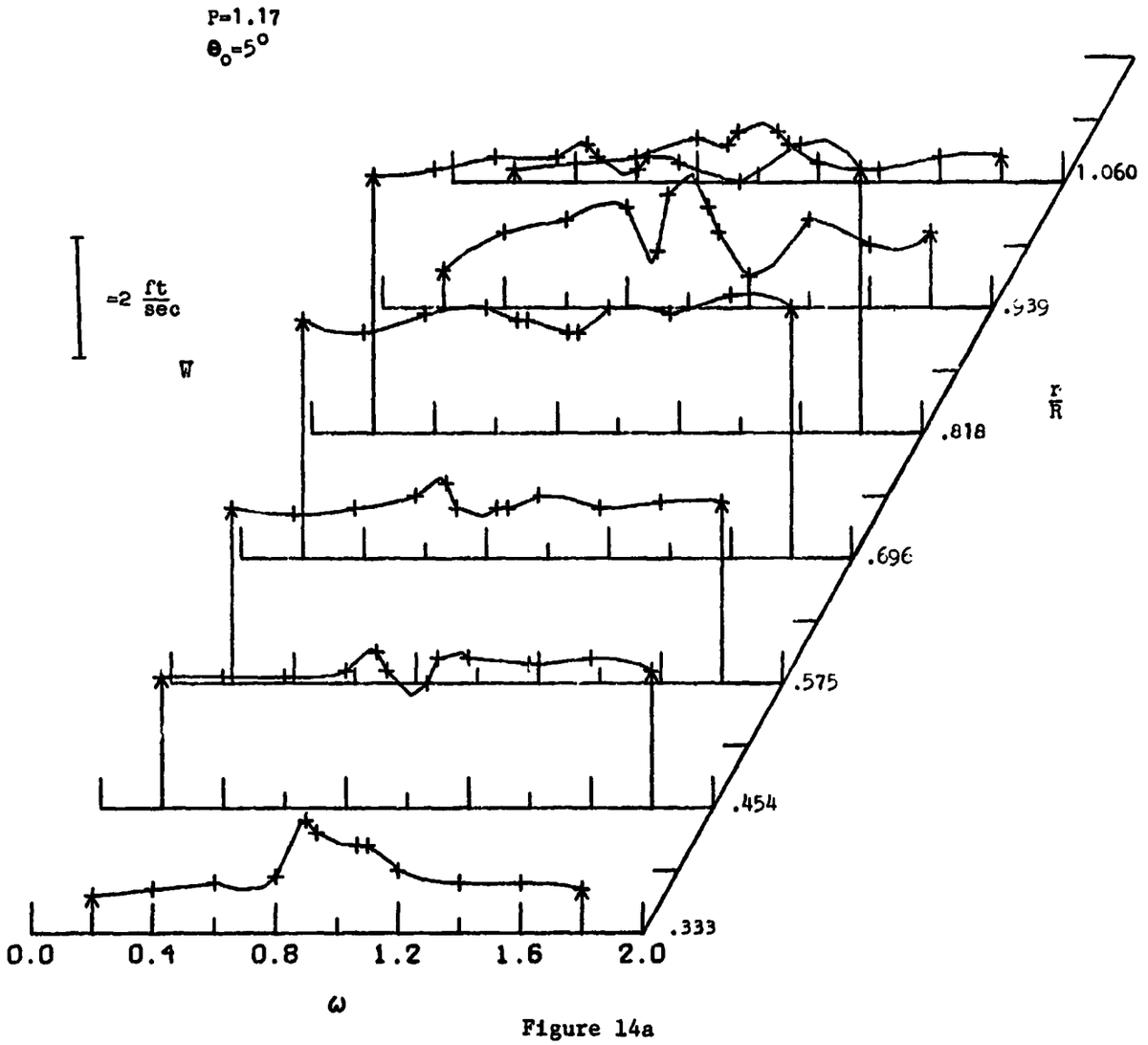

Figure 14a

Figure 14 $\theta_o = 5^o$, $\omega_1 = 1.17$ Harmonic Test Downwash Measurements

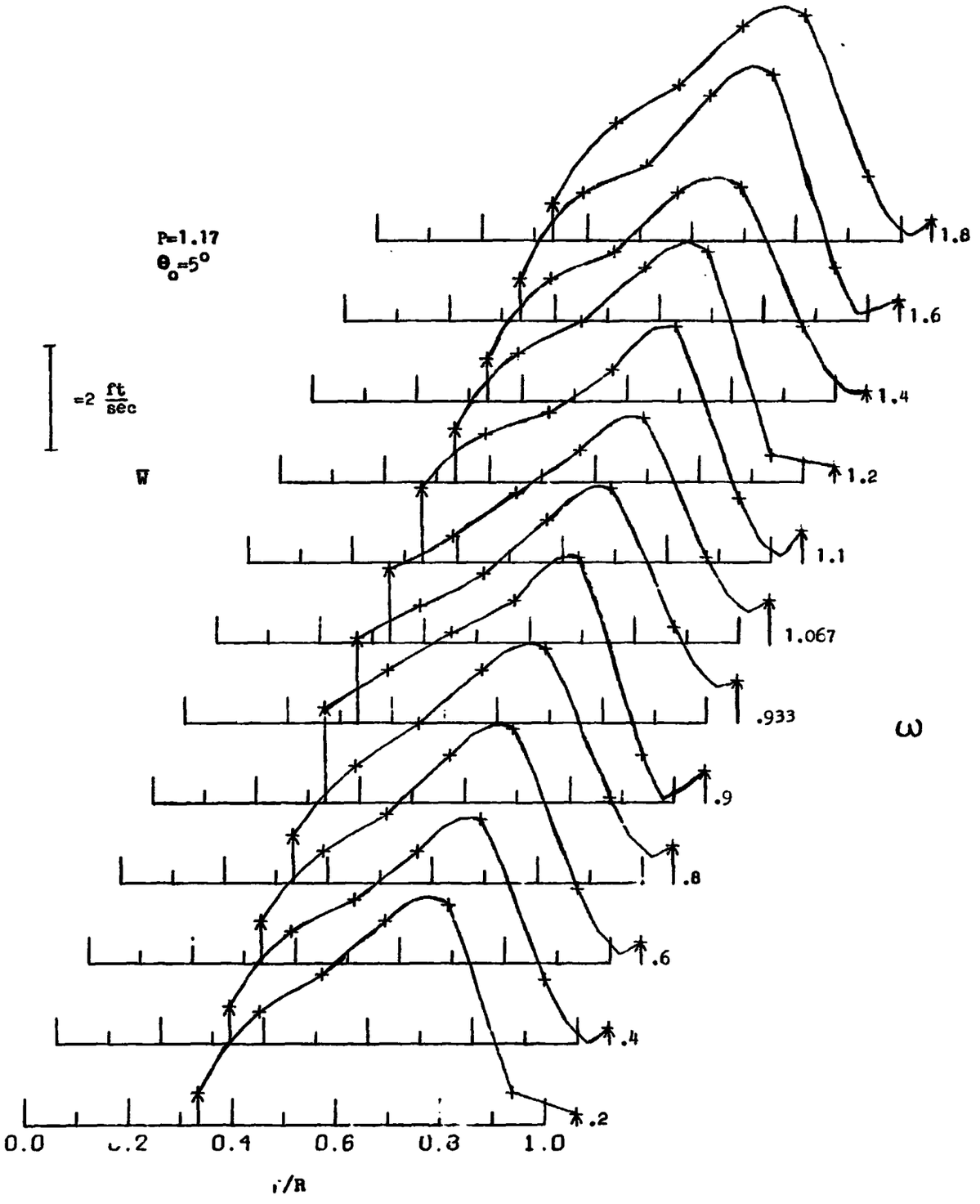
P=1.17
θ_o=5°
=2 ft/sec
W
ω
1.8
1.6
1.4
1.2
1.1
1.067
.933
.9
.8
.6
.4
.2
0.0
0.2
0.4
0.6
0.8
1.0
r/R

Figure 14b

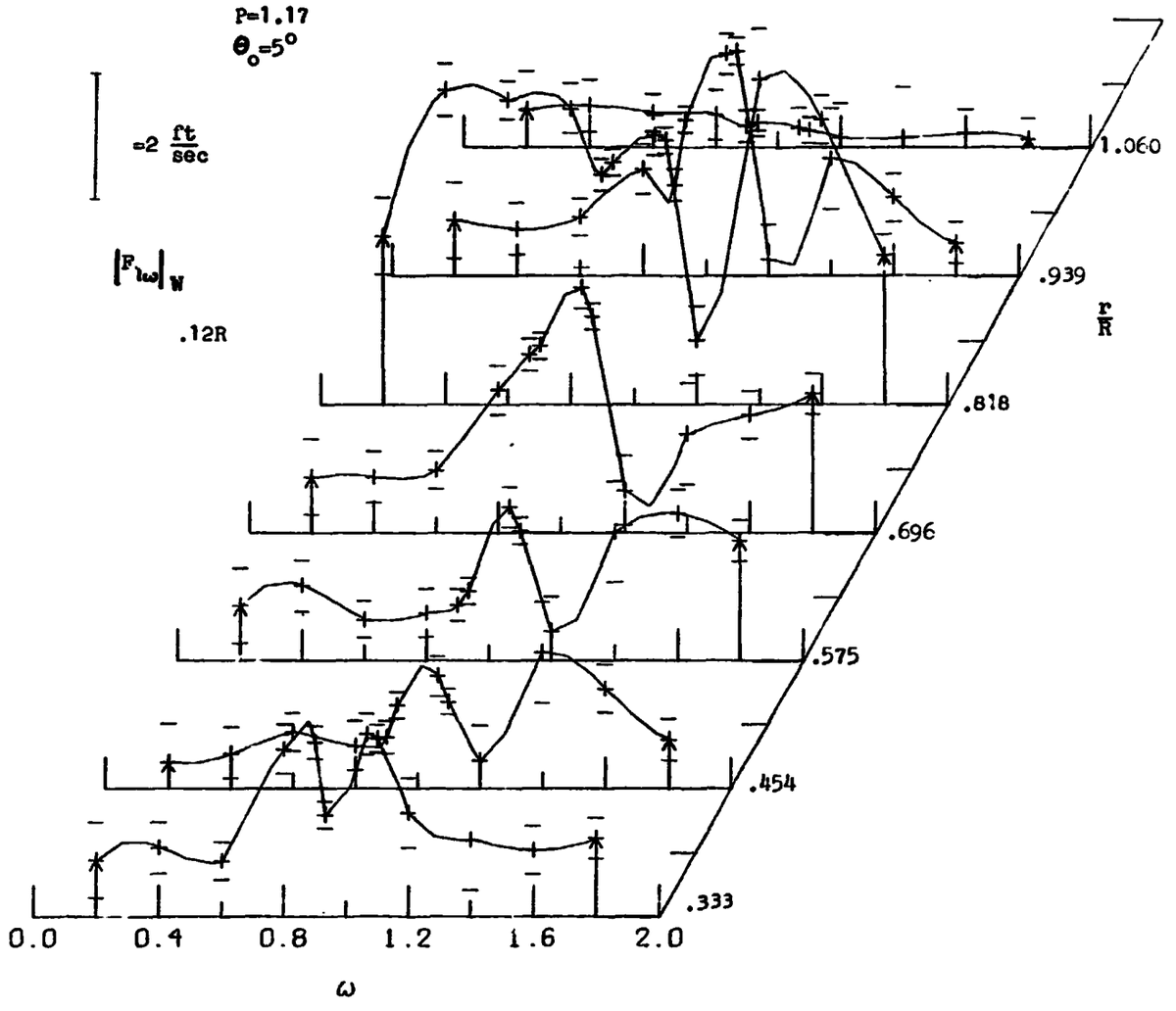
P=1.17
θ_o=5°
=2 ft/sec
$|F_{1\omega}|_W$
.12R
1.060
.939
.818
.696
.575
.454
.333
r/R
0.0
0.4
0.8
1.2
1.6
2.0
ω

Figure 14c

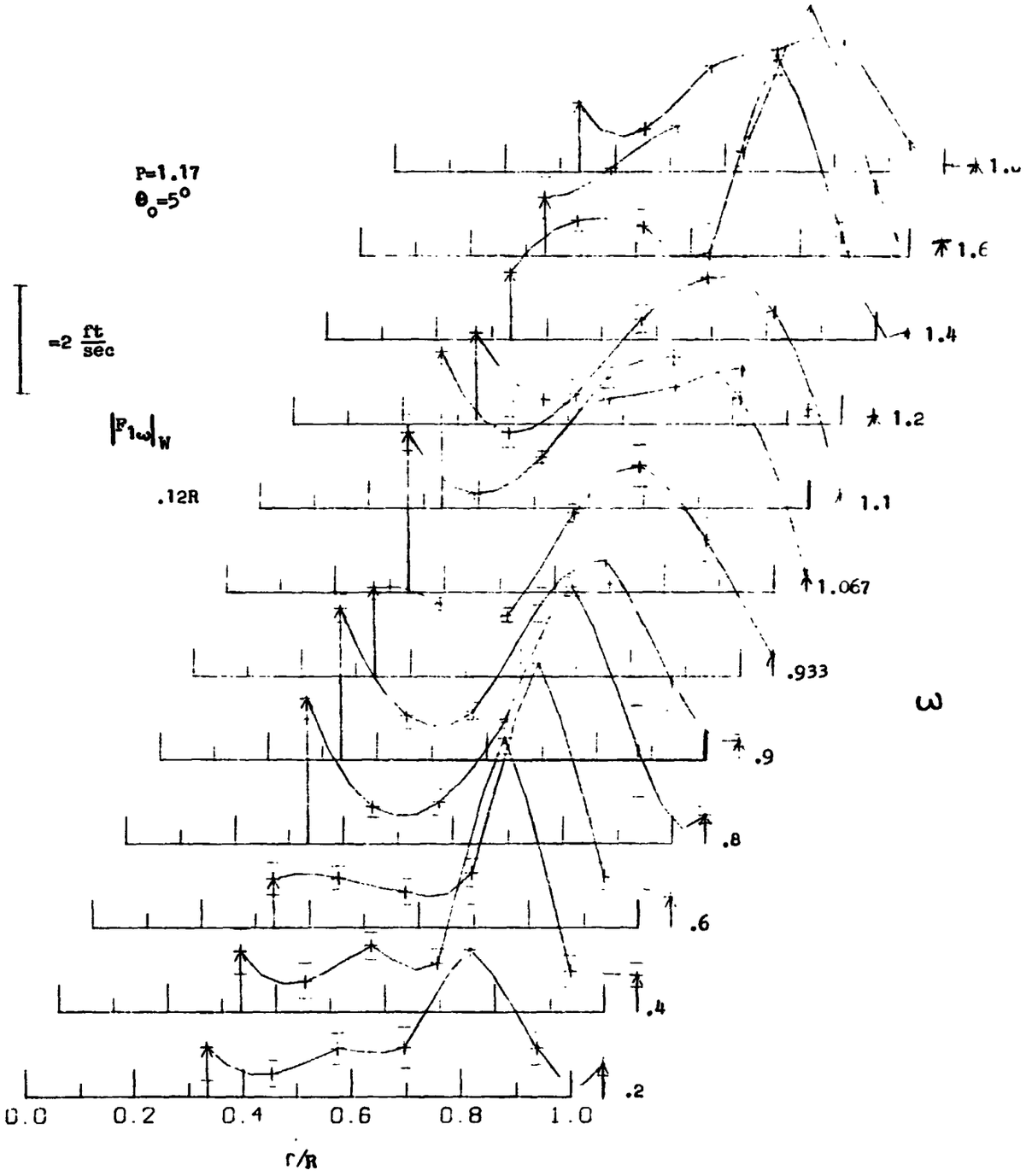
P=1.17
θ_0=5°
=2 ft/sec
$|F_{1\omega}|_W$
.12R
1.6
1.4
1.2
1.1
1.067
.933
.9
.8
.6
.4
.2
ω
0.0
0.2
0.4
0.6
0.8
1.0
r/R

Figure 14d

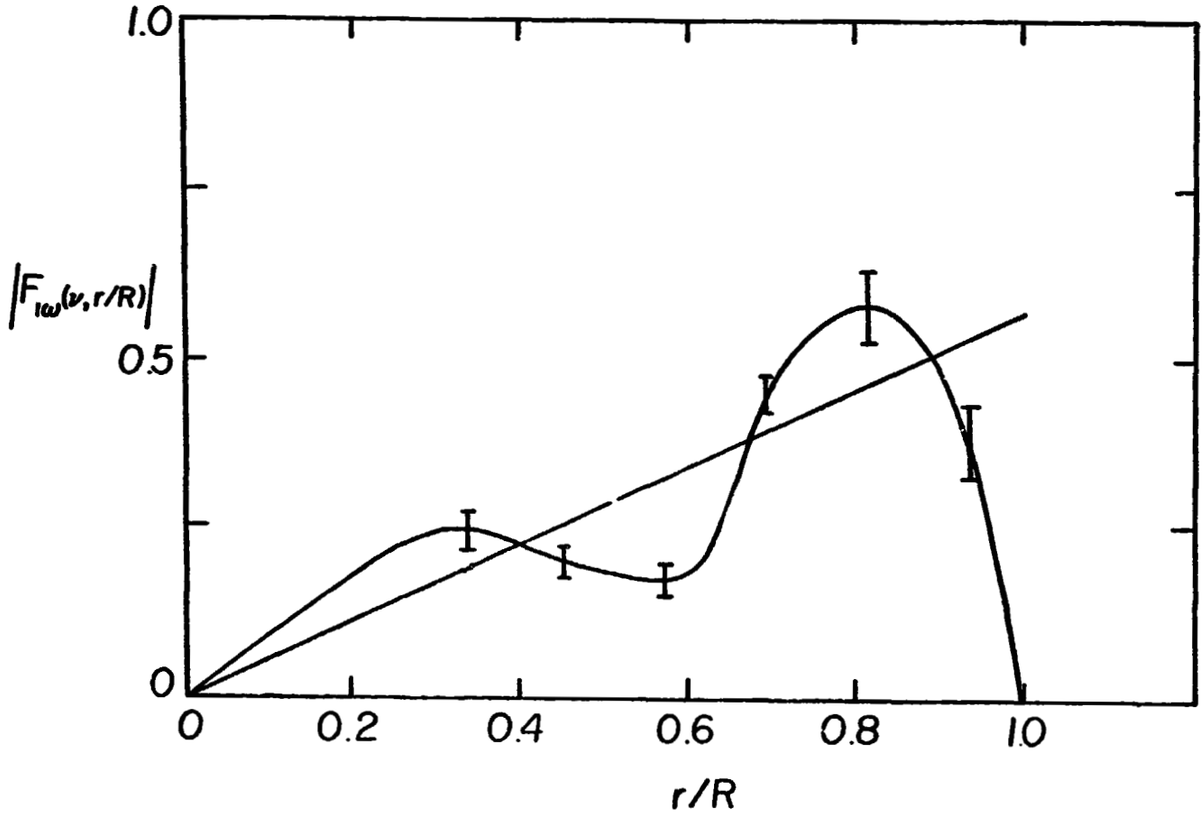

Figure 15 $\theta_o = 5^o$, $\omega_1 = 1.17$, $\omega = .933$ Equivelent Linear Dynamic Downwash

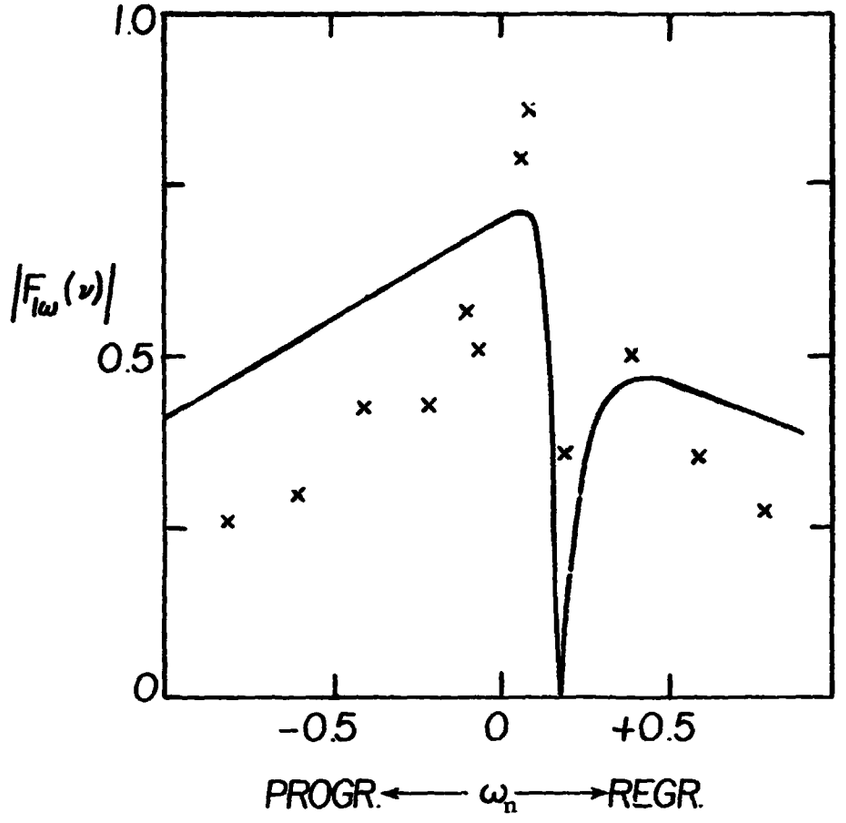

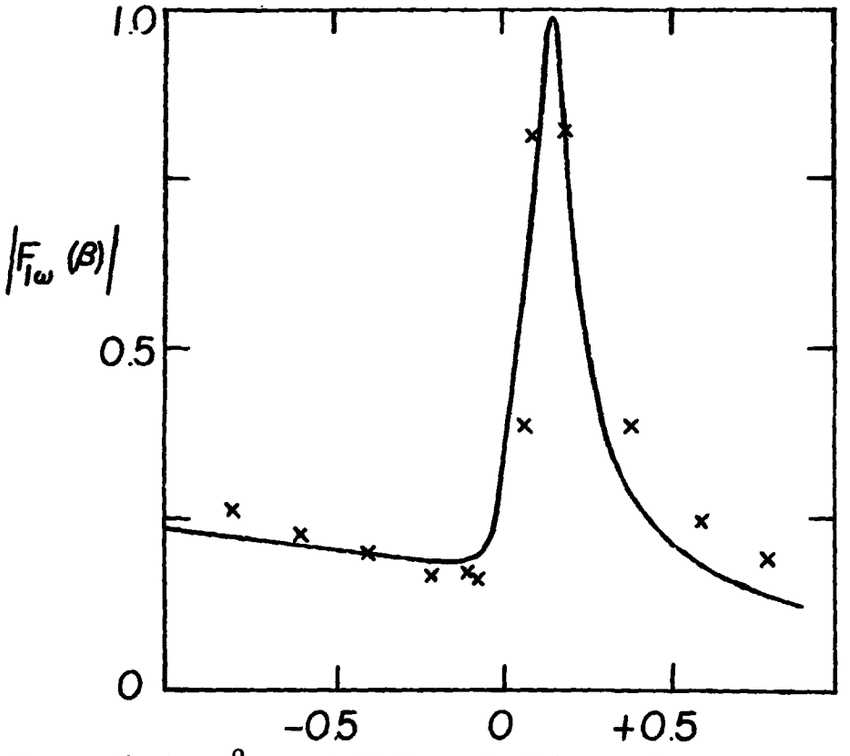

Figure 16 $\theta_o = 2^o$, $\omega_1 = 1.17$ Harmonic Stirring Test

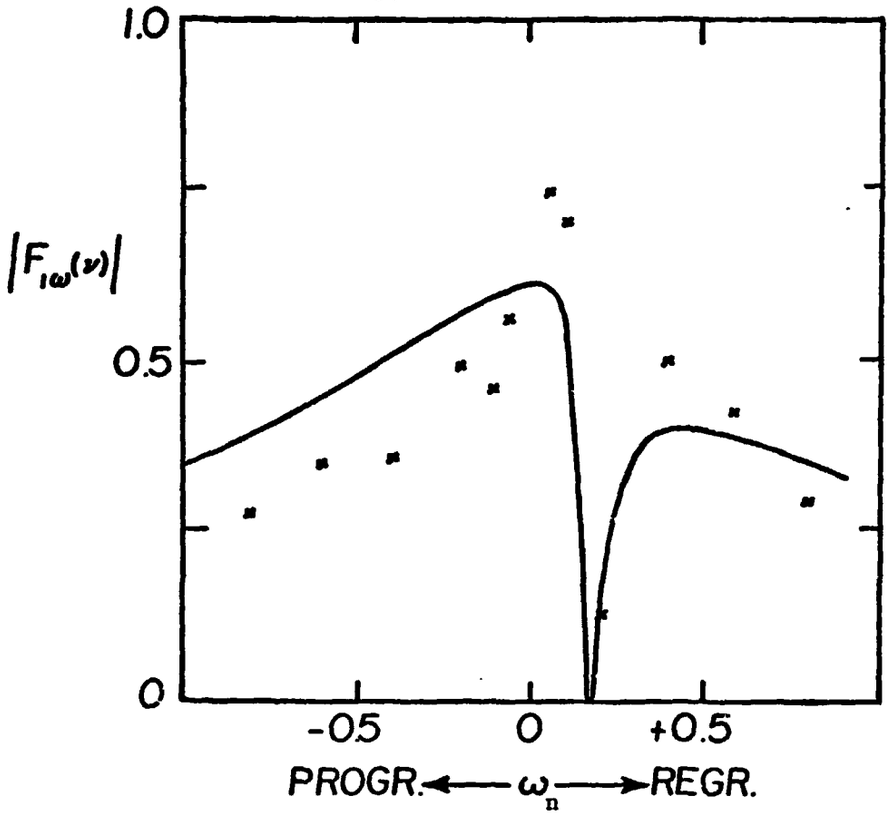

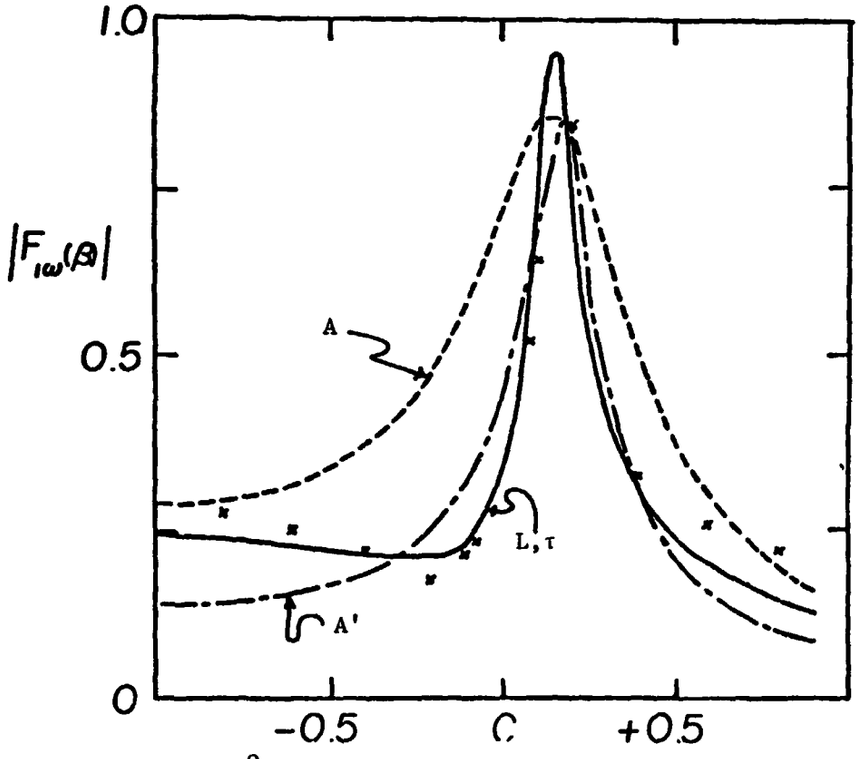

Figure 17 $\theta_o = 5^o$, $\omega_1 = 1.17$ Harmonic Stirring Test

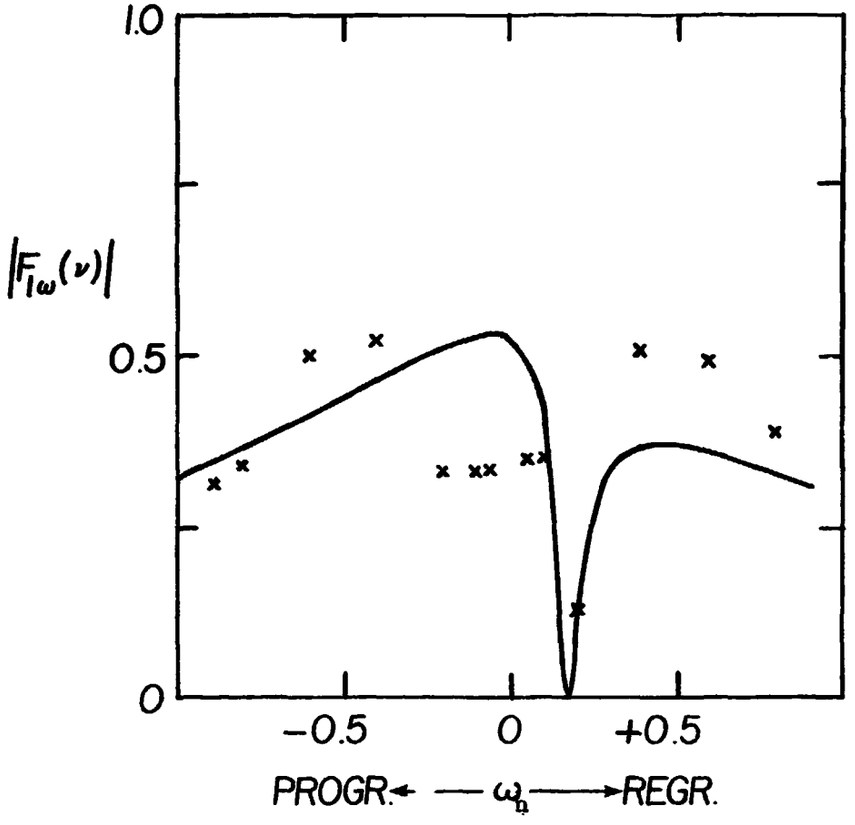

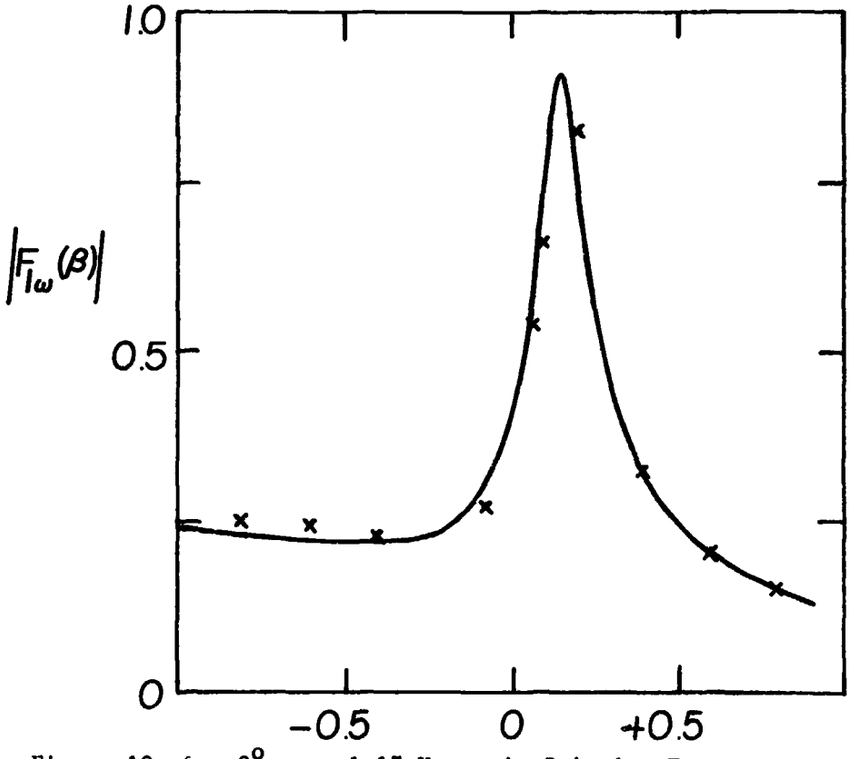

Figure 18 $\theta_o = 8^o$, $\omega_1 = 1.17$ Harmonic Stirring Test

6.2 DATA LENGTH STUDIES

Most of our early failures in developing the parameter identification methods were due to using insufficient data lengths. Therefore considerable effort was devoted toward determining how much data should be used to identify selected numbers of parameters for different models. Data length studies were made of an arbitrarily chosen test condition ($\theta_o = 5^o$, $\omega_1 = 1.18$, $h/R = 1.02$) for several different models.

Two different data length studies were made for each model. The first consisted of finding the shortest data length to give parameter convergence and then identifying the parameters using increasing amounts of data to the end of the data set. The interval of data length was approximately .25 rotor revolutions. This produced plots of parameters identified versus data length. This direct study was compared with the method of optimal data utilization developed in Reference 42, which was built into the identification algorithm (Section 5). The whole data length was used to identify the parameters. On the iteration following parameter convergence the program inverts M every 15 time steps (Section 5.3.3), thus the M^{-1} data length study is a by-product of the identification process.

The results of the data length studies for the quasisteady wake model (12) are presented in Figure 19. A' does not converge to a constant value with data length nor does $(M^{-1})^{\frac{1}{2}}$ level off with increasing data length. Thus no particular data length is optimal for identifying A'. The reason for this is related to the fact that the A' model has basic limitations, see Figures 17 and 27. An arbitrary data length of 9.0π was used in identifying the A' quasisteady wake model.

The results of a 2 parameter (L, τ) data length study of the unsteady wake model, which contains 4 parameters (P2, A, L, τ) are presented in Figure 20. P2 = .3924, the structural parameter, is assumed known. A = .385 comes from blade element momentum theory. After $t = 10\pi$ both the square root of the diagonals of M^{-1} and the identified parameter values have reached a steady state condition. Both studies produce the same optimal data length. A data length of 10π is used in identifying the L and τ first order unsteady wake model.

The results of a 3 parameter (A, L, τ) data length study of the unsteady wake model are presented in Figure 21. Although A is identified as .385, the same as the specified value of A in the

2 parameter model, it takes at least 12π for the parameter values and the square roots of the diagonal terms of M^{-1} to reach steady-state values. A data length of 12π is used in identifying A, L, and τ.

The results of the 4 parameter (P2, A, L, τ) data length studies are presented in Figure 22. Neither the parameter values nor the square roots of the diagonals of M^{-1} reach steady state by the end of the data set, although they are apparently very close to doing so. The identified value of P2 is .38 which is very close to its true value .39. The four parameter unsteady wake model was not identified except for the one collective pitch presented in Figure 22.

Figures 20, 21, and 22 show that as the number of identified parameters is increased for a particular model, longer data lengths must be used to identify the model. They also show that both data length studies produce approximately the same result. Since the M^{-1} study is on the order of 15 times less time consuming than the identified parameter data length study, it is to be preferred over the identified parameter study.

From Figure 27 one may suspect that the reason for the improvement in the identified parameters when using data beyond $\psi = 8\pi$ is that the input becomes more like a constant amplitude oscillation. However, as can be seen from Figure 30, a short input transient results in a response that extends over 8π beyond the end of the input. As discussed later identification from this short input transient using a data length of 10π, yielded almost the same parameters as the input shown in Figure 22.

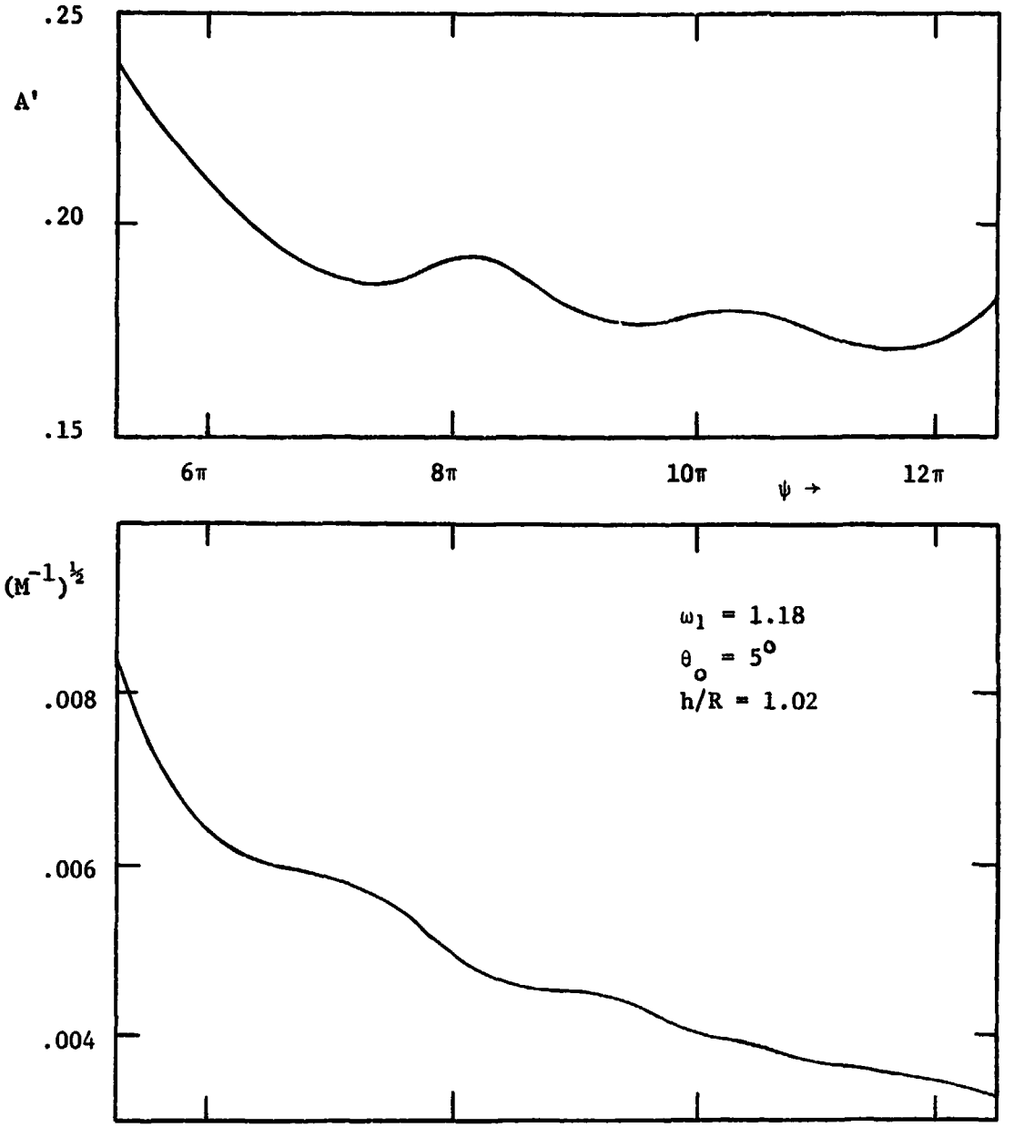

Figure 19 A' Data Length Study

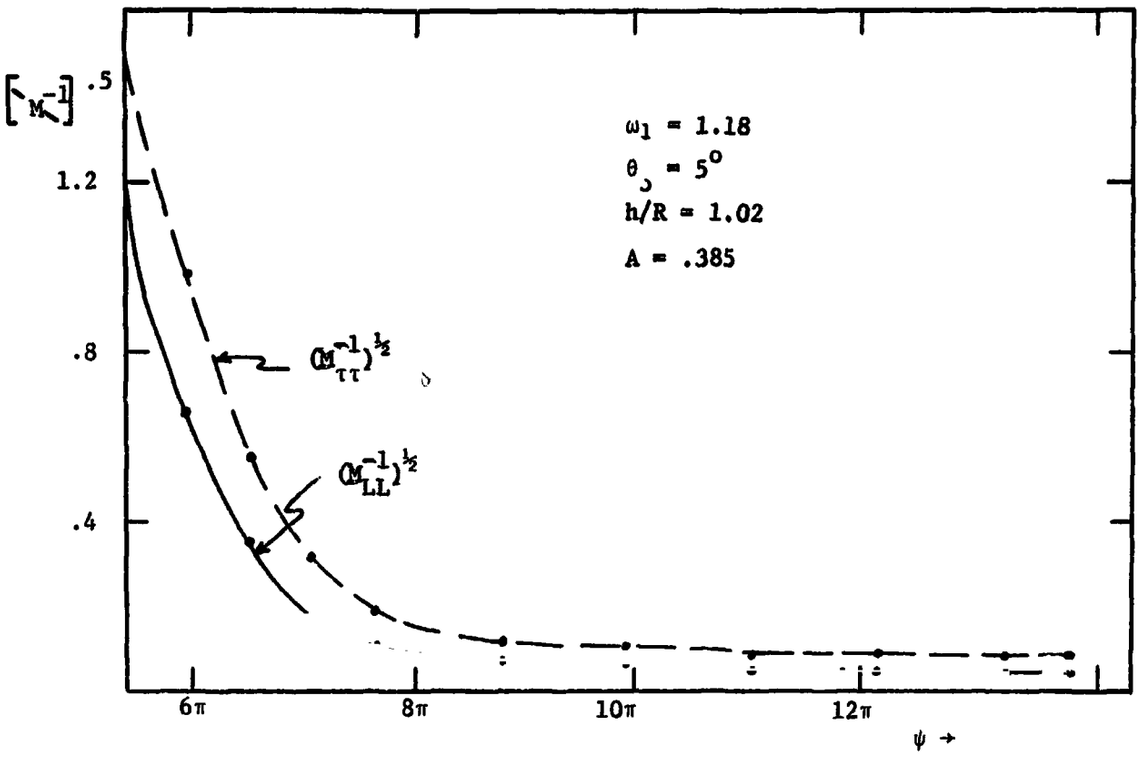

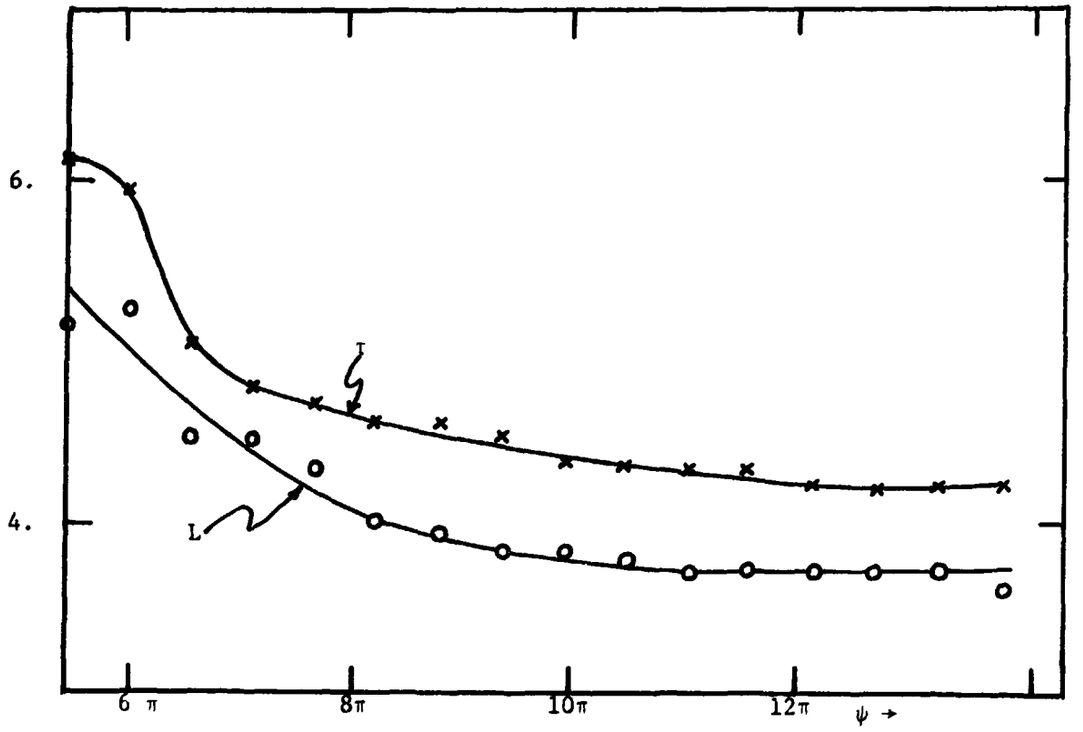

Figure 20 L,τ Data Length Study

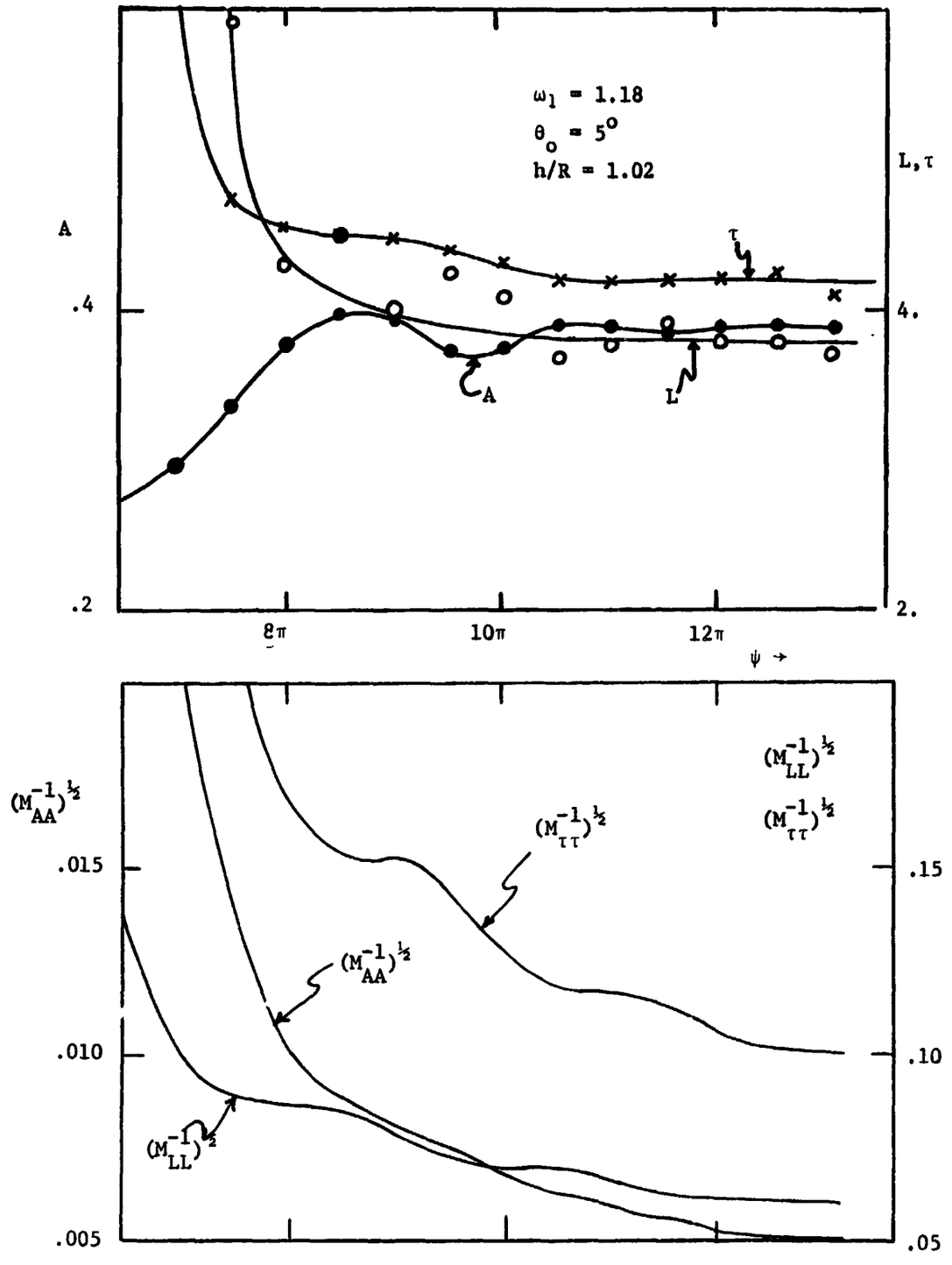

Figure 21 A, L, τ Data Lenth Study

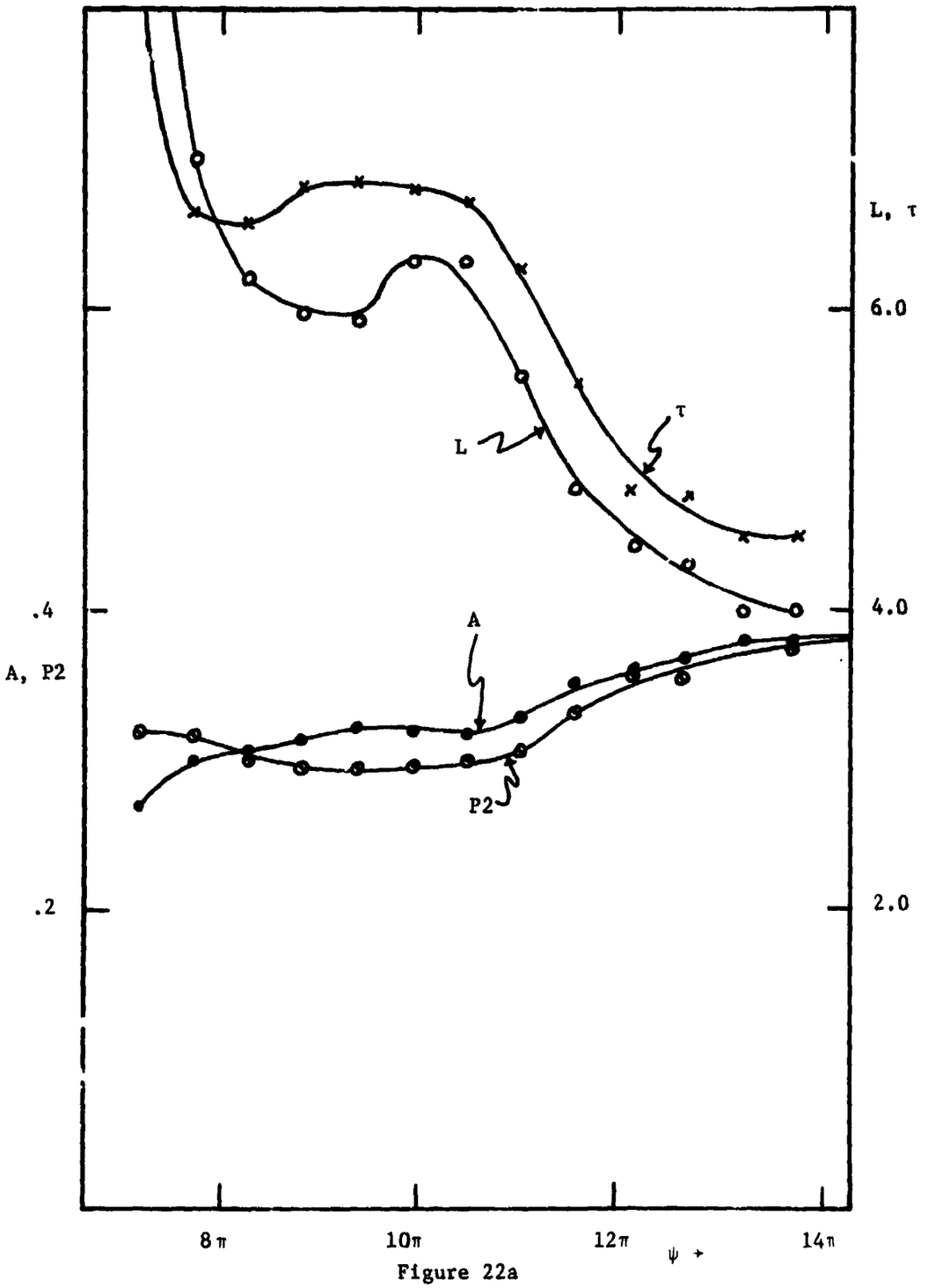

Figure 22a

Figure 22 P2, A, L, τ Data Length Study

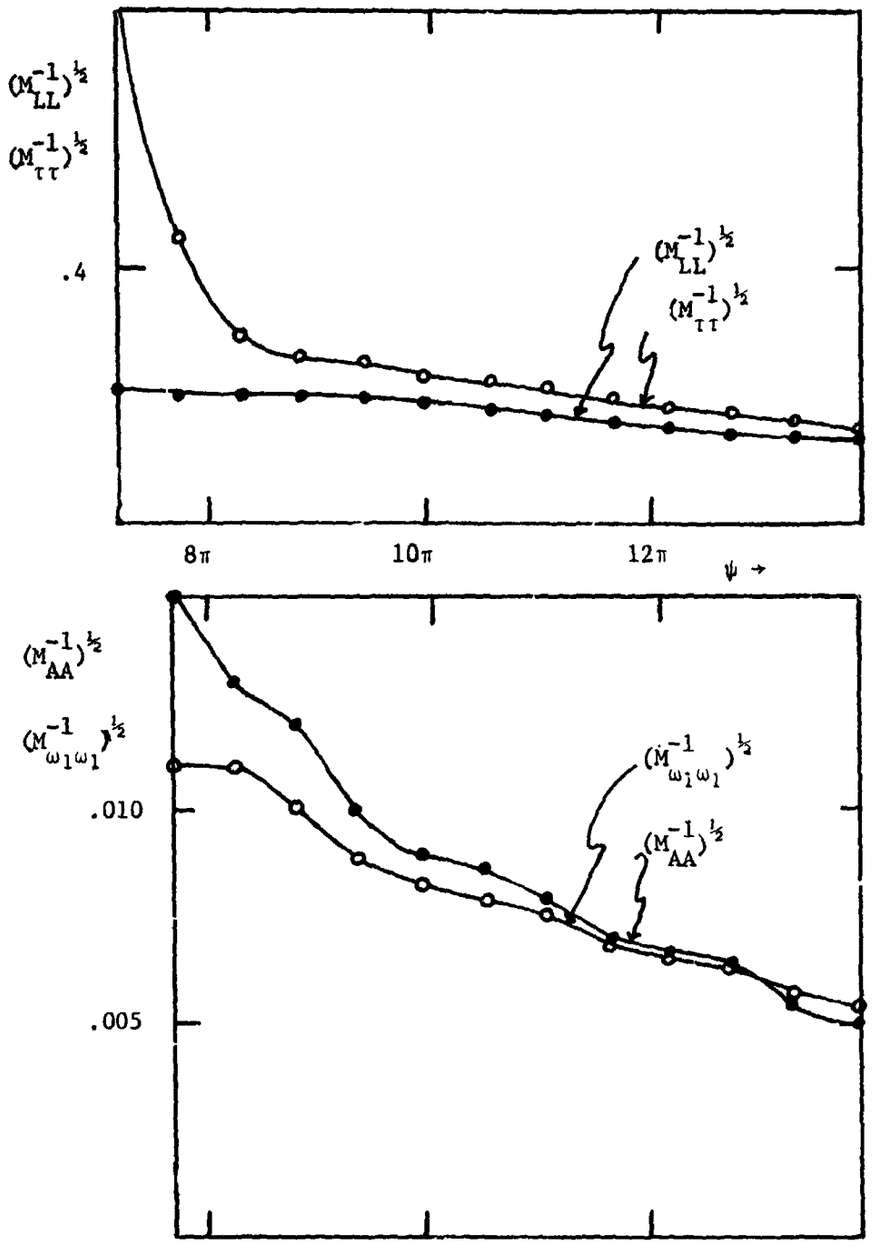
$(M_{LL}^{-1})^{\frac{1}{2}}$
$(M_{\tau\tau}^{-1})^{\frac{1}{2}}$
.4
$(M_{LL}^{-1})^{\frac{1}{2}}$
$(M_{\tau\tau}^{-1})^{\frac{1}{2}}$
8π
10π
12π
ψ →
$(M_{AA}^{-1})^{\frac{1}{2}}$
$(M_{\omega_1\omega_1}^{-1})^{\frac{1}{2}}$
.010
.005
$(M_{\omega_1\omega_1}^{-1})^{\frac{1}{2}}$
$(M_{AA}^{-1})^{\frac{1}{2}}$

Figure 22b

6.3 IDENTIFIED PARAMETERS

Figures 23, 24, 25, and 26 present identified parameters of the perturbation models for dynamic induced flow from progressing pitch stirring tests. Plotted are the fit factors, RR (22), versus collective pitch and the parameter values versus collective pitch for each data set.

Figure 23 presents the results of identifying the quasisteady wake model, (12), from Transient Tests Sets 1 and 2 of Table 4.

Figure 24 presents the results of identifying 2 parameters (L, τ) of the 4 parameter (A, P2, L, τ) first order unsteady wake model from the Transient Tests Sets 1, 2, and the first part of 3 of Table 4. The measured parameter P2 varied slightly from experiment to experiment and was adjusted to the correct value for each data set. A = .385 was assumed constant, and is the calculated value of A at a collective pitch of 5 degrees.

Figure 25 presents the results of identifying 3 parameters (A, L, τ) of the 4 parameter first order unsteady wake model from the Transient Tests Sets 1, 2, and part of 3 of Table 4.

The average fit factors (root mean square error over all the data set), RR, for the three models are shown in Table 8. Also shown

Table 8

Averaged Fit Factors

Model	RR	Comparison
A'(12)	.0774	2.19
L, τ(8)	.0442	1.25
A,L,τ(8)	.0353	1.00
A,L,τ,H(9)	.0346	.98

in Table 8 is the average fit factor of identifying 4 parameters (A, L, τ, H) of the 5 parameter (P2, A, L, τ, H) first order unsteady wake model with wake cross-coupling (Equation (9)). The A, L,τ (8) model is 25% better than the L,τ (8) model and 119% better than the A'(12) model. The A, L, τ, H (9) model is only a slight, 2%, improvement on the A, .. τ (8) model. Figure 24a shows that the fit factors for the A' (12) model get slightly better with increasing

collective pitch. Figure 25a shows that the fit factors for the L, τ (8) model are best around $\theta_o = 5^o$ and worsen with both increasing or decreasing collective pitch. Figure 26a shows that the fit factors for the A, L, τ (8) model does not vary with collective pitch. Thus the identified A, L, τ (8) perturbation model shown in Figures 25a and b is clearly the best of the 3 perturbation models in Figures 23 to 25, since it has the best average fit factor and no fit factor variation with collective pitch.

When the wake cross-coupling term, H, from Equation (9) was identified along with A, L, and τ, the identified values of A typically increased by .5%, the identified values of L typically decreased by 1.5%, and the identified values of τ typically increased by 7%. The identified value of wake cross-coupling was always in the direction of rotor rotation and was not an obvious function of collective pitch. The average value of H for all data sets was .15. The arctangent of .15 is 8.5 degrees. Therefore the induced flow from rotor drag in the direction of rotor rotation is approximately 2% of the rotor velocity.

The 5 parameter 2nd order unsteady wake model (P2, A, L, T_1, T_2) of Equation (11) could not be successfully identified from the progressing pitch stirring transients.

Figure 26 presents the results of identifying the A, L, τ (8) model from Transient Tests Set 3 of Table 4. These results show that the identified values are not functions of ω_1. A, L, and τ are all rotor aerodynamic or aerodynamic terms and should be independent of ω_1 which is strictly a structural property of the rotor.

The simulation studies of Reference 38 determined that progressing pitch stirring transients should be used over regressing pitch stirring transients. Table 9 presents comparisons of identification results, fit factors, and the square root of the related diagonal term of M^{-1} from different experimental transients. Regr stands for a regressing pitch stirring transient test, prog stands for a progressing pitch stirring transient test, and pspring stands for a progressing spring driven pitch stirring (Section 2.2 1) transient test. Two different regressing excitations were used for identifying parameters. These excitations can be seen in Figures 28, 29, and 30 of Section 6.4. The

smaller the $(M^{-1})^{\frac{1}{2}}$ terms are, the better the excitation is (Section 5.2).

Table 9 shows that the progressing pitch stirring excitation is somewhat better than the slow regressing pitch stirring excitation, since the $(M_{AA}^{-1})^{\frac{1}{2}}$'s for the progressing cases are better than those of the regressing cases and A is the strongest parameter. Both these excitations produce almost the same parameter values. The fast regressing pitch stirring excitation will not converge for the 3 parameter model and does not produce good results for the 2 parameter model.

Table 9 shows that the progressing spring excitation is not sufficient for identifying the three parameter model, but does better than the progressing pitch stirring excitation for identifying L and τ if A is specified at the identified value from the progressing tests. The L values identified are almost equal, but the τ values are about 20% less for the progressing spring excitation.

Figure 23b shows how A', the quasisteady wake parameter, should vary with ground effect and collective pitch according to blade element momentum theory. A' was calculated from A' = A/(1+AL) where A was assumed to be .385. L was calculated from (14). v_o was calculated from blade element momentum theory corrected for ground height variation by the relations found in Reference 36. The experimental curves for the smallest (h/R = .78) and largest (h/R = 1.28) ground heights from Figure 23a are also shown. For h/R = 1.28 the experimental and theoretical curves are close, however they deviate increasingly with decreasing ground height. The experimental curves show A' increasing with decreasing ground height.

The three average induced flow values measured with h/R = 1.28 shown in Table 7 (Section 6.1) can be used to calculate L and τ from (14). The results of these calculations are shown in Table 7. By comparing these values with those of Figure 24b for h/R = 1.28 it is seen that there is reasonable agreement between the theoretical values of L and τ and those identified from transients.

Figure 25c presents theoretical values of L and τ plotted as a function of ground height and collective pitch. L and τ were calculated from (14). The average induced flow values were calculated from blade element momentum theory corrected for ground height variation by the relations found in Reference 36 (Section 6.1). These curves show

excellent agreement with the experimental curves of 25b for L above collective pitch settings of 5^{o}. At low collective pitch settings the identified L values are lower than the theoretical ones. The identified τ values agree with the theoretical ones at very low collective pitch. As collective pitch increases the identified τ values are proportionally larger than the theoretical ones. The theoretical and identified values both show the same effect of ground height on L and τ. As collective pitch increases, disk loading increases, and tip losses (B) should increase. This would cause A to decrease. Figure 25a shows the identified A increasing until the collective pitch reaches about 5^{o}. Above 5^{o} A decreases as predicted by the increasing tip loss factor.

Table 9

Transient Identification Comparisons

	A	$(M_{AA}^{-1})^{\frac{1}{2}}$	L	$(M_{LL}^{-1})^{\frac{1}{2}}$	τ	$(M_{\tau\tau}^{-1})^{\frac{1}{2}}$	RR
A, L, τ (8) model							
ω_1=1.18							
h/R =1.28 regr slow	.356	.0061	4.72	.10	7.80	.35	.0372
pspring	.277	.0092	3.43	.10	7.22	.54	.0367
=1.02 prog	.356	.0040	4.66	.13	8.50	.40	.0400
regr	.381	.0064	5.50	.10	7.80	.29	.0357
= .78 prog	.359	.0040	4.71	.14	9.25	.46	.0468
regr	.358	.0056	5.58	.10	8.31	.42	.0343
ω_1=1.26							
h/R =1.28 prog	.355	.0040	4.32	.14	7.86	.46	.0354
pspring	.455	.0338	4.94	.16	5.28	.42	.0616
L, τ (8) model							
ω_1=1.18							
h/R =1.28 regr slow	.360		4.73	.10	7.69	.32	.0372
regr fast	-		11.15	.90	19.76	2.25	.0538
pspring	-		4.02	.06	5.30	.24	.0382
ω_1=1.26							
h/R =1.28 prog	-		4.57	.15	7.71	.40	.0348
pspring			4.59	.14	5.98	.47	.0623

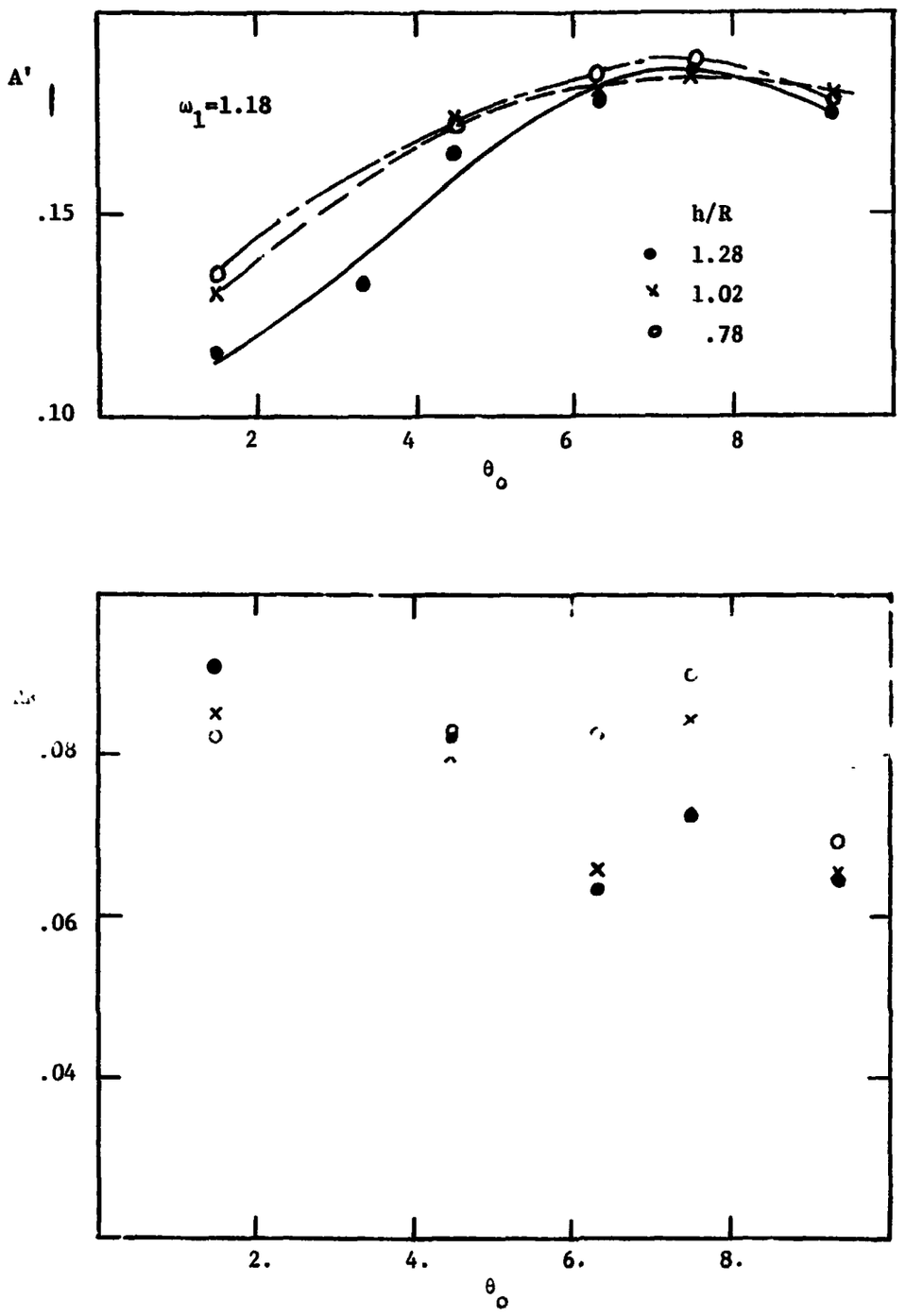

Figure 23a A' and Fit Factor Versus θ_o for the Quasisteady Wake Model

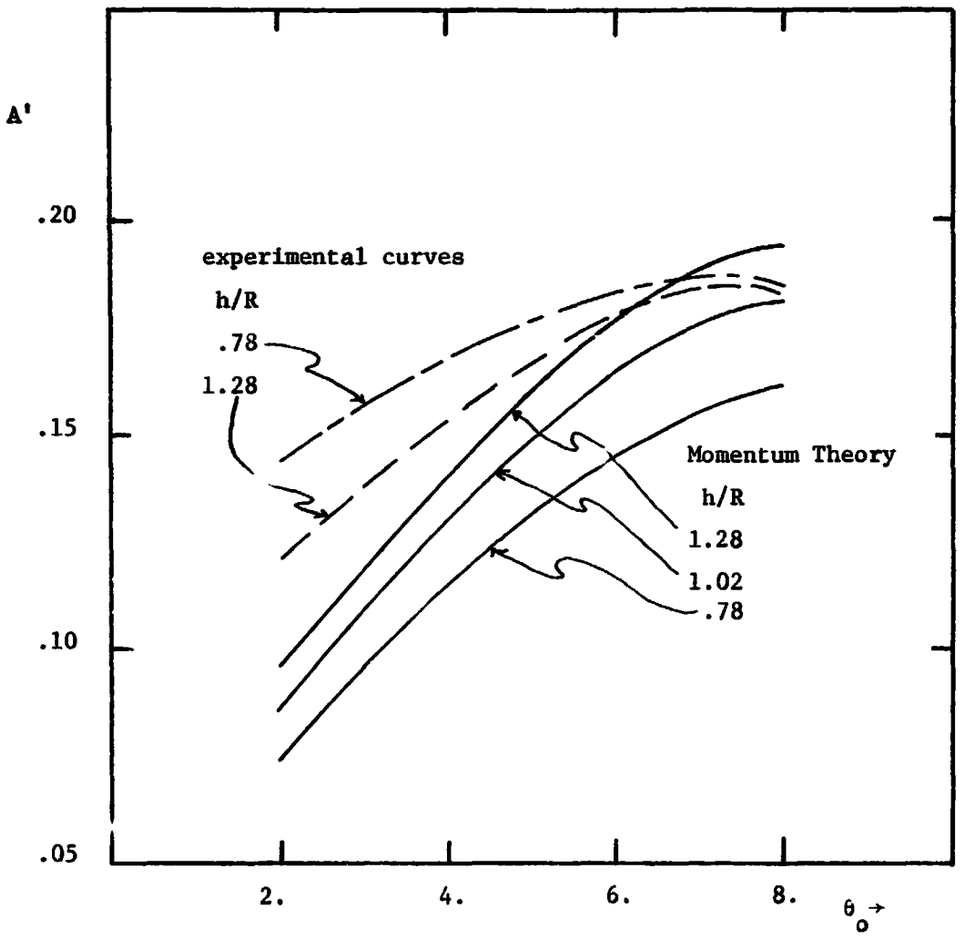

Figure 23b

Comparison Between Test and Theoretical Results for the Quasisteady Wake Model

$\omega_1 = 1.18$, A = .385

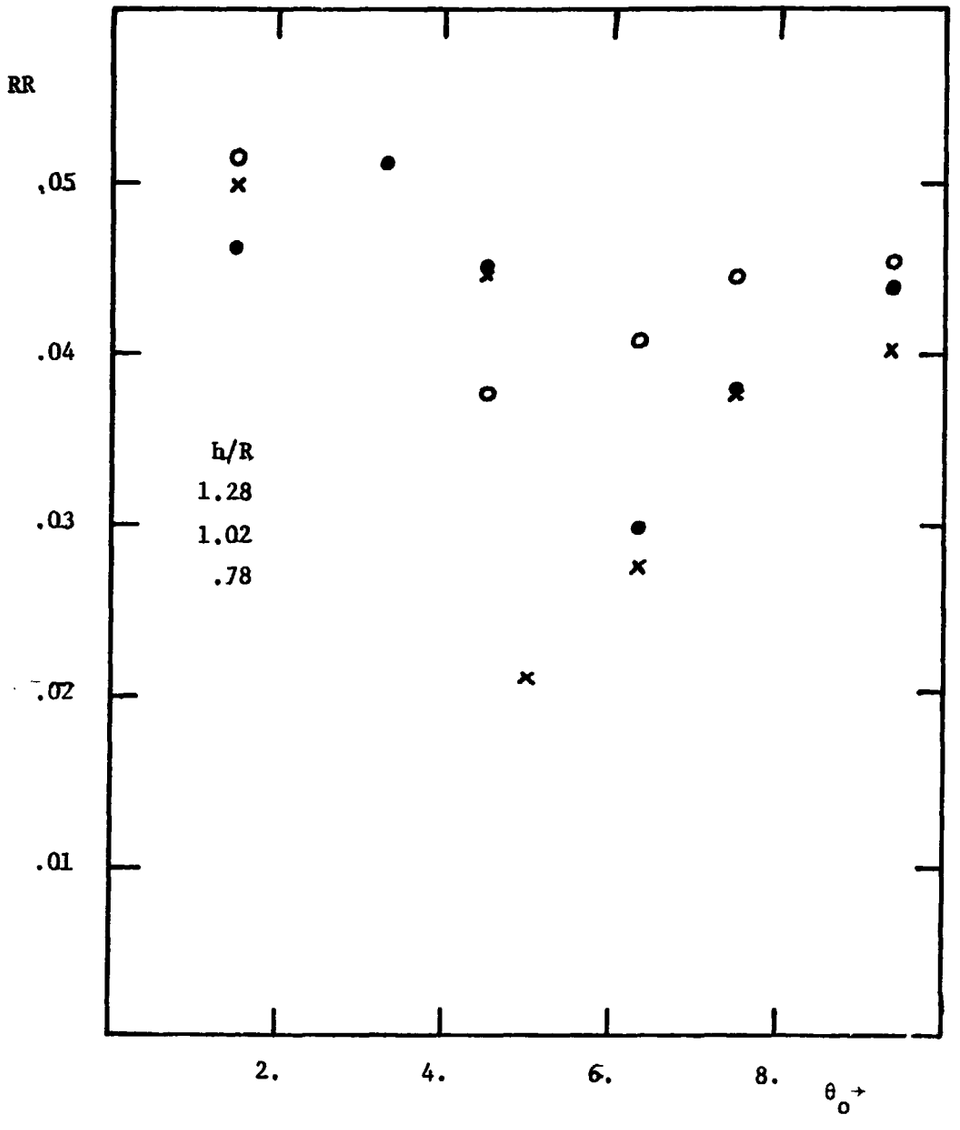

Figure 24a

Fit Factor RR Versus θ_o for the Two Parameter Unsteady Wake Model

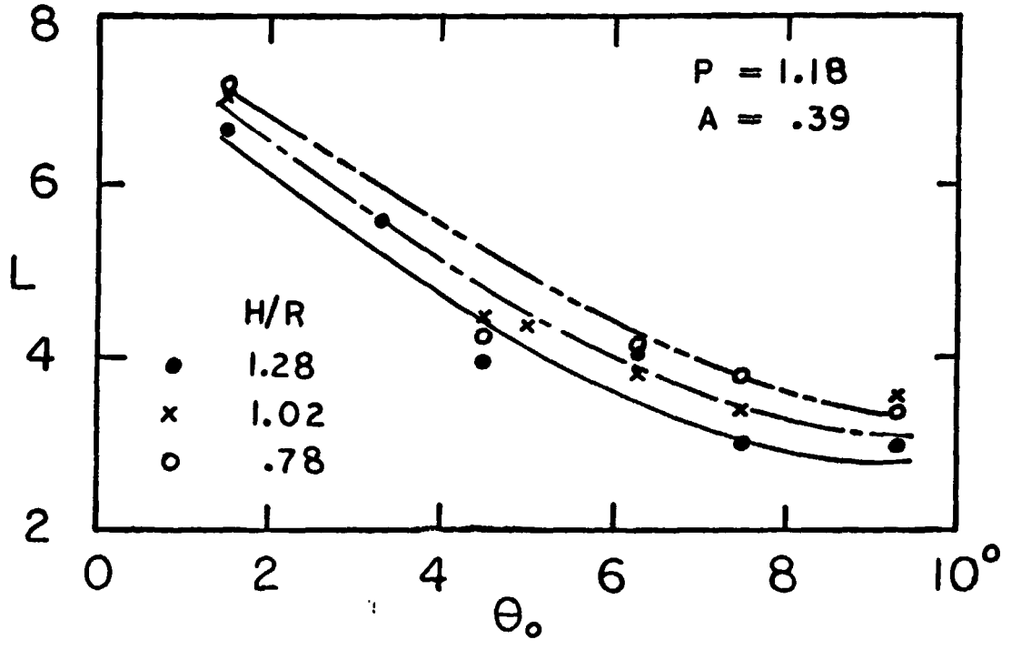

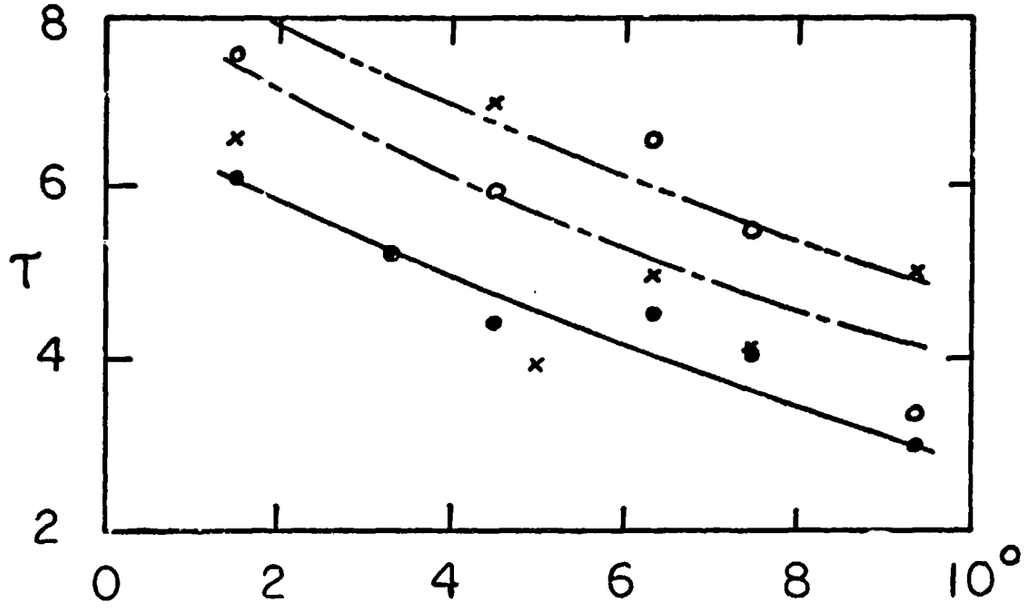

Figure 24b L and τ Versus θ_o for the Two Parameter Unsteady Wake Model

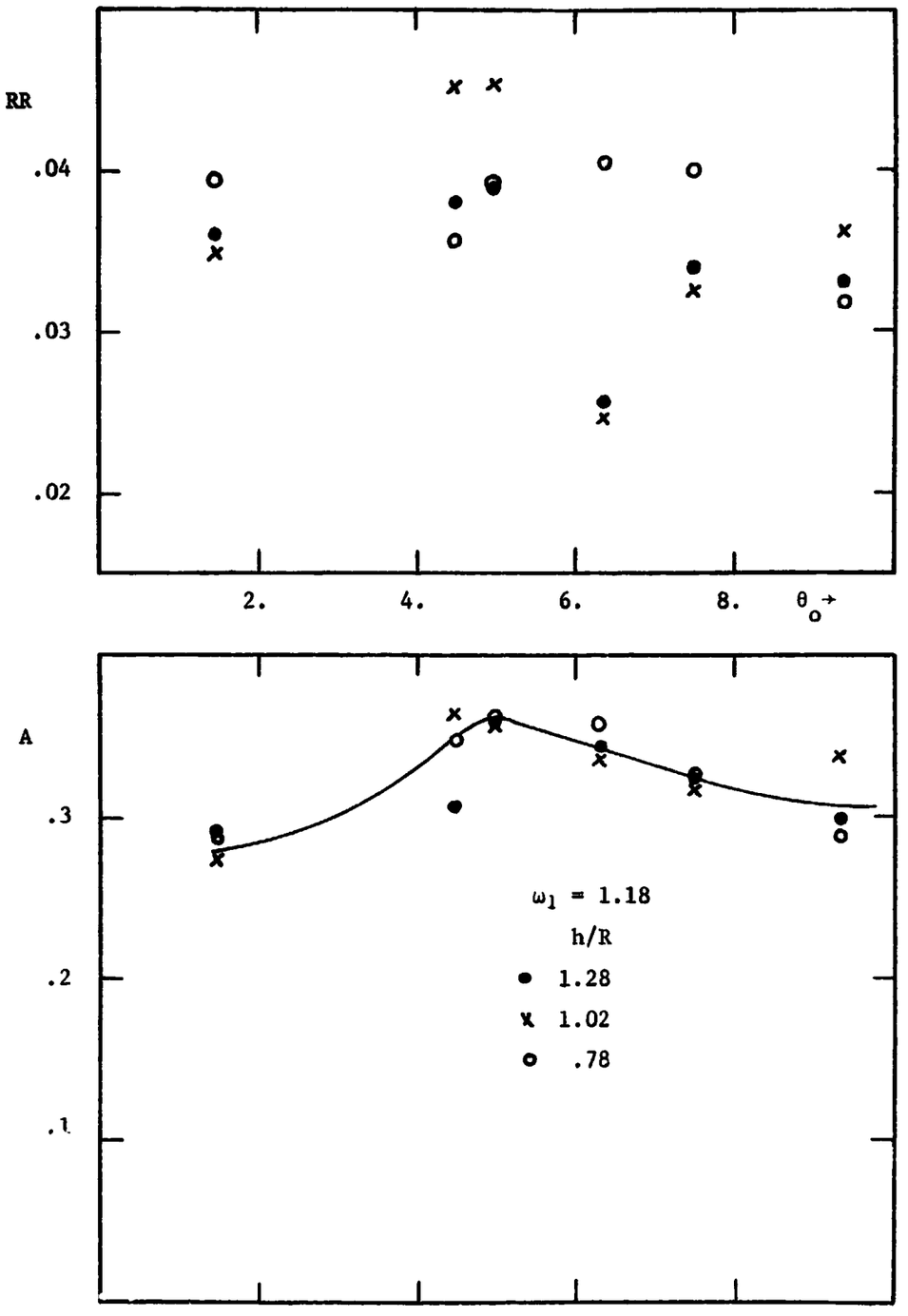

Figure 25a

Fit Factor and A Versus θ_o for the Three Parameter Unsteady Wake Model

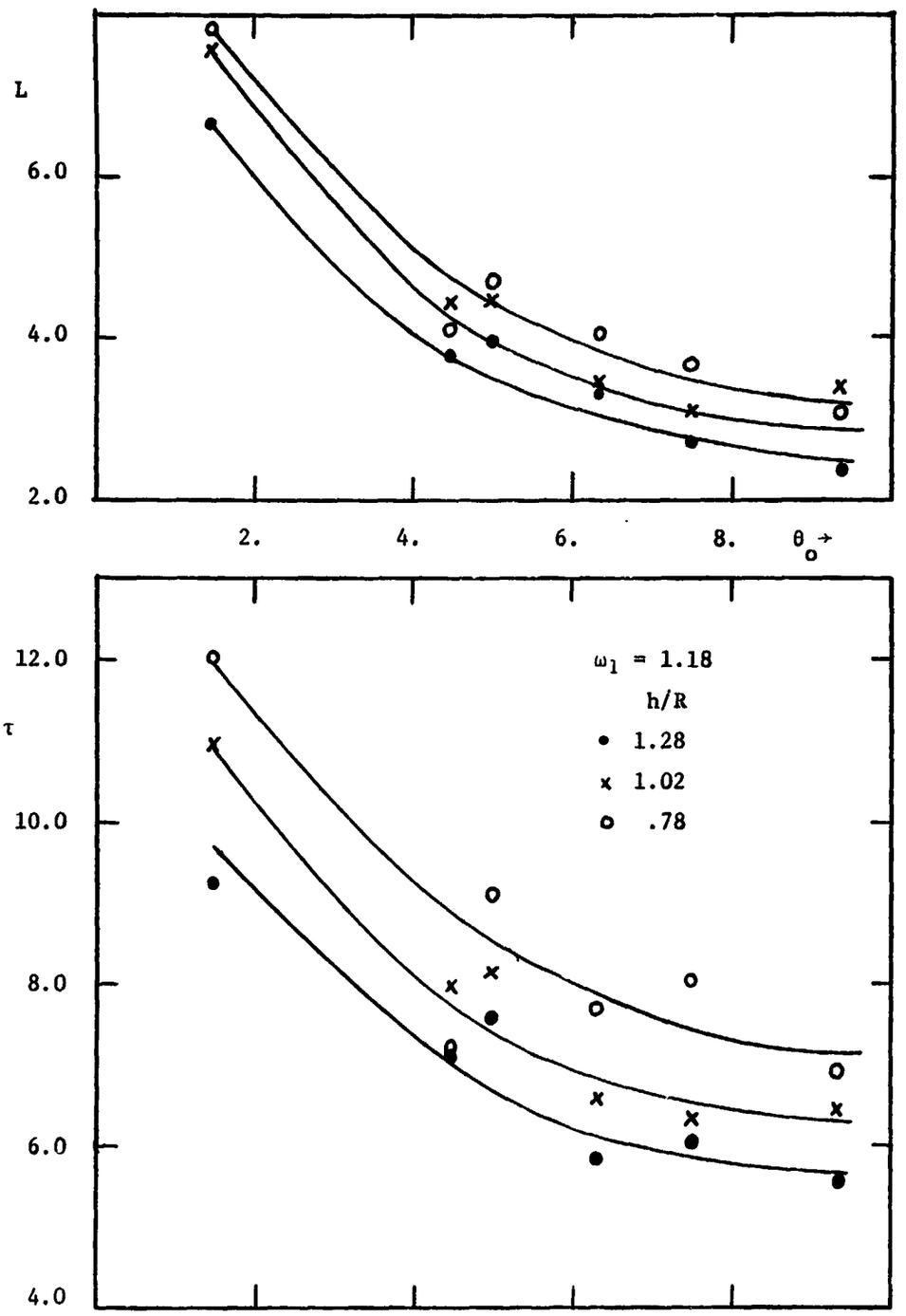

Figure 25b

L and τ Versus θ_o for the Three Parameter Unsteady Wake Model

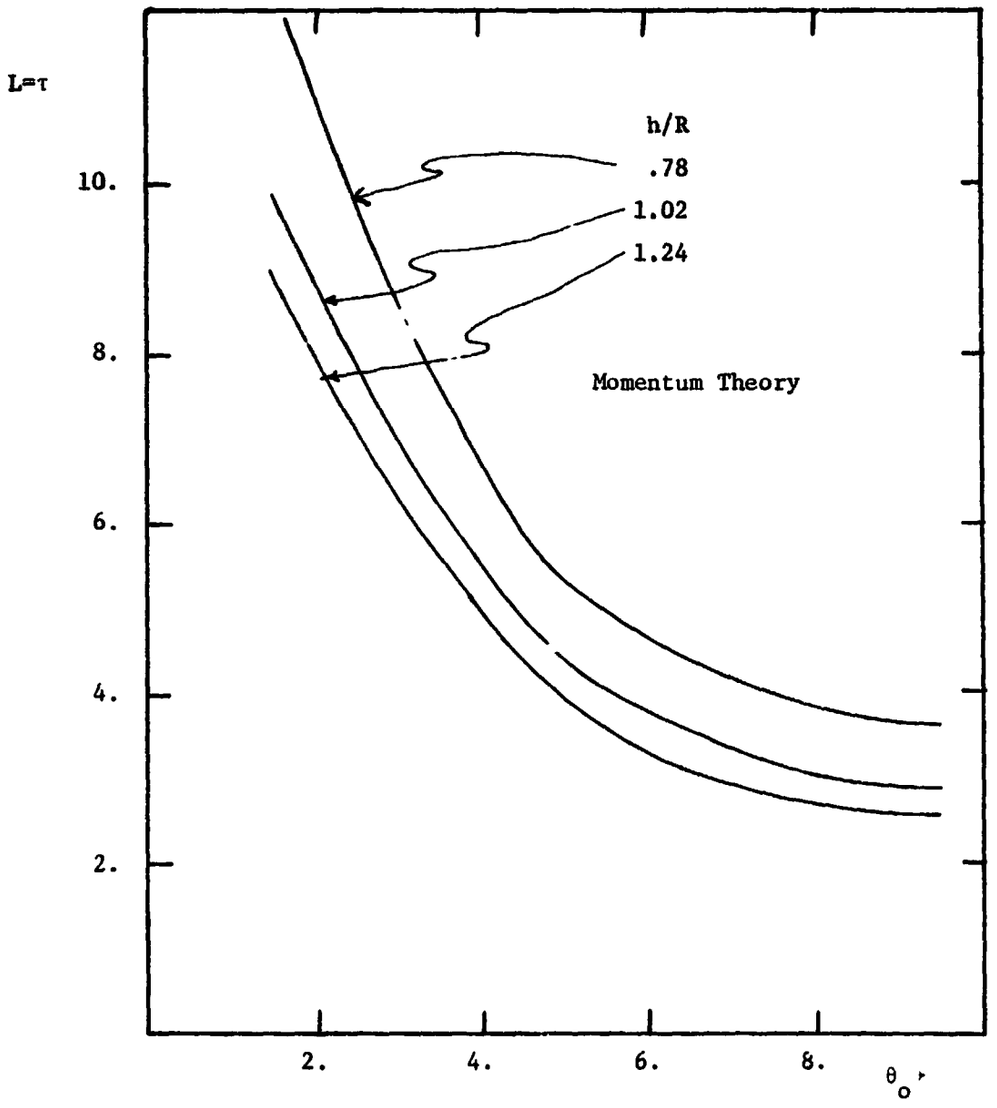

Figure 25c

Theoretical Values or L and τ Versus θ_o

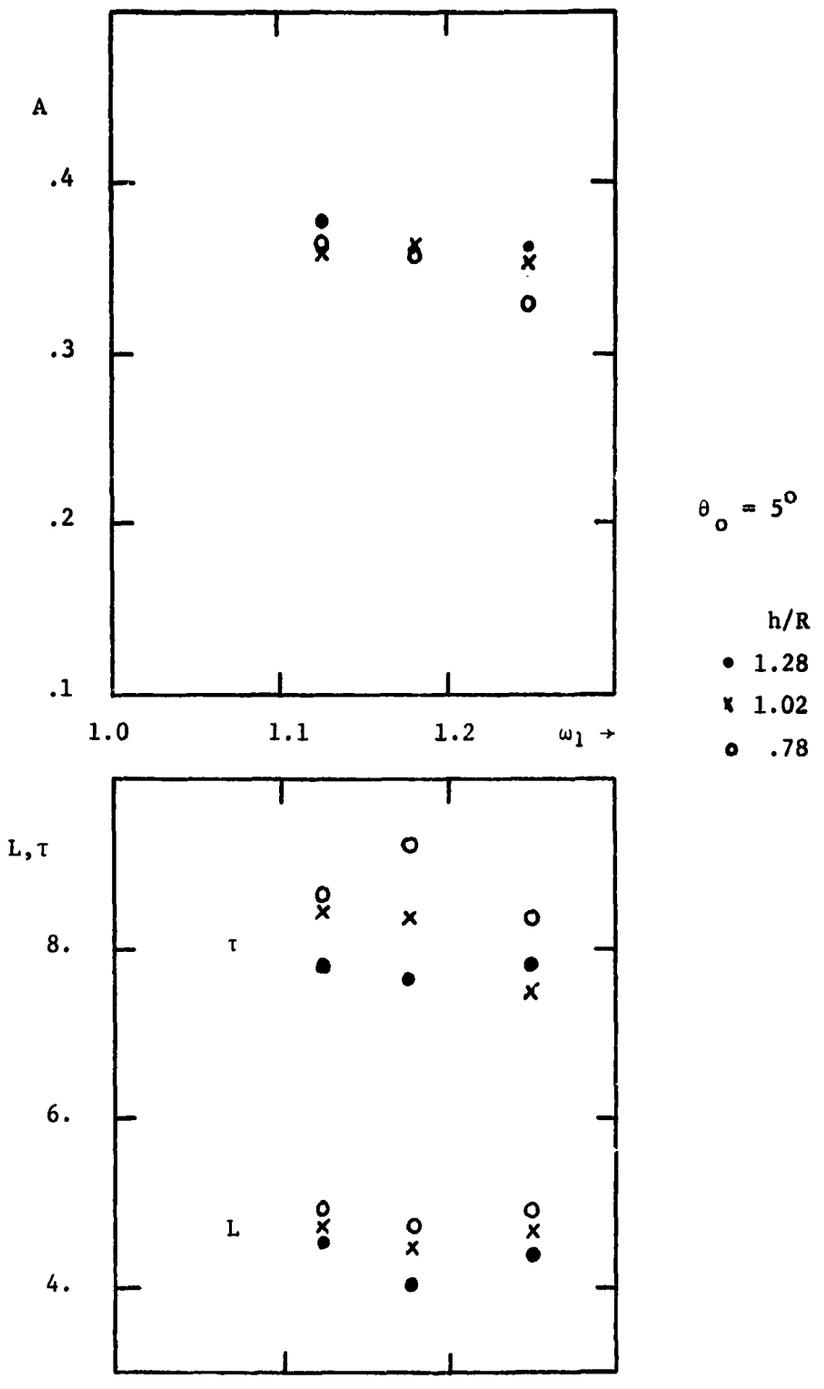

Figure 26 A, L, and τ Versus ω_1 for the Three Parameter Unsteady Wake Model

6.4 PREDICTIONS

Figures 16, 17, and 18 in Section 6.1 present frequency response test prediction results. The crosses are the measured data points discussed in Section 6.1. The solid lines in Figures 16, 17, and 18 are predictions for the L, τ (8) model of Figure 24. L and τ values for θ_o = 2, 5, and 8 degrees and h/R = 1.28 were picked from the solid line curves in Figure 24. A was assumed to be .385. The dashed line in Figure 17 is a prediction for A = .385 where the dynamic rotor inflow is omitted. The dot-dashed line in Figure 17 is a prediction for the A' (12) model of Figure 23. The A' value for $\theta_o = 5^o$ and h/R = 1.28 was picked from the solid line curve in Figure 23.

Omitting the dynamic inflow produces poor predictions of the experimental frequency flapping responses (Figure 17). The quasisteady wake model produces better prediction results (Figure 17) but cannot predict the measurement trends as a function of frequency. Though no flow measurements are used to establish the solid curves (the L, τ (8) identified model) in Figures 16, 17, and 18, and though the presented flow data (crosses) are derived from inaccurate measurements (see Figures 14c and d) the agreement in the dynamic flow Fourier coefficients is reasonable. The experimental frequency flapping responses agree even better with the L, τ (8) identified model predictions.

Figures 27 through 30 present real time prediction results. The dots are the measurements. Every 5th measurement is plotted. The experimental input for each transient excitation is plotted above the experimental and predicted responses. The root mean square fit between prediction and measured response over the length of the data is noted on the figures. Each of the experimental responses was used for identification purposes, consequently the data bias terms ($\overline{\beta}_I$ and $\overline{\beta}_{II}$) are known. Each prediction includes these bias terms. The parameter values for each prediction are determined by picking them from the curves (Figures 23, 24, and 25) for the model being considered.

Figure 27 presents prediction results, using the A, L, τ model and the A' (12) model, from a progressing pitch stirring transient input. This is the transient input used to produce the models shown in Figures 23, 24, and 25. The predicted dynamic downwash (from the A, L, τ (8) model) is plotted along with the flapping responses and the experimental input versus rotor azimuth angle. The quasisteady

model does not predict the measured response very well. The first order unsteady wake model predicts the measured response adequately.

Figure 28 presents prediction results, using the A, L, τ (8) model, from a slow regressing pitch stirring excitation. The prediction is excellent.

Figure 29 presents prediction results, using the A, L, τ (8) model, from a fast regressing pitch stirring transient input.

Figure 30 presents prediction results, using the A, L, τ (8) model, from a short progressing pitch stirring excitation. This is the excitation produced by the spring loaded drive described in Section 2.2.1. There is a two per rotor revolution component in the measured response. Aside from this, the prediction is excellent. It has also been shown (Table 9) that the L, τ (8) model can be identified from this transient.

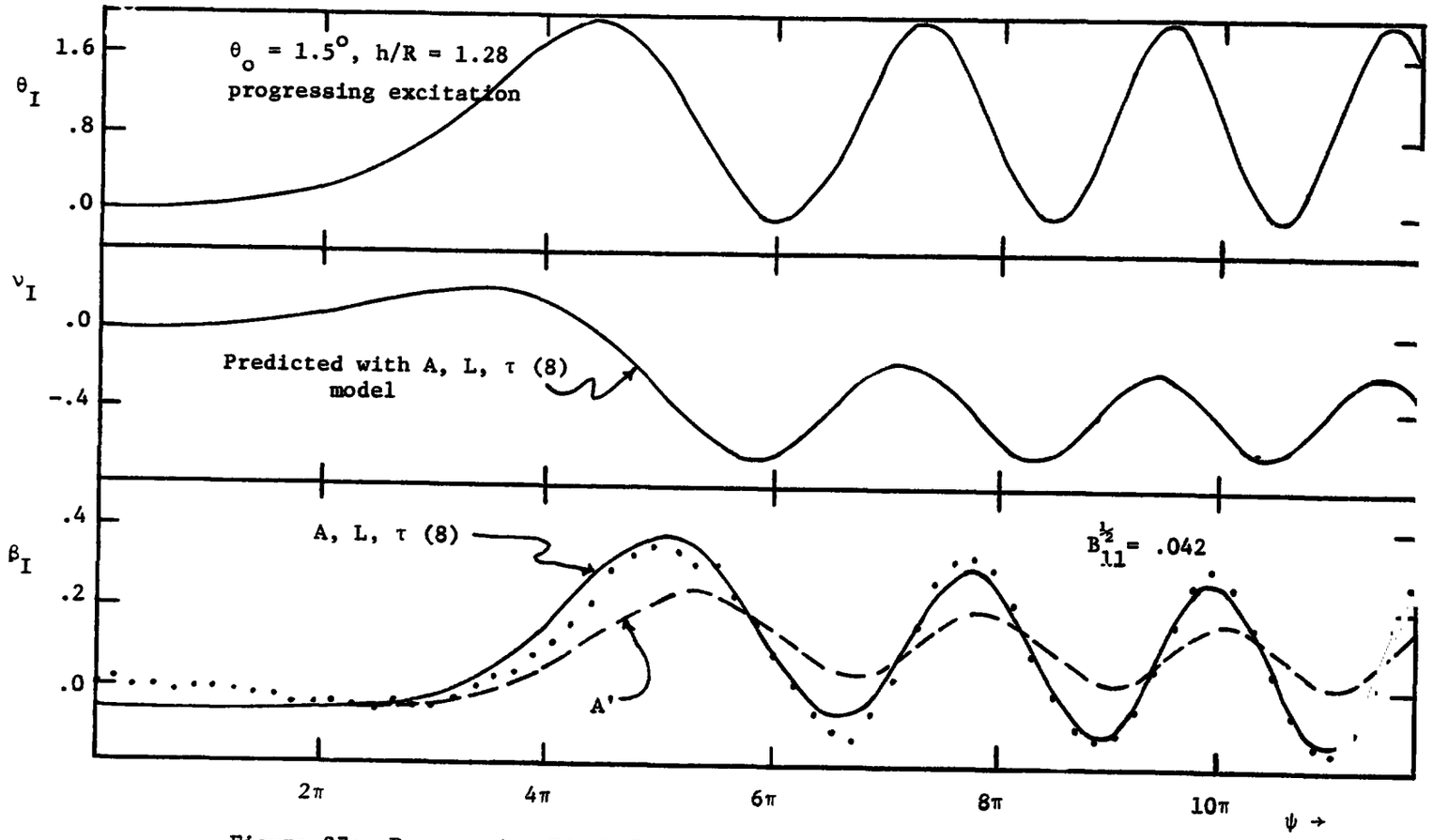

Figure 27a Progressing Pitch Stirring Transient Test Prediction

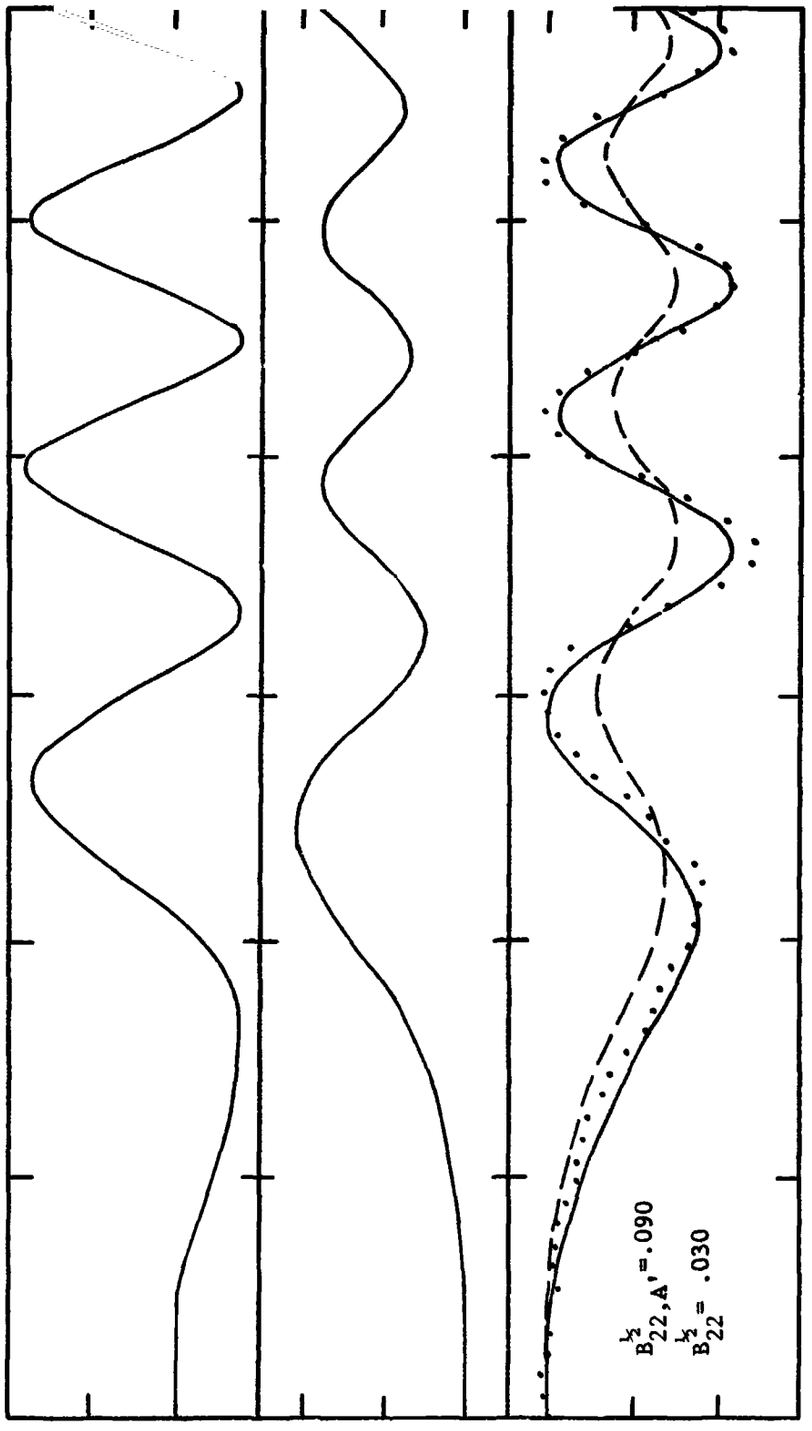
.8
.0
θ_{II}
.8
.4
.0
ν_{II}
.0
-.2
-.4
β_{II}
$B^{\frac{1}{2}}_{22,A'}$=.090
$B^{\frac{1}{2}}_{22}$= .030
2π
4π
6π
8π
10π

Figure 27b

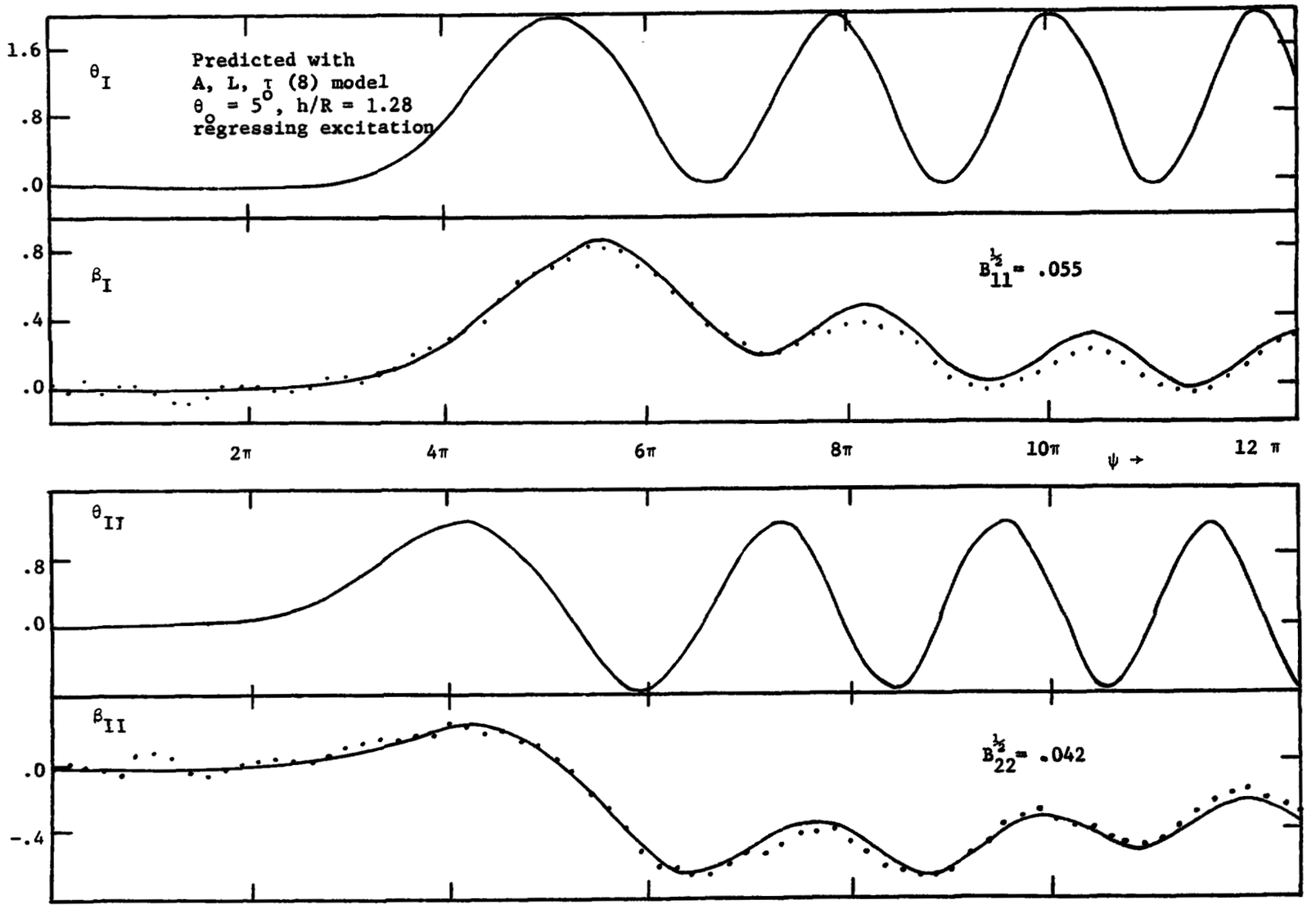

Figure 28 Regressing Test Prediction Slow Transient

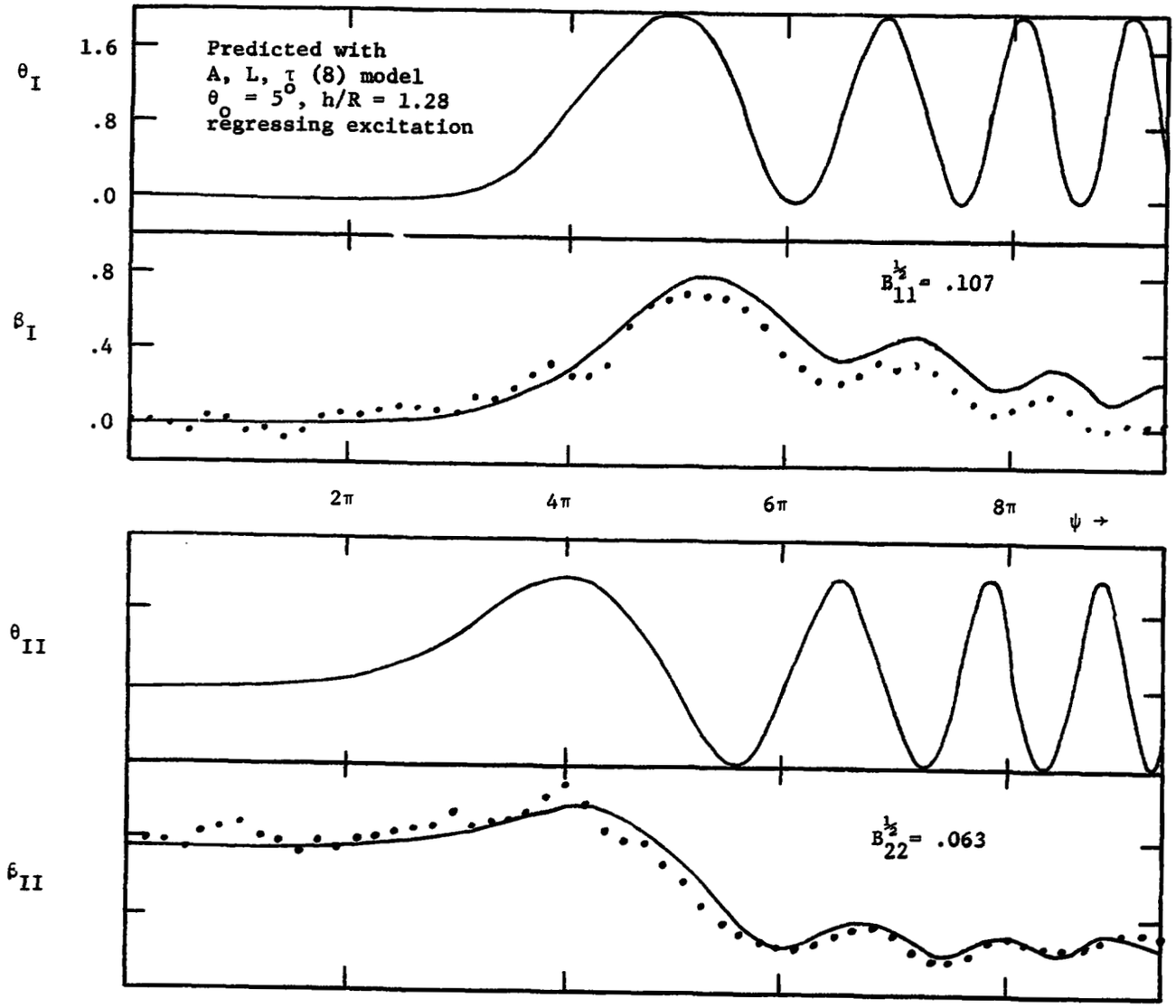

Figure 29 Regressing Test Prediction Slow Transient

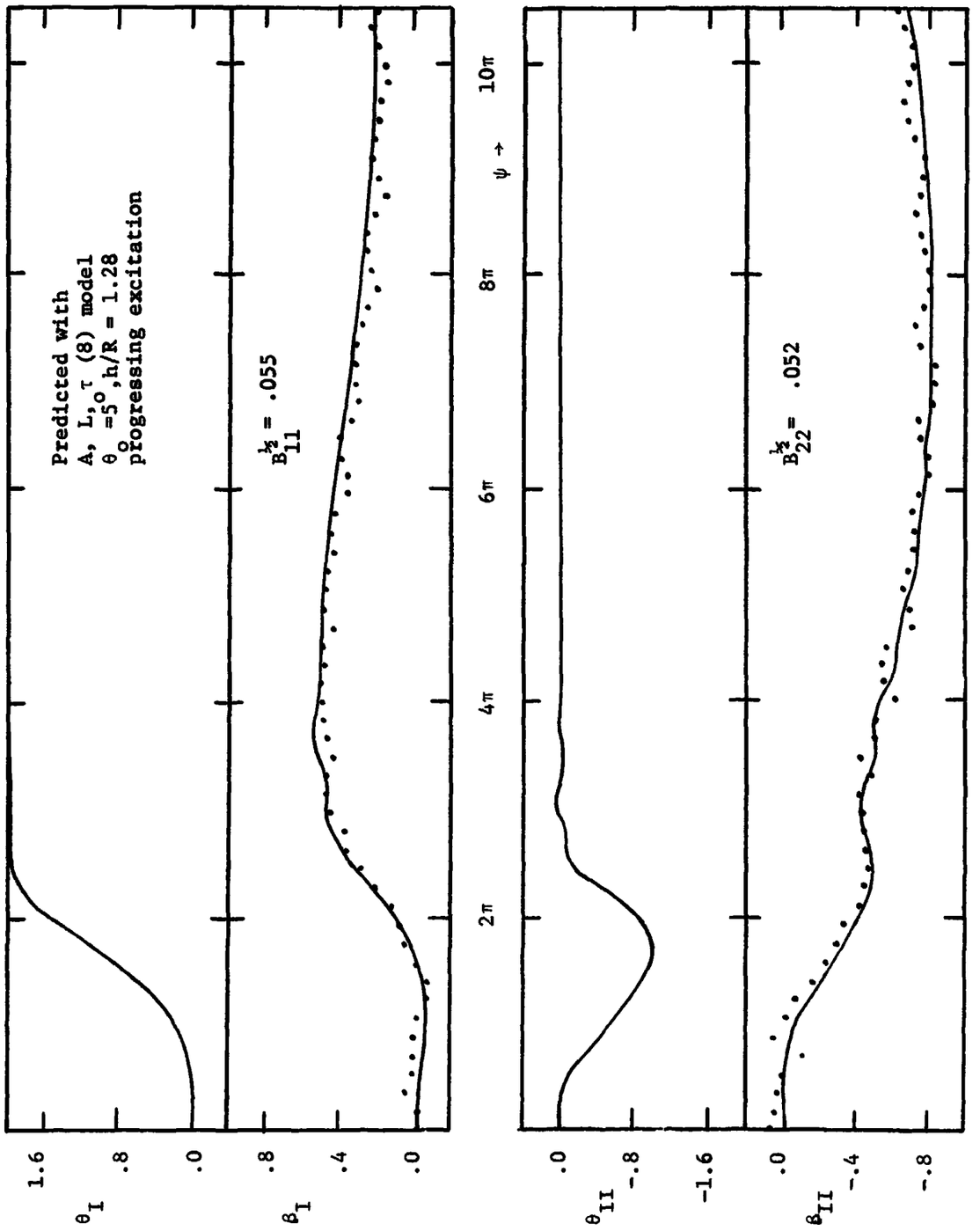

Figure 30 Progressing Test Prediction Short Transient

7. CONCLUSIONS

Since the objective was to gain a better understanding of rotor aeroelastic phenomena from dynamic rotor tests using both transient tests (with state variable and parameter identification evaluation techniques) and frequency response tests (with Fourier analysis evaluation techniques), there are two types of conclusions; the first type regarding methods used; the second type regarding the results for the selected aeroelastic problem.

7.1 CONCLUSIONS REGARDING METHODS

1.1 Transient tests evaluated by a simplified version of the maximum likelihood state variable and parameter identification method reduced model testing time by a factor of 80 over harmonic tests evaluated by frequency response methods for each rotor condition studied.

1.2 The parameter identification method provided the model parameter values directly while model parameter values must be determined from curve matching from frequency response tests.

1.3 The method of optimal data utilization based on the time history of the inverse of the sensitivity matrix can be effectively used to prevent inaccuracies from insufficient data utilization.

7.2 CONCLUSIONS REGARDING ROTOR DYNAMIC INFLOW EFFECTS

2.1 Transient cyclic pitch stirring is a simple and effective test technique to extract linear perturbation models including dynamic inflow effects from blade flapping measurements. The perturbation model used is only valid in the frequency regime typical for flight mechanical or ground and air resonance phenomena.

2.2 The analysis using identified rotor dynamic inflow parameters is in good agreement with transient and frequency response test results not used in the identification; thus the extracted perturbation is validated within the stipulated frequency range.

2.3 The extracted perturbation model is in reasonable agreement with a simple dynamic inflow theory especially above collective pitch settings of 5 degrees, thus confirming the previously deduced phenomenon of a substantial reduction of the regressing flapping mode damping caused by dynamic rotor inflow.

2.4 The ground proximity within the tested range ($h/R = .78$ to 1.28)

has a pronounced effect on the dynamic rotor downwash parameters which become larger with decreasing ground-rotor distance.

8. REFERENCES

1. Molusis, J. A., "Helicopter Stability Derivative Extraction and Data Processing Using Kalman Filtering Techniques", 28th Annual National Forum of the American Helicopter Society, May 1972.

2. Molusis, J. A., "Rotorcraft Derivative Identification from Analytical Models and Flight Test Data", AGARD Flight Mechanics Panel Specialists Meeting, NASA Langley, November 1974.

3. Gould, D. G. and Hindson, W. S., "Estimates of the Lateral-Directional Stability Derivatives of a Helicopter from Flight Measurements", Canadian Aeronautical Report LR-572, December 1973.

4. Gould, D. G. and Hindson, W. S., "Estimates of the Stability Derivatives of a Medium Sized Single Rotor Helicopter from Full Scale Flight Tests", AGARD Flight Mechanics Panel Specialists Meeting, NASA Langley, November 1974.

5. Condon, C. W., "Rotor System Research Aircraft Requirements for, and Contributions to, Rotorcraft State Estimation and Parameter Identification", AGARD Flight Mechanics Panel Specialists Meeting, NASA Langley, November 1974.

6. Lebacqz, J. V., "The Efficient Application of Digital Identification Techniques to Flight Data from a Variable Stability V/STOL Aircraft", AGARD Flight Mechanics Panel Specialists Meeting, NASA Langley, November 1974.

7. Kuczynski, W. A., Sharpe, D. L., and Sissingh, G. J., "Hingeless Rotor Experimental Frequency Response and Dynamic Characteristics with Hub Moment Feedback Controls", 28th Annual National Forum of the American Helicopter Society, May 1972.

8. Kuczynski, W. A. and Sissingh, G. J., "Characteristics of Hingeless Rotors with Hub Moment Feedback Controls Including Experimental Rotor Frequency Response", Volume I, CR-114427, January 1972, NASA.

9. Hohenemser, K. H. and Crews, S. T., "Unsteady Wake Effects on Progressing/Regressing Forced Rotor Flapping Modes", AIAA 2nd Atmospheric Flight Mechanics Conference, September 1972.

10. Hohenemser, K. H. and Crews, S. T., "Model Tests on Unsteady Rotor Wake Effects", Journal of Aircraft, January 1973.

11. Crews, S. T., Hohenemser, K. H., and Ormiston, R. A., "An Unsteady Wake Model for a Hingeless Rotor", Journal of Aircraft, December 1973.

12. Giansante, N. and Flannelly, W. G., "Identification of Structural Parameters from Helicopter Dynamic Test Data", AHS/NASA-Ames Specialists' Meeting on Rotorcraft Dynamics, February 1974.

13. Daughaday, H., DuWaldt, F., and Gates, C., "Invertigation of Helicopter Blade Flutter and Load Amplification", Journal of the American Helicopter Society, July 1957.

14. Ormiston, R. A. and Bousman, W. G., "A Study of Stall-Induced Flap-Lag Instability of Hingeless Rotors", 29th Annual National Forum of the American Helicopter Society, May 1973.

15. Carpenter, P. J. and Fridovich, B., "Effect of Rapid Blade Pitch Increase on the Thrust and Induced Velocity Response of a Full Scale Helicopter Rotor", NACA TN3044, November 1953.

16. Bousman, W. G., Sharpe, D. L., and Ormiston, R. A., "An Experimental Study of Techniques for Increasing the Lead-Lag Damping of Soft Inplane Hingeless Rotors", Forum of the American Helicopter Society, May 1976.

17. Bousman, W. G., "An Analog Technique for the Measurement of Damping from Transient Decay Signals", NASA TMX-73, 121, June 1976.

18. Peters, D. A., "Hingeless Rotor Frequency Response with Unsteady Inflow", AHS/NASA Ames Specialists' Meeting on Rotorcraft Dynamics, February 1974.

19. Landgrebe, A. J. and Cheney, M. C., "Rotor Wakes - Key to Performance Prediction", AGARD-CP-11, September 1972.

20. Baskin, V. E., Vil'dgrube, L. S., Vozhdayev, Ye. S., and Maykapar, G. I., "Theory of the Lifting Airscrew", NASA TT F-823, February 1976.

21. Ormiston, R. A., "An Actuator Disc Theory for Rotor Wake Induced Velocities", AGARD-CP-111, September 1972.

22. Curtiss, H. C. and Shupe, N. K., "A Stability and Control Theory for Hingeless Rotors", 27th Annual National Forum of the American Helicopter Society, Preprint No. 541, May 1971.

23. DeDecker, W., "Static Test of Monocyclic Control on a Full-Scale Boeing-Vertol 76 Rigid Propeller", AMC(t)-01-63-20, R-339, Volume 1, Boeing-Vertol, June 1965.

24. Ormiston, R. A. and Peters, D. A., "Hingeless Rotor Response with Nonuniform Inflow and Elastic Blade Bending -- Theory and Experiment", AIAA 10th Aerospace Sciences Meeting, January 1972.

25. Miller, R. H., "Rotor Blade Harmonic Airloading", AIAA Journal, July 1964.

26. Loewy, R. G., "A Two Dimensional Approach to the Unsteady Aerodynamics of Rotary Wings", Journal of Aerospace Science, Vol. 24, 1957.

27. Crews, Samuel T., "Development and Testing of a New Type of Wind Tunnel Model Rotor", Master of Science Thesis, Washington University, June 1975.

28. Hohenemser, K. H. and Crews, S. T., "Further Experiments with Progressing/Regressing Rotor Flapping Modes", Phase VII-C Report under NAS2-4151, June 1973.

29. Hohenemser, K. H. and Crews, S. T., "Experiments with Progressing/Regressing Forced Rotor Flapping Modes", Phase VI-B Report under Contract NAS2-4151, June 1972.

30. Critzos, C. C., Heyson, H. H., and Boswinkle, R. W., "Aerodynamic Characteristics of NACA 0012 Airfoil Section at Angles of Attack from 0^{o} to 180^{o}", NACA TN 3361, January 1955.

31. Knight, Montgomery and Hefner, Ralph A., "Static Thrust Analysis of the Lifting Airscrew", NACA TN 626, June 1937.

32. Gessow, A. and Meyers, G. C., "Aerodynamics of the Helicopter", Ungar, 1952.

33. Hohenemser, K. H. and Crews, S. T., "Development of Experimental Methods", PhaseV-C Report under NAS2-4151, June 1971.

34. Hohenemser, K. H. and Crews, S. T., "Additional Experiments with a Four-bladed Cyclic Pitch Stirring Model Rotor", Part II of the Second Yearly Report under Contract NAS2-7613, CR-137965, June 1975.

35. Hohenemser, Kurt H. and Yin, S. K., "Some Applications of the Method of Multiblade Coordinates", Journal of the American Helicopter Society, July 1972.

36. Knight, Montgomery and Hefner, Ralph A., "Analysis of Ground Effect on the Lifting Airscrew", NACA TN 835, December 1941.

37. Hayden, T. S., "The Effect of the Ground on Helicopter Hovering Power Required", Preprint #1000, presented at the 32nd Annual National Forum of the American Helicopter Society, May 1976.

38. Hohenemser, K. H., Banerjee, D., and Yin, S. K., "Method Studies on System Identification from Transient Rotor Tests", Part I of the Second Yearly Report under Contract NAS2-7613, NASA CR-137965, June 1975.

39. Hohenemser, K. H., Banerjee, D., and Yin, S. K., "Rotor Dynamic State and Parameter Identification from Simulated Forward Flight Transients", Part I of the Third Yearly Report under Contract NAS2-7613, NASA CR-137963, June 1976.

40. Stepner, D. E. and Mehra, R. K., "Maximum Likelihood Identification and Optimal Input Design for Identifying Aircraft Stability and Control Derivatives", NASA CR 2200, March 1972.

41. Chen, R. T. N., "Input Design for Parameter Identification - A New Formulation and a Practical Solution", Proceedings, 1974 Joint Automatic Control Conference, June 1974.

42. Banerjee, D. and Hohenemser, K. H., "Optimum Data Utilization for Parameter Identification with Application to Lifting Rotors", Journal of Aircraft, Volume 13, Number 12, December 1976.

9. APPENDIX

9.1 NOMENCLATURE

A	$= B^4\gamma/8$ aerodynamic blade constant, (4)*
A'	$= A/(1+AL)$ aerodynamic blade constant assuming quasisteady wake, (12)
A''	aerodynamic wake constant, (4)
B	blade tip loss factor
B	measurement equation error covariance, (19)
$F_{1\omega}$	first Fourier coefficient of frequency ω
H	wake cross coupling term, (9)
H'	$= H/\tau$, (9)
I	$= a\rho cR^4/\gamma$ blade moment of inertia
J	scalar cost criterion, (17)
K	1024 words
L	dynamic induced flow gain, (5), (13)
L*	$= AL/\tau$, (8)
L'	$= AL/T_1^2$, (11)
M	information or sensitivity matrix, (20)
$M_{\omega_1\omega_1}$, M_{AA}, M_{LL}, $M_{\tau\tau}$	diagonal terms of M
M_b	blade moments
N	number of measurement vectors
P2	$= (\omega_1^2 - 1)$ non-dimensional non-rotating blade flapping natural frequency (8)
R	rotor radius
RR	fit factor, (28)
T	$= T_2/T_1$, (11)
T_1	acceleration term of the second order unsteady wake model, (10)

* Numbers in brackets here and in the text refer to equations

T_2	rate cerm of the second order unsteady wake model, (10)
T'	$(1 + AL)/T_1^2$, (11)
W	hot wire anemometer wake measurement
$\overline{W}$	average wake measurement
a	blade section lift slope
b	number of blades on the rotor
c	blade cord
$f(\cdot)$	function of variables in parentheses in the system equation, (15)
h	rotor to ground plate distance
$h(\cdot)$	function of variables in parentheses in the measurement equation, (16)
n	rotor speed
r	distance from rotor center along blade span
u	input control vector, (15)
v	measurement noise vector, (16)
w	system or process noise vector, (15)
x	state vector, (15)
y	measurement vector, (16)
β_k	flapping angle of the kth blade, positive up
β_I, β_{II}	multiblade flapping coordinates: longitudinal and lateral cyclic flapping
$\overline{\beta}_I$, $\overline{\beta}_{II}$	measurement bias values
β_{I_m}, β_{II_m}	multiblade flapping coordinate measurements
$\hat{\beta}$	estimated values of flapping angles
ψ, t	rotor azimuth angle
ψ_k	azimuth angle of the kth blade, (5)
ψ_p	inner shaft or cyclic pitch azimuth angle, (1)
ψ_{po}	a constant ψ_p value, (2)
λ_k	generalized wake velocity, (4)

ω	cyclic pitch stirring excitation frequency in the rotating system
ω_n	cyclic pitch stirring excitation frequency in the space-fixed reference system
ω_l	non-dimensional rotating blade flapping natural frequency
ν_j	innovation vector at time j, (18)
ν_o, ν_I, ν_{II}	uniform, longitudinal and lateral perturbation induced inflow components
$\overline{\nu}_o$	r weighted average inflow
ρ	air density
γ	blade Lock number
θ	vector of unknown parameters, (15)
θ_k	pitch angle of the kth blade positive when leading edge is up
θ_o, θ_I, θ_{II}	collective, nose down cyclic and left cyclic pitch angles, respectively, (6)
σ	rotor solidity ratio ($b \cdot c/\pi R$)
τ	dynamic induced flow time constant, (5)
τ^*	$= (1 + AL)/\tau$, (8)

Superscripts

$\cdot$	time derivetive
$\hat{}$	estimate
T	transposed matrix
$\bar{}$	bias value

Subscripts

j	value for jth data sample
k	value for kth blade
m	measured variable
p t	pretransient
t	transient

o, I, II	multiblade variables
1_ω	first Fourier coefficient

```
OS/8  FORTRAN IV  3.03              APR 24  1977          PAGE  ONE

      C  HVPRT4 IS A PARAMETER IDENTIFICATION
      C  PROGRAM DESIGNED TO IDENTIFY 4 TO 6
      C  PARAMETERS (L,TAU,BIAS1,BIAS2,A,P2)
      C  FORM HOVERING TRANSIENT TESTING.
0002        DIMENSION BM(3,500),RJ(6),Y(42),RM(6,6),RRR(2,2)
0003        DIMENSION PRMT(3),G(2,15),PR(20),Z(6,2,15),RR(6),AUX(42)
0004        COMMON M,MM,Y,AUX,PR,NP,NSD,BM,G,Z,RM,RJ,RR,RRR
0005        EXTERNAL FC4THV,DU4THV,MINV
      C  READ IN DATA
0006        READ(5,20)IJK,PNTS,FIRZO,PITO
0007   20   FORMAT(I4,3F15.9)
0010        DO 10 I=1,3
0011        READ(5,21)(BM(I,J),J=1,IJK)
0012   21   FORMAT(10F7.3)
      C  IJK=NUMBER OF MEASUREMENT VECTORS
      C  PNTS=NUMBER OF MEASUREMENTS PER ROTOR REVOLUTION
      C  FIRZO=NUMBER OF MEASUREMENTS INTO THE DATA SET
      C        THAT THE FIRST ZERO AZIMUTH ANGLE OCCURS
      C  PITO=INITIAL CONDITION OF THE PITCH AZIMUTH ANGLE
0013   10   CONTINUE
      C  BM(1, )=PITCH AZIMUTH
      C  BM(2, )=BETA1
      C  BM(3, )=BETA2
      C  **********************
      C  NP=#OF PARAMETERS
0014        NP=5
      C  **********************
      C           4 YEILDS L,TAU,BIAS
      C           5 YEILDS L,TAU,BIAS,A
      C           6 YEILDS L,TAU,BIAS,A,P**2,-1.
0015        NSD=6
      C  NSD=DIMENSION OF STATE EQN.
0016        NIC=(NP-1)*NSD
      C  NIC=#OF INITIAL CONDITIONS
0017        PRMT(1)=FIRZO
0020        PRMT(2)=6.8318531/PNTS
      C  PRMT(2) IS THE TIME UNIT BETWEEN SAMPLE POINTS
      C  IN RADIANS AND THE INTERVAL OF INTEGRATION.
0021        RR(1)=400.
0022        RR(2)=0.
0023        RR(4)=400.
      C  RR(1-4) IS THE COST FUNCTION NORMALIZATION MATRIX.
      C  **********************
      C  INITIAL PARAMETER ESTIMATES AND/OR SPECIFIED
      C  PARAMETER VALUES.
0024        A=.400
0025        XL=4.
0026        TAU=4.
0027        P2=.3924
0030        BR=.976
0031        BR=BR**4.
0032        XKAPPA=.1
      C  **********************
      C  PR(1-20) IS THE PARAMETER ASSOCIATED VECTOR
      C  PASSED TO SUBROUTINES.
```

```
 05/8  FORTRAN IV  3.03              APR 24  1977          PAGE  TWO

0033            PR(6)=P2
      C  P2=P SQUARED MINUS 1.
0034            PR(1)=XL
0035            PR(2)=TAU
0036            PR(5)=A
0037            PR(10)=SIN(PITO)
0040            PR(11)=COS(PITO)
      C  **********************
      C  INITIAL BIAS VALUES
0041            PR(3)=.0
0042            PR(4)=.0
      C  **********************
0043            WRITE(3,22)IJK
0044            WRITE(3,23)A,XL,TAU,P2
0045       22   FORMAT(15X,'# OF MEASUREMENTS=',I4)
0046       23   FORMAT(3X,'INITIAL ESTIMATES',3X,'A=',F7.3,3X,
           '  'L=',F7.3,3X,'TAU=',F7.3,'  P2=',F7.4)
0047            WRITE(3,171)PR(3),PR(4)
0050       171  FORMAT(20X,'B1 BIAS=',F8.5,'     B2 BIAS=',F8.5)
0051            WRITE(3,172)BB,XKAPPA
0052       172  FORMAT(20X,'B**4.=',F8.5,'    KAPPA=',F8.5)
      C  **********************
      C  CALCULTAE MULTIPLYING FACTORS
      C  IKK=15=THE NUMBER OF DATA POINTS USED IN IDENTIFICATION.
0053            IKK=20
      C  **********************
0054       24   FORMAT(I4)
      C  **********************
      C  MM SPECIFIES THE #OF PARAMETER ITERATIONS.
      C  ITERATION LOOP
0055            DO 80 MM=1,5
      C  **********************
      C  SET STATE VECTOR INITIAL CONDITIONS TO ZERO.
0056            DO 70 I=1,NIC
0057       70   Y(I)=0.
      C  ZERO THE PARTIAL J/PARTIAL PARM AND THE M ARRAYS.
0060            DO 71 I=1,NP
0061            RJ(I)=0.
0062            DO 71 J=1,NP
0063            RM(I,J)=0.
0064       71   CONTINUE
      C  AVDAGR IS THE AVERAGE OF THE DIAGONAL OF B
0065            AVDAGR=(RR(1)+RR(4))/2.
0066            RRR(1,1)=AVDAGR
0067            RRR(2,2)=AVDAGR
0070            RRR(1,2)=0.
0071            RRR(2,1)=0.
      C  RRR(1,1)=RR(1) FOR NORMALIZING COST WITH B
      C  RRR(2,2)=RR(4) FOR NORMALIZING COST WITH B
      C  RRR(1,2)=RR(2) FOR NORMALIZING COST WITH B
      C  RRR(2,1)=RR(2)   "       "          "    "  "
0072            DO 72 I=1,4
0073            RR(I)=0.
0074       72   CONTINUE
      C  COMPUTE NEW PARAMETER ASSOCIATED VECTOR FOR EACH
```

```
  OS/8  FORTRAN IV  3.03              APR 24  1977          PAGE  THREE

      C  PARAMETER ITERATION.
0075          PR(20)=PR(1)/PR(2)
0076          PR(19)=(PR(5)*PR(1)+1.)/PR(2)
0077          PR(18)=PR(5)*PR(1)/PR(2)
0100          PR(17)=1./PR(2)
0101          PR(16)=PR(5)/PR(2)
0102          PR(15)=PR(5)+(PR(5)*4.*.028*XKAPPA)/88
0103          PR(14)=PR(15)*PR(1)/PR(2)
      C  SET UP WORKING VECTOR FOR INTEGRATING SUBROUTINE.
0104          DO 73 I=1,NIC
0105       73 AUX(I)=0.
      C  OUTER INTEGRATION LOOP
0106          DO 60 M=1,IKK
0107          NUMSTP=15
0110          NDIM=NIC
      C  INTEGRATE THROUGH 15 TIME STEPS.
0111          CALL RK4THV(PRMT,NUMSTP,NDIM,FC4THV,OU4THV)
      C  RETAIN PARTIAL SUMS OF INTEGRATION RESULTS
0112          CALL SEN4TS(IKK,MTNV)
0113       60 CONTINUE
0114          CONTINUE
0115       80 CONTINUE
0116          CALL EXIT
0117          END
```

OS/8 FORTRAN IV 3.03 APR 24 1977 PAGE ONE

```
C  FC4THV IS THE FUNCTION SUBROUTINE TO BE USED IN
C  IN THE EVALUATION OF HOVERING PARAMETER
C  IDENTIFICATION.  IT IS CALLED BY RK4THV.
         SUBROUTINE FC4THV(N,DERY,J)
         DIMENSION Y(42),DERY(42),BM(3,500),PR(20),AUX(42)
         COMMON M,MM,Y,AUX,PR,NP,NSD,BM
C  I IS THE TIME AT THE START OF THE INTERVAL OF
C  INTEGRATION.  II=I+1 IS THE TIME OF THE END OF THE
C  INTERVAL OF INTEGRATION.
         I=(M-1)*15+N
         II=(M-1)*15+N+1
C  COMPUTE LEFT AND FORWARD CYCLIC PITCH INPUT
C  FROM THE PITCH AZIMUTH ANGLE.
C  SUBTRACT THE INITIAL CYCLIC PITCH INPUT ANGLES
C  (PR(10,11)).
         GO TO (10,11,11,12),J
   12    THA1=-COS(BM(1,II))+PR(11)
         THA2=-SIN(BM(1,II))+PR(10)
         GO TO 14
   11    THA1=((-COS(BM(1,I))-COS(BM(1,II)))/2.)+PR(11)
         THA2=(-SIN(BM(1,I))-SIN(BM(1,II)))/2.+PR(10)
         GO TO 14
   10    THA1=-COS(BM(1,I))+PR(11)
         THA2=-SIN(BM(1,I))+PR(10)
   14    CONTINUE
C  NII= THE NUMBER OF DIFFERENTIAL EQUATIONS TO
C  BE SOLVED.
         NII=NSD*(NP-1)
C  PR(20)=L/TAU
C  PR(19)=(A*L+1)/TAU
C  PR(18)=A*L/TAU
C  PR(17)=1./TAU
C  PR(16)=A/TAU
C  PR(15)=A'
C  PR(14)=A'*L/TAU
C  PR(11)=-THETA1 AT T=0
C  PR(10)=  "   2 "   "
C  *************
C  DO LOOP THAT SOLVES THE KERNAL OF THE SYSTEM
C  EQUATIONS AND THE SENSITIVITY EQUATIONS.
         DO 15 I=1,NII,NSD
         DERY(I)=Y(I+1)
         DERY(I+1)=-PR(6)*Y(I)-PR(15)*Y(I+1)-PR(15)*Y(I+2)
     '   -2.*Y(I+3)+PR(5)*Y(I+4)
         DERY(I+2)=Y(I+3)
         DERY(I+3)=PR(15)*Y(I)+2.*Y(I+1)-PR(6)*Y(I+2)
     '    -PR(15)*Y(I+3)+PR(5)*Y(I+5)
         DERY(I+4)=PR(14)*Y(I+1)+PR(14)*Y(I+2)-PR(19)*Y(I+4)
         DERY(I+5)=-PR(14)*Y(I)+PR(14)*Y(I+3)-PR(19)*Y(I+5)
   15    CONTINUE
C  **********
C  ADD ON THE FORCING FUNCTIONS TO THE DIFFERENTIAL
C  EQUATIONS
         DERY(2)=DERY(2)+PR(5)*THA2
         DERY(4)=DERY(4)-PR(5)*THA1
```

```
 OS/8  FORTRAN IV  3.03              APR 24  1977          PAGE  TWO

0034            DERY(5)=DERY(5)-PR(18)*THA2
0035            DERY(6)=DERY(6)+PR(18)*THA1
      C   (2-6) ARE SYSTEM EQUATION FORCING FUNCTIONS.
0036            DERY(11)=DERY(11)+PR(16)*Y(2)+PR(16)*Y(3)-PR(16)*Y(5)
     '           -PR(16)*THA2
0037            DERY(12)=DERY(12)-PR(16)*Y(1)+PR(16)*Y(4)-PR(16)*Y(6)
     '           +PR(16)*THA1
0040            DERY(17)=DERY(17)-PR(17)*DERY(5)
0041            DERY(18)=DERY(18)-PR(17)*DERY(6)
0042            IF(NP-5)20,21,22
0043     22     DERY(26)=DERY(26)-Y(1)
0044            DERY(28)=DERY(28)-Y(3)
0045     21     DERY(20)=DERY(20)-Y(2)-Y(3)+Y(5)+THA2
0046            DERY(22)=DERY(22)+Y(1)-Y(4)+Y(6)-THA1
0047            DERY(23)=DERY(23)+PR(20)*Y(2)+PR(20)*Y(3)-PR(20)*Y(5)
     '           -PR(20)*THA2
0050            DERY(24)=DERY(24)-PR(20)*Y(1)+PR(20)*Y(4)-PR(20)*Y(6)
     '           +PR(20)*THA1
      C  (11-24) ARE SENSITIVITY EQUATION FORCING FUNCTIONS.
0051     20     CONTINUE
0052            RETURN
0053            STOP
0054            END
```

```
OS/8  FORTRAN IV  3.03              APR 24  1977          PAGE  ONE

      C  OU4THV IS THE OUTPUT SUBROUTINE CALLED FROM
      C  RK4THV TO BE USED WITH HOVERING DATA ANALYSIS.
0002            SUBROUTINE OU4THV(II,DERY,NDIM,PRMT)
0003            DIMENSION DERY(42),Y(42),PRMT(3),G(2,15),Z(6,2,15)
0004            DIMENSION BM(3,500),PR(20),AUX(42)
0005            COMMON M,MM,Y,AUX,PR,NP,NSD,BM,G,Z
      C  BEST ESTIMATES OF LEFT AND FORWARD TILTS AT THE END
      C  OF THE INTERVAL OF INTEGRATION ARE SAVED.
0006            G(1,II)=Y(1)
0007            G(2,II)=Y(3)
      C  **********
      C  PARTIAL J/PARTIAL PARAMETER VALUES ARE SAVED.
0010            Z(1,1,II)=Y(7)
0011            Z(1,2,II)=Y(9)
0012            Z(2,1,II)=Y(13)
0013            Z(2,2,II)=Y(15)
0014            Z(3,1,II)=1.
0015            Z(3,2,II)=0.
0016            Z(4,1,II)=0.
0017            Z(4,2,II)=1.
0020            IF(NP-5)30,31,32
0021     32     Z(6,1,II)=Y(25)
0022            Z(6,2,II)=Y(27)
0023     31     Z(5,1,II)=Y(19)
0024            Z(5,2,II)=Y(21)
      C  **********
0025     30     CONTINUE
      C  **********
      C   INPUT, OUTPUT, AND STATE VECTORS AS A
      C  FUNCTION OF TIME CAN BE GENERATED DURING
      C  ANY ITERATION BY SUBSTITUTING 25 FOR 40.
0026            GO TO (40,40,40,40,40,40),MM
      C  **********
0027     40     RETURN
0030     25     I=(M-1)*15+II+1
0031            THA1=-COS(BM(1,I))+PR(11)
0032            THA2=-SIN(BM(1,I))+PR(10)
      C  Y1 AND Y3 ARE THE BEST ESTIMATES OF THE
      C  TILTING STATES.
0033            Y1=Y(1)+PR(3)
0034            Y3=Y(3)+PR(4)
      C  BIN1 AND BIN2 ARE THE BEST ESTIMATES OF THE
      C  WAKE STATES.
0035            BIN1=Y(5)
0036            BIN2=Y(6)
      C  BM(2,I) AND BM(3,I) ARE THE TILTING MEASUREMENTS.
0037            WRITE(3,24)BM(2,I),Y1,BIN1,BM(3,I),Y3,BIN2,THA1,THA2
0040     24     FORMAT(4X,8F8.3)
0041            RETURN
0042            END
```

```
 OS/8  FORTRAN IV  3.33              APR 24  1977          PAGE  0'E

       C  SE!4TS COMPUTES THE PARTAIL SUMS OF THE SE.STTIVITY
       C  SEQUENCES.
0002           SUBROUTINE SEN4TS(IKK,MINV)
0003           DIMENSION DH(4),G(2,15),Z(6,2,15),RM(6,6),BM(3,500),RRR(2,2)
0004           DIMENSION RJ(6),LV(6),MV(6),PR(20),Y(42),GRM(36),RR(6),AUX(42)
0005           DIMENSION DIAGM(6)
0006           COMMON M,MM,Y,AUX,PR,NP,NSD,BM,G,Z,RM,RJ,RR,RRR
0007           II=(M-1)*15
       C  FORM INOVATION SEQUENCE FOR THIS 15 SAMPLES G.
       C  ALSO CALCULATE B MATRIX.
0010           DO 12 J=1,15
0011           III=II+J+1
       C  COMPUTE INOVATION SEQUENCE
0012           G(1,J)=BM(2,III)-G(1,J)-PR(3)
0013           G(2,J)=BM(3,III)-G(2,J)-PR(4)
       C  COMPUTE B MATRIX
0014           RR(1)=RR(1)+G(1,J)*G(1,J)
0015           RR(2)=RR(2)+G(1,J)*G(2,J)
0016           RR(4)=RR(4)+G(2,J)*G(2,J)
0017    12     CONTINUE
       C  COMPUTE PARTIAL  PARTIAL PRAMS,RJ.
0020           DO 14 JJ=1,NP
0021           DO 14 J=1,15
0022           RJ(JJ)=RJ(JJ)+G(1,J)*(Z(JJ,1,J)*RRR(1,1)+Z(JJ,2,J)*RRR(2,1))
     '           +G(2,J)*(Z(JJ,1,J)*RRR(1,2)+RRR(2,2)*Z(JJ,2,J))
0023    14     CONTINUE
       C  COMPUTE M
0024           DO 47 I=1,NP
0025           DO 47 J=1,NP
0026           DO 47 K=1,15
0027           RM(I,J)=RM(I,J)+(Z(I,1,K)*RRR(1,1)+Z(I,2,K)*RRR(2,1))*Z(J,1,K)
     '           +(Z(I,1,K)*RRR(1,2)+Z(I,2,K)*RRR(2,2))*Z(J,2,K)
0030    47     CONTINUE
       C  SUPSTITUTE 31 FOR 33 FOR PRINTING OUT TIME HISTORY
       C  OR M INVERSE
0031           GO TO (33,33,33,33,33),MM
0032    33     IF(M.EQ.IKK) GO TO 31
0033           GO TO 32
       C  CHANGE RM TO GENERAL MATRIX GRM.
0034    31     NB=0
0035           DO 49 J=1,NP
0036           DO 49 I=1,NP
0037           NB=NB+1
0040           GRM(NB)=RM(I,J)
0041    49     CONTINUE
0042           NP2=NP*NP
       C  **********
0043    23     FORMAT(4X,5F14.6)
       C  **********
       C  INVERT M
0044           CALL MINV(GRM,NP,DT,LV,MV)
0045           WRITE(3,24)M,DT
0046    24     FORMAT(5X,I3,3X,'INVERSE OF M-MATRIX','    DTM=',E14.8/)
0047           WRITE(3,23)(GRM(I),I=1,NP2)
0050           WRITE(3,26)
```

```
0051      26      FORMAT(5X,'SQ RT OF DIAG M')
0052              DO 27 I=1,NP
0053              ILM=(I-1)*NP+I
0054      27      DIAGM(I)=(ABS(GRM(ILM)))**.5
0055              WRITE(3,23)(DIAGM(I),I=1,NP)
0056              WRITE(3,25)(RJ(I),I=1,NP)
0057      25      FORMAT(3X,'PART.(J/THETA)=',6F9.0/)
0060      32      CONTINUE
0061              IF(M.EQ.IKK) GO TO 30
0062              RETURN
          C  CHANGE GRM(K) TO MATRIX RM(I,J)
0063      30      NB=0
0064              DO 50 J=1,NP
0065              DO 50 I=1,NP
0066              NB=NB+1
0067              RM(I,J)=GRM(NB)
0070      50      CONTINUE
0071      90      FORMAT(4F10.4)
          C  UPDATE UPDATES PARAMETER ESTIMATES AFTER EACH
          C  ITERATION.
0072              DO 55 I=1,NP
0073              DH(I)=0.
0074              DO 55 J=1,NP
0075              DH(I)=RM(I,J)*RJ(J)+DH(I)
0076      55      CONTINUE
0077              DO 56 I=1,NP
0100              PR(I)=PR(I)+DH(I)
0101      56      CONTINUE
0102              RR(3)=RR(2)
0103              XN=15*IKK
0104              DO 34 I=1,4
0105      34      RR(I)=RR(I)/XN
0106              RRP=((RR(1)+RR(4))/2.)**.5
          C  RRP IS THE FIT FACTOR
0107              WRITE(3,61)RRP
0110      61      FORMAT(/'RRP=',F20.8,/'RR=')
0111              WRITE(3,62)(RR(I),I=1,4)
0112      62      FORMAT(2F20.8)
0113              CALL MINV(RR,2,DT,LV,MV)
0114      63      FORMAT(4F18.7)
0115              A=PR(5)
0116              TAU=PR(2)
0117              XL=PR(1)
0120              P2=PR(6)
0121              WRITE(3,20)MM,A,XL,TAU,P2
0122      20      FORMAT(' ITERATIONS=',I1,'  A=',F6.3,' L=',F6.3,' TAU=',
                  '  F6.3,'  P2=',F8.5)
0123              WRITE(3,21)PR(3),PR(4)
0124      21      FORMAT(20X,'B1 BIAS=',F8.5,'     B2 BIAS=',F8.5)
0125              RETURN
0126              END
```